STRESS CONCENTRATIONS IN FILLETS

Thesis by

Robert Solverson

In Partial Fulfillment of the Requirements

For the Degree of

Doctor of Philosophy

California Institute of Technology

Pasadena, California

1953

ACKNOWLEDGEMENTS

The author wishes to acknowledge Him who makes all things possible, and his loved ones whose encouragement has been unbounded.

He wishes also to express special thanks to his supervisor, Dr. E. E. Sechler, for suggesting this problem and arranging financial support with the Cooperative Wind Tunnel. He is indeed grateful to the Cooperative Wind Tunnel for its support of the program.

Appreciation is also expressed to Mr. Beverly Morant, Mr. John Wall, and Mr. Charlton Dunn who prepared models and conducted many of the stress concentration and fringe value tests; to Mrs. Dorothy Eaton and Miss Joan Benson for their assistance in computation; to Mrs. Betty Wood for preparation of the figures; and to Mrs. Virginia Boughton for typing this manuscript.

ABSTRACT

The stress concentrations arising in the fillets of fan and turbine blades, tie down rods, and bolt heads from axially symmetric centrifugal or static force loadings are treated two dimensionally by photoelastic and theoretical methods. The effects of the fillet radius, the height of the base, the mode of application of retention forces, and the distance between the retention reactions and fillet tangencies are considered. The stress concentration factor, K, was found to increase with decreasing radius and decreasing base height and, for small radii, to decrease at first with the distance between the reaction and fillet tangency but, in general, to increase with this distance. Comparisons with other experiments and stress concentration configurations are also made.

An approximate theoretical solution is derived by selecting a convenient region from the whole base and replacing, where necessary, the exact boundary conditions with relaxed or integral conditions. The problem is formulated in terms of the classical Airy stress function. Agreement between theory and experiment is reasonable.

TABLE OF CONTENTS

LIST OF FIGURES

LIST OF FIGURES (Cont'd)

EXPLANATION OF SYMBOLS

a = overall width of base

b = narrowest dimension across shank above fillets or narrowest dimension of tensile specimen

R = fillet radius

c = smallest height of base

e = width of shoulder

ℓ = distance between center of reaction and fillet tangency point

f = height of base at load application for recessed fillets

α = angle of inclination of loading shoulder

p, q = principal stresses

t = thickness of model

n = fringe number

C = stress optic coefficient

f = fringe value in psi shear per fringe per inch thickness at λ = 5460 A

λ = wave length of light in angstroms

w = R + b/2

h = R + c

σ_x, σ_y = normal stresses in rectangular cartesian coordinates; positive value ~ tension, negative value ~ compression

τ_{xy} = shear stress in rectangular cartesian coordinates

σ_r, σ_θ = normal stresses in polar coordinates; positive values ~ tension, negative values ~ compression

$\tau_{r\theta}$ = shear stress in polar coordinates

φ = Airy stress function

σ_Q = stresses on side of base

Q = sum of horizontal stresses

σ_P = stress on shoulder due to reaction

P = applied load in simplified problem

R_o = distance from center of fillet circle to centroid of side load Q

θ_o = $\tan^{-1} e/R$

X_o = distance between fillet tangency point and region of uniform tensile stress

I. INTRODUCTION

In order to predict the useful life of a wind-tunnel fan blade and to design such a blade for maximum life, it is necessary to know the stress distribution in the fillet near the retention bearing. (Figure 1.) Due principally to the large centrifugal force and, secondarily, to the thrust and drag forces on the fan blade in operating conditions, a stress concentration arises in the fillet which is a function of the geometry of the butt of the blade and the manner in which the retaining forces are applied. It was due to a stress concentration of this type that a fatigue failure occurred at the root of a fan blade at C. W. T. * in 1948, which resulted in extensive damage to the tunnel and necessitated a lengthy shutdown. That failure, and the subsequent investigation, prompted this experimental and theoretical study of the factors which affect the stress rise.

The retention configuration shown in Figure 2 is only one of several possible configurations. Due to other design and manufacturing requirements, however, this configuration was chosen for the fan blades of the new supersonic wind tunnel development at C. W. T. and was consequently studied to the exclusion of other possibilities.

This retention configuration is by no means confined to propellers and wind-tunnel fan blade butts, but also occurs in helicopter rotor attachments**, bolt heads, turbine blades, and recently in the tie-down

---

* Southern California Cooperative Wind Tunnel, Pasadena, California

** See, for instance, the design details of the British Cierva "Air Horse" in Aeroplane, April 8, 1949, pp. 391 and 393.

rods of a 50,000 ton capacity forging press designed for the production of aircraft components. (Reference 1.) In all of these applications the design requirement is maximum fatigue life. Since, in general, the loading spectrum is only roughly known, the designer can only choose the configuration which has the lowest maximum stress, and if possible, treat the surface where the concentration occurs to delay fatigue cracking.

Some published work on this problem is known by the author. Following the failure at C.W.T., H. D. McGinness of the wind tunnel staff conducted several experimental studies with both two- and three-dimensional models. (References 2, 3, 4, 5, and 6.) It was shown that the amplitude of vibration of the blade due to the non-uniform flow coming from the upstream straightening vanes was negligibly small. (Reference 6.) In 1949 the N.A.C.A.,* Moffett Field, conducted several two-and three-dimensional strain gage studies but did not officially publish their findings. (Reference 7.) Professor W. D. Murray of the Massachusetts Institute of Technology studied recessed fillets in bolt heads; one of his studies appears on pages 151 and 196 in Reference 8. In the design analysis of a 50,000 ton capacity forging press, F. T. Morrison and R. G. Sturm made a two-dimensional photoelastic study of eleven configurations. (Reference 1.) The fatigue problem was also considered at Farnborough in the redesign of their wind-tunnel fan blades. (Reference 8.)

Little work on turbine blade stress concentrations has been

---

* National Advisory Committee for Aeronautics.

published and what has come to the author's attention has been in the classified literature and is not available for publication here. In the case of relatively short turbine life and the use of ductile-metal blades, multiple-land or fir-tree retention configurations had proven satisfactory. Volume production and low cost production of turbine blades were the important problems together with vibration and starting shock problems. Higher operating temperatures and rotational speeds have indicated that brittle fracture materials such as ceramics, ceramets, etc., may be used for turbine blades. These materials are particularly sensitive to stress concentrations and unless very small tolerances are adhered to in the production of these blades, multiple-land configurations fail prematurely due to the local concentration at one of the lands. This fact has motivated designers to consider new configurations such as the Dovetail and Interlock; these resemble the second configuration illustrated in Figure 1.

Undoubtedly much other experimental work has been done by various companies in determining the strength and fatigue life of bolts (and rotor attachments) but most of this information has not been published in the usual journals.

A review of the experimental studies of the N.A.C.A. and C.W.T. indicated that the factors which affected the stress concentration were the fillet contour, the depth of the base, the distance of the load from the end of the fillet, and the method of loading. In the case of a circular arc fillet these factors could be expressed in terms of dimensionless ratios, R/b, c/b, and ℓ/b, the method of loading being indescribable in terms of a simple ratio. (Figure 2.) The few

data also indicated that the stress concentration in three dimensions varied similarly to the two-dimensional concentration as a function of these ratios but that the magnitude of the stress concentration factor* in three dimensions was substantially lower than the two-dimensional factor for the same R/b, c/b, and ℓ/b ratios. In view of this observation and the urgent need of C. W. T. for a suitable configuration for its supersonic tunnel, it was decided to investigate a series of two-dimensional contours photoelastically to obtain the apparent optimum design in as short a time as possible, and then, knowing the behavior of the stress concentration as a function of the geometrical ratios, to develop a theory which would predict the stress concentration factor under the C. W. T. operating condition and a variety of other loadings.

Besides the propeller hub problem, there are many other aircraft structural problems, such as fittings, which are difficult to treat by the Theory of Elasticity either because the boundary conditions, though simple to formulate physically, are not easily expressed analytically in functions which satisfy equilibrium and compatability requirements, or because too many variables are present to permit a reasonably simple analysis. Many of these problems are, however, amenable to experimental treatment by strain gage and two- or three-dimensional photoelastic study. (Reference 9.) If experimental methods, moreover, are first used to investigate a problem, it is

---

* The stress concentration is the ratio of the maximum fillet stress to the applied axial load divided by the minimum cross-sectional area.

not likely that important variables will be overlooked or that assumptions inconsistent with experimental fact will be made in a theoretical analysis. (See Timoshenko's discussion of Navier's treatment of the "free torsion" problem on page 228, Reference 11.) It is therefore fitting that the initial approach to these problems be of an exploratory experimental nature.

In order that the experimental approach be practical it must be rapid and low cost. Strain gage studies of stress concentrations are neither rapid nor low cost because the models must be large and require much time to prepare and instrument. To study a large number of propeller hubs in three dimensions by strain gage methods would be very costly and time consuming. Three-dimensional photoelastic studies are limited by the materials suitable for "frozen stress" studies. The only photoelastic material currently available in large sizes is Fosterite which is very expensive. Other photoelastic materials have maximum thicknesses in the order of one inch; use of these materials would necessitate very small models and consequently yield relatively inaccurate experimental results.

In view of these time and cost requirements, a conventional two-dimensional photoelastic analysis is certainly justified for plane-stress problems and even relatively justified for axially-symmetric problems because in certain cases the axially-symmetric distribution can be obtained directly from the two-dimensional distribution. Examination of the equilibrium equations shows that the stress distribution in the axially-symmetric case is roughly similar to the two-dimensional distribution because a transformation of the type

$$\sigma_r = \frac{S_r}{r} \qquad \tau_{rz} = \frac{T_{rz}}{r} \qquad \sigma_z = \frac{S_z}{r}$$

changes the axially symmetric equations of equilibrium

$$\frac{\partial \sigma_r}{\partial r} + \frac{\partial \tau_{rz}}{\partial z} + \frac{\sigma_r - \sigma_\theta}{r} = 0$$

$$\frac{\partial \tau_{rz}}{\partial r} + \frac{\partial \sigma_z}{\partial z} + \frac{\tau_{rz}}{r} = 0$$

to

$$\frac{\partial S_r}{\partial r} + \frac{\partial T_{rz}}{\partial z} = \sigma_\theta$$

$$\frac{\partial S_z}{\partial z} + \frac{\partial T_{rz}}{\partial r} = 0$$

The two-dimensional equilibrium equations in rectangular cartesian coordinates are, with no body forces,

$$\frac{\partial \sigma_x}{\partial x} + \frac{\partial \tau_{xy}}{\partial y} = 0$$

$$\frac{\partial \sigma_y}{\partial y} + \frac{\partial \tau_{xy}}{\partial x} = 0$$

The quantities S_r, T_{rz}, and S_z may therefore be expected to behave like the stresses σ_x, σ_y and τ_{xy} because in the r, z coordinate system they satisfy the same boundary conditions, except for a factor, and satisfy almost identical equilibrium equations. (σ_θ may be treated as a body force and will of course affect S_r, T_{rz}, and S_z.)

Any development, furthermore, of the two-dimensional photoelastic technique (and three-dimensional technique) would be of value

not only to the author but to many aircraft companies whose problems warrant a similar approach. Research effort was therefore devoted to the application of castable plastics to photoelasticity - a study which was initiated at GALCIT by Roger Matzdorff. (Reference 12.)

From an experimental investigation the important factors may be determined and as simple a theory as will agree with experimental results may be developed. This was the underlying motivation of the stress concentration study which follows.

II. TWO-DIMENSIONAL EXPERIMENTAL PHOTOELASTIC STUDIES

Object and Models

The first object of these experiments was to derive a fan blade contour and butt shape which would yield the lowest possible fillet stress for the required loads. It became evident that the optimum design was one which had no shoulder fillet and to which the retention forces were applied as shear stresses on the cylindrical end of the blade. (The blades could not be continuous across the axis of rotation of the fan because each blade was required to feather.) Since this configuration was impractical, the configuration shown in Figure 2, with the possible modifications indicated in Figures 3 and 4, was chosen as the basic configuration. Since an infinite variety of fillet contours could be drawn, it was decided to confine the initial studies at least to circular-arc contours until the importance of the R/b ratio on the stress concentration could be determined. Many non-circular-arc contours could, moreover, in the neighborhood of the stress rise be approximated by circular arcs. An example would be an elliptical contour in which the major axis was parallel to the axis of symmetry of the propeller hub.

The contour classes illustrated in Figures 3 and 4 seemed promising variations of the basic contour: that of Figure 3 because a large radius could be obtained and the retention force had a compressive component to reduce the fillet stress, and that of Figure 4 because recessed fillets had previously been used in bolt heads.

Loads

The loads which the butt must support are due to the centrifugal force and the thrust and drag forces on the blade. The centrifugal force was simulated by a uniform axial stress at section A-A, Figures 2, 3, and 4, a small distance from the fillet. The thrust and drag forces were simulated by a shear and bending moment at A-A. The stresses arising from the shear and bending moment were small compared to the axial stress and were neglected in the two-dimensional studies.

The reactions were developed on the shoulders outboard of the fillet tangency points. In the case of the axially-symmetric uniform loading at A-A, these reactions were equal. In case of bending at A-A, these reactions became unequal, their moment being equal to the applied bending moment for equilibrium.

Two types of reactions were studied: uniformly distributed reactions and point load reactions. The first reactions were obtained by inserting thick cardboard cushions between the shoulder and the holding rig to distribute the forces evenly over the whole shoulder from the fillet tangency point to the end of the shoulder. The point load reactions were developed at the fillet tangency point. Several experiments were designed to show how the stress concentration was affected by moving the point load away from the fillet tangency point.

One could not hope to study all possible reaction types but several types at least needed investigation. According to St. Venant's principle the stress rise is not sufficiently far removed from the point of loading that the mode of loading has insignificant effect on it.

Description of Test Equipment

The models were loaded in the loading frame in the photoelastic laboratory. (Figure 5.) The frame is a conventional loading frame which may be translated vertically and horizontally so that different regions of a large model may be brought to the center of the collimated light field. Two special jigs were built to support the propeller-hub models and facilitate alignment. The loading frame rests on a table whose legs have adjusting screws so that the plane of the frame can easily be made vertical.

The polariscope is a conventional one except that mirrors replace the collimating lenses. The light source is a General Electric 100 watt AH-4 air-cooled, glass-enclosed lamp which is operated in an upright position in series with a step-up transformer, type 89 G 144, and has an arc length of one and one-fourth inches. The principal visible radiations of this lamp are the dark violet, 4060A; blue violet, 4360A; bright green, 5460A; yellow, 5780A; and a band of red.

The plano-convex lenses, items 2 and 3, Figure 6, are light collecting lenses. If the light source is considered a point source, analysis shows that the total flux of useful light falling on the mirror, item 8, depends only on the stop diameter, item 6, and the aperture of the mirror. Since the source is a line source, however, analysis shows that the best combination of collecting lenses is one in which the aperture of the second lens, item 3, is the same as that of the mirror, and that its size and that of the first lens, item 2, is determined to catch as much light from the source container as possible. The stop

could not be placed near enough to the light source to collect as much useful light as the present system does. More light could be obtained from a BH-6, 1000 watt arc, but this would necessitate water or forced-air cooling. The 100 watt bulb together with an efficient collecting lens system provides sufficient intensity at the photographic plate so that with a sensitive emulsion rapid enough exposures can be made to stop all normal vibrations. The chief source of vibrations was the GALCIT 10 Foot Wind Tunnel.

The main light requirement is a large field of collimated light of high intensity. Analysis shows that deviation from perfectly collimated light depends on the ratio of the stop diameter to the mirror diameter and a function of the aperture of the mirror. The optimum mirror aperture is near 5 because greater apertures make severe space demands for small perfections in collimation. As the stop diameter is reduced the collimation improves, but the flux of useful light also decreases, so clearly a compromise must be reached. The spherical aberration of the mirror and a 3/16 inch diameter stop limit the number of distinct interference fringes to about 20 per inch, model dimensions, but this proved to be no handicap for this analysis.

The stop, item 6, is located at the focal point of the mirrors to simulate a point source. The mirrors have an overall diameter of eight inches and a focal length of thirty-nine inches. The angle which the mirror makes with the incident light is small so that the effects of coma are minimized.

The principal law of photoelasticity is the stress-optic law which states:

$$\frac{P-Q}{2} = \frac{n\lambda}{2Ct} = \frac{n}{t}f$$

where P, Q are principal stresses

n is the fringe order of the interference fringe

λ is the wave length of light

C is the stress-optic coefficient for the photoelastic material

t is the thickness of the specimen

f is the material fringe value in psi shear for a given wave length of light

Since n is inversely proportional to λ , the lowest possible wave length of light should be used. The GALCIT polariscope, nevertheless, uses the mercury green, 5460A wavelength, because it facilitates visual work. A Wratten 77A filter which transmits about half of the incident mercury green and high wave-length red light is used. The presence of the red light does not affect visual work because the red light is clearly distinguishable from the green and black fringes; nor does it affect the photographic work because plates sensitive only to the 5460 radiation are used.

The polarizer and analyzer are Polaroid sheet and are fixed into rings which can be rotated. The quarter-wave plates were also made by the Polaroid Corporation and are placed in the same ring as the polarizer and analyzer. These elements were aligned and their relative axes determined. Most of the experimental work was done using the quarter-wave plates since they eliminate the isoclinics of

which there was little need because the stress concentration occurred on a free boundary.

Shields were placed over most of the optical system to cut down the scattered light for photographic purposes. A focal plane shutter was used to determine exposures. An exposure of 1/50 sec. was found to be the longest possible satisfactory exposure because of wind-tunnel vibrations. The photographic plates were 4 x 5 Kodak Spectroscopic 103-G type plates and were exposed from plate holders held on a wooden frame. The 103-G Spectroscope plate is sensitive only to the mercury green radiation and is very suitable for low intensity exposures. (Reference 13.)

Model Preparation

The models were made from either Paraplex P-43 (Reference 14), a thermosetting resin manufactured by Rohm and Haas and several other manufacturers, or CR-39 (References 15 and 16), also a thermally set plastic developed by the Pittsburgh Plate Glass Company and manufactured by the Cast Optics Corporation of Riverside, Connecticut. Appendix I is a summary of the photoelastic properties of these materials. The model contours were laid out on the material and sawed out roughly on an ordinary band saw. Chipping was not bad if recommended blades and speeds were used; the band saw cuts were as close as 1/16 inch to the finish line. The models could then have been finished on a milling machine with a high speed end mill, but in the case of the propeller-hub model each was finished on a hand router with a high speed rotary file (10,000 rpm). (Figure 9.) Tolerances on the hand

router operations are poor compared to those on a mill but are, nevertheless, quite satisfactory for most photoelastic work.

Test Procedure

After each model was machined it was bolted to pull-off plates. The plates in turn were bolted to a pull-off rod which was connected to the lever arm of the loading frame which had been appropriately counterbalanced so that the load on the model was zero when no weight was in the pan. (Figure 10.) The model was placed on the supports on the arms of the loading frame and then adjusted so as to make it perpendicular to the beam of collimated light by centering its reflection on the mirror. This alignment operation was conducted with a small weight in the pan.

The supporting arms were set horizontal and the model was further aligned by making its centerline vertical and locating it in the center of the frame by eye and scale. The model was then partially loaded until a few fringes were observed. Lack of symmetry in the fringe pattern was corrected by raising or lowering the supporting arms. This adjustment permitted corrections for non-uniformly distributed loadings as well. Each model, after being properly aligned, was then cleaned and loaded to produce a reasonable number of fringes in the fillet.

Photographs of both fillets of each model were taken - with the fillet centered in the light field. The Kodak Spectroscopic plate, 103-G, proved very satisfactory for the short, low-intensity exposures after its development time was pushed to eight minutes.

The developer used was commercially prepared D-19. The plates were then fixed for twenty minutes, washed in water for one-half hour, and air dried. A sampling of over four hundred plates is shown in Figures 10 to 18 inclusive.

Estimation of Fringe Order

The fillet stress was determined by projecting a several-times enlarged image of each configuration on a white paper. The point of maximum fillet stress was observed and a line normal to the fillet contour at that point was drawn on the paper. The various fringe orders and model edge were located on this line. Later the fringe orders were plotted directly above this line and extrapolated to the edge. Results for both fillets of a specimen were averaged to eliminate asymmetrical effects.

This method of data reduction or a similar extrapolation was necessary to obtain readings to the nearest quarter of a fringe in seven or eight fringes instead of to the nearest half fringe which is about the best the eye can do on interpolation. It was felt that by graphical extrapolation the error in estimating the fillet fringe order could be reduced from 7.0 percent to 3.5 percent. Due to the little chippings at the edges in the fillet from machine operations the fringes did not always appear as clear, smooth lines. But if, many times enlarged, the borders of the fringes were carefully smoothed out and the centers of the full and half fringes carefully determined and at these points the appropriate fringe value plotted, a smooth curve could

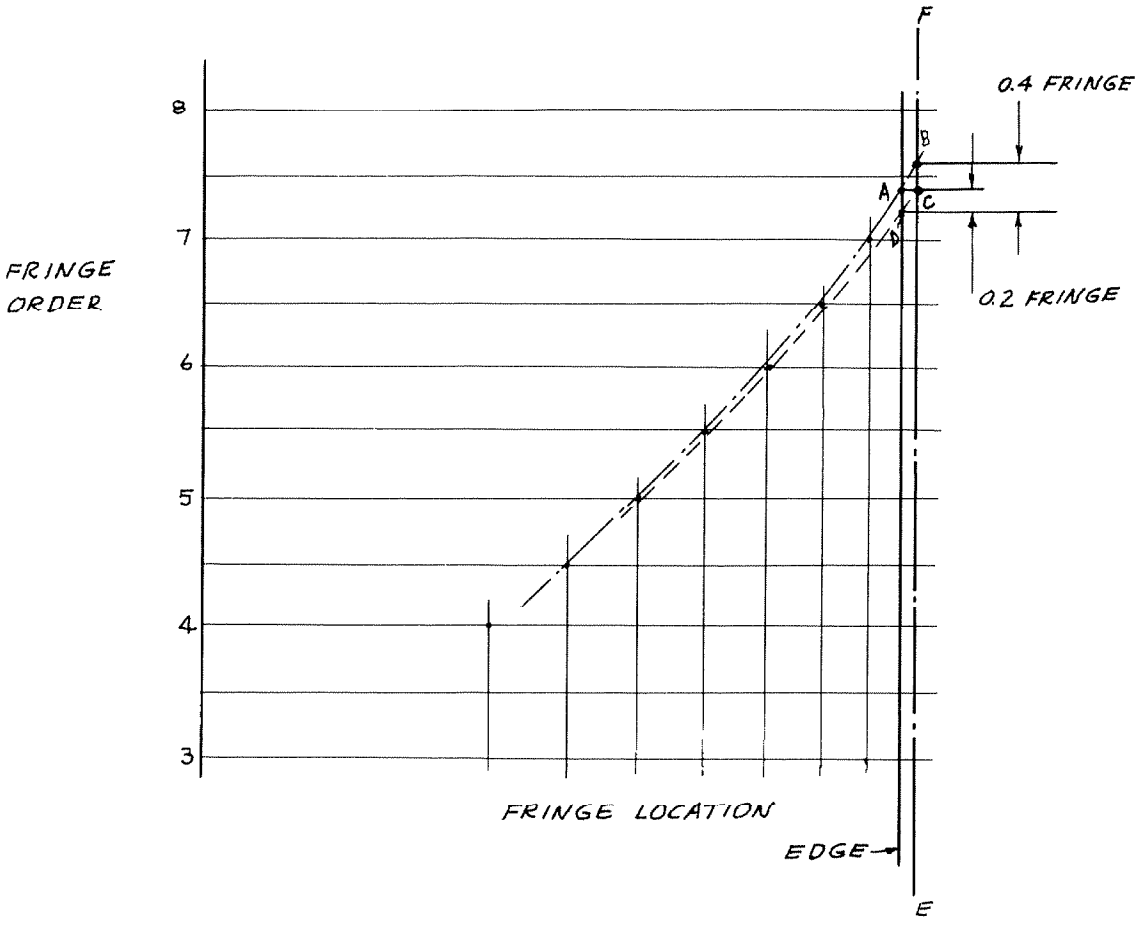

be passed through these values such that there was very little scatter of points about the line. Extrapolation to the edge could therefore be made using four points whose distances apart were greater than the distance from the last point to the edge.

In the sketch above, a typical extrapolation plot is presented. The most unfavorable lines through these fringe orders intersect the edge at A and D which differ at most by 0.2 fringe orders and differ from their average by 0.1 fringe order. The error involved in estimating the fringe order is therefore about 1.5 percent at eight fringes. The edge however is not always an infinitesimally thin line. Due to the rounding of the edge corners or beveling of them (during layout

with a scribe) and due to anticlastic curvature which the surface suffers under large stresses, the edge appears as a line sometimes as wide as one quarter of the neighboring fringe. This width is indicated in the figure by the line labeled EDGE and the line FE. The most unfavorable lines intersect the outermost position of the edge at B and C. At worst, the correct fringe order lies between B and D which at most are about 0.4 fringe order apart. If the average of A, D, B, and C is taken as the fringe order, the error is at most $\pm$ 4 percent. The true position of the edge can be easily determined however so that the error in estimating the fringe order is less than 4 percent.

Calculation of Stress Concentration Factor, K

The stress concentration factor K is the ratio of the maximum fillet stress to the load divided by the nominal minimum cross-sectional area or,

$$K = \frac{\sigma \text{ fillet max}}{\frac{P}{tb}}$$

Since the applied load P was four times the pan load W, and σ fillet max is calculated from the stress optic law,

$$\sigma_{\text{fillet max}} = \frac{2nf}{t} ,$$

K, therefore is given by the formula

$$K = 1/2 \ \frac{nfb}{W} .$$

Discussion of Errors

An estimate of the maximum cumulative error in K may be made in the following manner:

$$\log K = \log 1/2 + \log n + \log f + \log b - \log W$$

and

$$\frac{dK}{K} = \frac{dn}{n} + \frac{df}{f} + \frac{db}{b} - \frac{dW}{W}$$

The maximum error may be first estimated as

$$\left|\frac{dK}{K}\right| = \left|\frac{dn}{n}\right| + \left|\frac{df}{f}\right| + \left|\frac{db}{b}\right| + \left|\frac{dW}{W}\right|$$

$\left|\frac{dn}{n}\right| = 0.04$ from the previous discussion. $\left|\frac{df}{f}\right|$ is the sum of the error in the initial fringe determination which is no greater than 0.01 for the data presented because only CR-39 was used for the models, and the error due to creep which was not accounted for in the reduction of the data. This is assessed at 0.04 at most; see Appendix I. $\left|\frac{df}{f}\right| = 0.05$. $\left|\frac{db}{b}\right|$ is a dimension tolerance which was less than 0.003. $\left|\frac{dW}{W}\right|$ including friction in the loading frame is $\leq$ 0.005. $\left|\frac{dK}{K}\right| = 0.04 + 0.05 + .003 + 0.005 = 0.098$ or $\pm$ 9.8 percent.

This error does not include the errors due to tolerances on the radius or base depth. The tolerances on the base depth were at most about 0.007 and on the radius about 0.02. An error of 0.02 in the radius causes an error in K of about 0.015 at R/b = 0.1 and causes less error if R/b $>$ 0.1. Including these effects the maximum

possible error is estimated at 12 percent.

These errors are reasonably larger than those claimed by other photoelasticians. Were the models milled to 0. 005 inches the sum of the tolerance errors could be reduced by 0. 015. If Bakelite were used, the creep would be substantially less so that the error in $\left|\frac{df}{f}\right|$ due to creep would be reduced 0. 025. With precision loading rigs, etc., the error in initial fringe value determination may be reduced 0. 005 making possible a total reduction of 0. 03 in $\left|\frac{df}{f}\right|$, and a reduction in $\left|\frac{dW}{W}\right|$ of 0. 003. By using special methods, the error in $\left|\frac{dn}{n}\right|$ may be reduced by 0. 02. The total reduction is 0. 015 + 0. 03 + 0. 01 + 0. 003 = 0. 058 making their maximum error about 5 percent. This reduction in error is obtained at the expense of model preparation time and cost and did not appear justified for the present experimentation.

Results

The results of the investigation of the basic contour (Figure 2) with the point load reactions applied at the fillet tangency points are shown in Figures 19 and 20. It is seen for any R/b ratio in the range studied that increasing the c/b ratio beyond 0. 6 has little effect on the stress concentration factor K. It is also seen that the radius (R/b) has little effect on the stress concentration for R/b $>$ 0.25. In this range the c/b ratio is the controlling factor. In the case of the point reactions, the ℓ/b ratio corresponds to the distance between the fillet tangency point and the reaction, and

also affects the stress rise. For $R/b < 0.25$ and $c/b < 0.3$, it is seen that the controlling factors are the R/b and the ℓ/b ratios.

This seems reasonable because, when R/b is in the neighborhood of 0.1, the c/b ratio at which c/b ceases to affect K should be less than 0.6, most probably near 0.3. It follows therefore that the increase in K with large R/b for small c/b is also reasonable from geometrical similarity considerations. The fact that the R/b ratio has little effect on K for these regions implies that other contours whose minimum radii of curvature are comparable to the R/b ratio of the circular-arc fillet to which they correspond would have little effect on the stress concentration factor K.

The effect of the ℓ/b ratio is shown in Figure 20. Due to the fact that loads had been on the models about an hour before these data were taken, creep correction was made. The broken line indicates a day's wait between tests. Agreement at $\ell/b = 0$ with Point Load Data is reasonably good.

It is not surprising to find that the stress concentration factor first decreases with ℓ/b in spite of the fact that the bending moment on section B-B (Figure 2) increases with ℓ/b. The reason for this is shear transfer or shear lag. As ℓ/b increases, the shear stress across B-B becomes more parabolic and the gradient of the shear stress in the vertical direction decreases. In other words, $-\frac{\partial \tau_{xy}}{\partial x}$ decreases as ℓ/b increases because there is an opportunity for the load to redistribute itself in the distance ℓ/b. But the rate of change in fillet stress $\frac{\partial \sigma_y}{\partial y} = -\frac{\partial \tau_{xy}}{\partial x}$ from equilibrium considerations. The fillet stress at the tangency point therefore grows less

rapidly if ℓ/b is large. Beyond a certain value of ℓ/b, however, the shear transfer contributes no further favorable effect and the stress concentration increases as ℓ/b increases.

A uniformly distributed loading permits a more favorable shear distribution along section B-B and therefore causes lower stress concentrations. (Figure 21.) The effect is larger for smaller R/b ratios, but this is again in accordance with St. Venant's principle.

An investigation of recessed fillets (Figure 4) was also conducted and the results are presented in Figures 22 and 23. Figure 22 shows the results of tests in which the R/b, ℓ/b, and f/b ratios were held constant and the c/b ratio varied. The work was done visually so that the error was larger than normal; this fact is indicated in the figure by shading the region of observation. It is seen that the stress concentration factor K for a recessed fillet is only slightly lower than the factor for the corresponding basic contour with the same R/b, ℓ/b, and c/b ratios. Figure 23 shows the effect of a second fillet on K plotted against the R/b ratio for a given c/b ratio but varying ℓ/b ratio. It is observed for small R/b ratios that recessing the fillet reduces the stress concentration. These few tests indicate that the recessed fillet contours behave in approximately the same way as the basic contours for the same R/b, c/b, and ℓ/b ratios. The recessed contours should therefore be considered for cases of small R/b, and large c/b; these conditions are manifest in bolt heads.

Several contours with inclined bearing surfaces were also studied. (Figures 17 and 18.) For the R/b and c/b ratios defined

according to Figure 3 these contours yielded stress concentrations about the same or slightly higher than the basic contours of similar geometry. The optimum angle α appears near 20 degrees; if large α are employed a large shear stress unfavorable to the fillet stress may develop to make this configuration inferior to the basic set.

The main advantage of contours of this class appears when the dimension a, the overall width of the base is given or required to be less than a certain value. For a given R/b and c/b ratio, the resulting b is always much larger than the corresponding basic contour b and for a given load, therefore, the resulting fillet stress is lower than the corresponding basic contour fillet stress.

Discussion

Using the results of the point load and distributed load tests, curves were faired through the unofficial N.A.C.A. two-dimensional results. For a c/b ratio = 0.5 comparison was made between these strain gage studies and the photoelastic investigations. (Figure 24.) The N.A.C.A. data fell between the distributed load and the point load results. Since the exact mode of loading was not observed all that can be said is that the strain gage results should fall between the two limiting cases. Certainly the strain gage results should not exceed the photoelastic results because the strain gages are finite in length and integrate over their length; they also may not have been placed at the exact maximum stress location.

A comparison between stress concentrations arising in the propeller-butt two-dimensional configurations, circular notches in tension, and circular-arc fillets in tension is made in Figure 25. (References 17 and 18.) The stress concentrations arising in the fillet with point and distributed loads are substantially higher than either the semicircular notch concentration or conventional fillet. To assume that Neuber's notch theory is applicable to the propeller-hub problem is unjustified.

DESIGN APPLICATIONS

In a design problem, the load that the butt must support is known, at least approximately, and the allowable stress is known from fatigue studies. The function $b/K = P/\sigma_{\text{fillet max}}$, $K = K(R/b, c/b, e/b)$, must then be determined. If there are no auxiliary conditions, K may be chosen as low as possible and b can be determined to satisfy the design requirements. After K has been chosen, R/b, c/b, and e/b can be determined from the figures; knowing b - R, c, and e can be calculated.

If auxiliary conditions such as minimum weight or an overall dimension are imposed, determination of the optimum design is not always easy.

If an overall dimension such as the maximum distance, a, across the base is specified and the bearing surface e is also specified then the derivation of the optimum configuration is relatively simple. It is observed that

$$a = b + 2R + 2e$$

$$\sigma_{fillet} = K\frac{P}{b}, \quad \text{per unit thickness}$$

$$\sigma_{fillet} = \frac{KP}{a - 2R - 2e} = \frac{P}{a}\left(\frac{K}{1 - \frac{2R}{a} - \frac{2e}{a}}\right)$$

For the maximum load P for the given dimension a, the function $\left(\frac{K}{1 - 2\frac{R}{a} - 2\frac{e}{a}}\right)$ must be minimized; K = K (R/b, c/b, e/b). e/b and R/b may be written in terms of R/a and e/a:

$$\frac{R}{b} = \frac{R}{a} \cdot \frac{1}{\frac{b}{a}} = \frac{R}{a}\left(\frac{1}{1 - 2\frac{R}{a} - 2\frac{e}{a}}\right)$$

$$\frac{e}{b} = \frac{e}{a} \cdot \frac{1}{\frac{b}{a}} = \frac{e}{a}\left(\frac{1}{1 - 2\frac{R}{a} - 2\frac{e}{a}}\right)$$

Since e/a is given, $R/b = f_1(R/a)$ and $e/b = f_2(R/a)$. A number of values for R/a may then be selected and the corresponding values of R/b and e/b calculated. For these values K(R/b, e/b, c/b = 0.6, 0.7) may be chosen and the value of the function $P(a\sigma_f)^{-1}$ determined and plotted against R/a to determine the maximum value.

If e/a is not given, assume various values of e/a and for each value determine the proper R/a to maximize $P(a\sigma_f)^{-1}$. These maxima may then be plotted against e/a and the optimum derived.

In the case of a minimum weight requirement, it is necessary to maximize the function b/K for smallest volume per unit thickness. The volume of the base below the fillet tangency point is

$$V = c(b + 2R + 2e) + 0.43R^2 + bR$$

The most direct procedure to determine the optimum configuration is to choose a number of b's and calculate the required K's.

For each K, several combinations of R/b, c/b, and e/b are possible. By holding combinations of two of these fixed and varying the third an optimum volume may be found. For example, for a given R/b, c/b, vary e/b and determine the minimum volume and the optimum e/b for that R/b, c/b. Then holding e/b = e/b optimum$_1$ and c/b, vary R/b until the optimum R/b is found. Then for R/b optimum, and e/b optimum vary c/b until its optimum is found. Then repeat the whole process holding R/b = R/b optimum, and c/b = c/b optimum, and find e/b optimum$_2$, etc. This must be done for each value of K. The optimum volume for each configuration may then be plotted against the K of that combination, and the absolute minimum volume obtained.

III. TWO DIMENSIONAL THEORETICAL ANALYSIS

Notation

The stress concentration which arises in the fillet of a fan blade butt may be formulated in two dimensions as a problem in plane stress without body forces. The only load considered is due to centrifugal force and it is simulated by a static load evenly distributed across the shank at a reasonable distance outboard of the fillet and is resisted by two equal static reactions on the shoulders. For circular arc fillets, the geometry may be represented, as shown in Figure 26, by the dimensions R, h, w, and e. R and e correspond to the R and e of the experimental investigation but $w = R + b/2$ and $h = R + c$. The reason for this change in notation will become evident after the approach to the problem is explained.

Formulation

The differential equations of equilibrium without body forces in the rectangular cartesian coordinate system x, y are

$$\frac{\partial \sigma_x}{\partial x} + \frac{\partial \tau_{xy}}{\partial y} = 0$$

$$\frac{\partial \tau_{xy}}{\partial x} + \frac{\partial \sigma_y}{\partial y} = 0$$

The material is assumed homogeneous and isotropic; Hooke's law therefore applies and the equation of compatibility may be written in terms of the stresses in the following way:

$$\nabla^2 (\sigma_x + \sigma_y) = 0 \qquad \text{where } \nabla^2 = \frac{\partial^2}{\partial x^2} + \frac{\partial^2}{\partial y^2}$$

This set of simultaneous partial differential equations may be solved in the classical manner by introducing an Airy stress function (page 24, Reference 11) $\varphi = \varphi(x, y)$ such that

$$\sigma_x = \frac{\partial^2 \varphi}{\partial y^2}$$

$$\sigma_y = \frac{\partial^2 \varphi}{\partial x^2}$$

$$\tau_{xy} = -\frac{\partial^2 \varphi}{\partial x \partial y}$$

By choosing the stress function φ in this way the equilibrium equations are identically satisfied and the compatibility equation becomes the classical equation of the theory of elasticity,

$$\nabla^4 \varphi(x, y) = 0 \qquad \nabla^4 = \left(\frac{\partial^2}{\partial x^2} + \frac{\partial^2}{\partial y^2}\right)\left(\frac{\partial^2}{\partial x^2} + \frac{\partial^2}{\partial y^2}\right)$$

Exact Boundary Conditions

A solution to this partial differential equation yielding a unique stress distribution may be obtained if suitable boundary conditions are prescribed. Suitable boundary conditions consist of the specification of the normal and shear stresses on the complete boundary. The exact boundary conditions of the propeller-hub problem are given below in the notation of Figure 26.

Due to the symmetry of the stress distribution the stress

function must be symmetrical about the centerline. A consequence of this symmetry is that the shear stress must vanish along the centerline since it is an odd derivative of an even function.

$$\tau_{xy}(x,0) = 0$$

The normal stress, $\sigma_x(x,0)$, must integrate to the applied side load. Since this is not an external boundary the normal and shear stresses should not be prescribed.

The bottom surface is free; therefore

$$\tau_{xy}(h,y) = 0$$

$$\sigma_x(h,y) = 0, \qquad -(w+e) \le y \le (w+e)$$

The side faces may have normal loadings $\sigma_q[x, \pm(w+e)]$. The boundary conditions are, therefore,

$$\tau_{xy}[x, \pm(w+e)] = 0$$

$$\sigma_y[x, \pm(w+e)] = \sigma_q$$

The boundary stresses on the shoulders are

$$\tau_{xy}(R,y) = 0$$

$$\sigma_x(R,y) = \sigma_p, \qquad -(w+e) \le y \le -w;\ w \le y \le w+e$$

The boundary conditions in the fillet can best be described by polar coordinate notation. For the fan blade problem*

$$\sigma_r(R,\theta) = 0$$

$$\tau_{r\theta}(R,\theta) = 0, \qquad 0 \le \theta \le \frac{\pi}{2}$$

---

* In the case of turbine blades where slightly different retention methods are used, $\sigma_r(R,\theta) \neq 0$.

On the vertical sides between the fillets and the nominal end of the shank, the faces are free of stress.

$$\tau_{xy}[x, \pm(w-R)] = 0$$

$$\sigma_y[x, \pm(w-R)] = 0, \qquad -\ell \leq x \leq 0$$

On the top surface, $x = -x_o$, where x_o is that value of x where the disturbance due to the fillet stress concentrations has vanished,

$$\tau_{xy}(-x_o, y) = 0$$

$$\sigma_x(-x_o, y) = \frac{e}{w-R}\sigma_p, \quad -(w-R) \leq y \leq (w-R)$$

These boundary conditions present formidable mathematical difficulties* not only because there are so many parameters but because the boundaries are hard to describe mathematically. Rather than solve this problem exactly or even approximately, a simpler problem which embodies the physics of the exact problem is studied.

---

* Alternative methods were also considered. Energy methods are not suited to this problem because the integrations tend to smooth out the stress concentration effects. Conformal mappings in general (Reference 19) present no simplifications either. One possible mapping, however, is that of the flow in a corner to flow in the half plane but this mapping has symmetry about the bisector of the corner angle and restricts the possible configurations to one.

Another approach was also contemplated. Polynomials φ_n of order n which satisfy $\nabla^4\varphi_n = 0$ possess arbitrary coefficients which may be determined by application of conditions at selected points on the boundary. Due to the enormity of the non-self-checking arithmetical calculations and the large probability of error this approach is rather impractical.

Simplified Problem

A geometrically simpler region of interest (Figure 27) is therefore considered for the case of axial symmetry and a more convenient choice of axes is made. Motivation for this simplification is the fact* that a polynomial stress function $\varphi(x, y)$ to which corresponds stresses σ_x, σ_y and τ_{xy} -stresses applicable to the straight boundaries - can be readily transformed to a stress function $\varphi(r, \theta)$ to which correspond stresses σ_r, σ_θ and $\tau_{r\theta}$, applicable to the fillet boundary. To this function can be added, from the general solution in polar coordinates a perturbation $\varphi'(r, \theta)$ with the corresponding stresses σ_r', σ_θ' and $\tau_{r\theta}'$ needed to satisfy the exact boundary conditions at the fillet but still be of such functional form that they vanish a short distance from the fillet. If the boundary conditions on the straight boundaries are applied before the perturbation stresses are added and the perturbation stresses do not tend to zero with r so that they are zero on the straight boundaries, then the conditions on the straight boundaries are not satisfied. The perturbation stresses are therefore chosen to vary with r^{-n} where n is as large as possible.

Simplified Boundary Conditions

This simplification of geometry implies new and less restrictive boundary conditions. The centerline is an external boundary in this

---

* This was essentially the method used to solve the problem of a circular hole in a tension field. See page 75, Reference 11.

simplified problem. One stress condition is known along this boundary, namely,

$$\tau_{xy}(x, w) = 0$$

For equilibrium in the y direction the integral of the normal stresses over the centerline must equal the sum of the forces in the horizontal direction applied on either half of the butt and, for no such forces, the integral must vanish. This may be formulated in the following way.

$$\int_{-x_o}^{h} \sigma_y(x, w)\,dx = Q$$

or

$$\int_{-x_o}^{0} \sigma_y(x, w)\,dx + \int_{o}^{h} \sigma_y(x, w)\,dx = Q$$

where x_o is a point $x_o > 0$, corresponding to the distance required for the stress concentration disturbance to vanish.

In the region $0 \leq x \leq h$, the only horizontal forces that are theoretically considered are pressures along the sides of the base, $y = 0$, and their sum is - Q. The integral $\int_{-x_o}^{0} \sigma_y(x, w)\,dx$ is therefore an estimation of the shear along the top of the region of interest, $\int_{R}^{w} \tau_{xy}(0, y)\,dy$. But sufficiently far from the top of the fillet, at $x = -x_o$, the stress is a uniform tension and $\int_{R}^{w} \tau_{xy}(-x_o, y)\,dy = 0$. The integral $\int_{-x_o}^{0} \sigma_y(x, w)\,dx$ which is equivalent to $\int_{R}^{w} \tau_{xy}(0, y)\,dy$ is therefore an estimation of the shear transfer needed for the perturbation or stress concentration at the fillet level to vanish.

An estimation of either $\int_R^w \tau_{xy}(0, y)\, dy$ or $\int_0^h \sigma_y(x, w)\, dx$ must be made because these are external forces in the simplified formulation and affect the fillet stress which is an interior stress. An estimation of either integral is sufficient if the equations of equilibrium are satisfied.

An approximation of this integral $\int_0^h \sigma_y(x, w)\, dx = Q - \int_{-x_o}^0 \sigma_y(x, w)\, dx$ may be made with the help of St. Venant's principle. According to his principle the disturbance must vanish in some characteristic length which in this case is R or w. The photoelastic studies indicate that w is the characteristic dimension and, therefore $x_o = w$.

For a first approximation, the functional form of $\sigma_y(x, w)$ may be considered linear, $-w \le x \le 0$. Photoelastic studies corroborate this choice. $\int_{-x_o}^0 \sigma_y(x, w)\, dx = \frac{1}{2} w\, \sigma_y(0, w)$ and $\int_0^h \sigma_y(x, w)\, dx = Q - \frac{1}{2} w\, \sigma_y(0, w)$. $\sigma_y(0, w)$ is not assigned a specific value as is Q so that this requirement is better expressed by the equation

$$\frac{1}{2} w\, \sigma_y(0, w) + \int_0^h \sigma_y(x, w)\, dx = Q$$

If $x_o = R$, the stress concentration factor is not seriously changed.* The main effect of changing x_o is the change in $\sigma_y(0, w)$ which is of little interest in this analysis.

---

* Subsequent calculations for R/h = 0.22, $w = h$, $Q = 0$ show that the percent change in stress concentration factor due to a change in x_o between w and R was -1 percent but the change in $\sigma_y(0, w)$ was + 56 percent, and in $\sigma_x(0, w)$ was + 1 percent based on the former values. A change in x_o therefore makes little change in the integral of the shear stresses along the top edge.

An alternative formulation of these boundary conditions may be inferred from the photoelasticity studies. The uniform stress across the shank is $\frac{P}{W-R}$. The stress at the center $\sigma_x(0,W) < \frac{P}{W-R}$ since $\sigma_x(0,R) > \frac{P}{W-R}$ and $\int_R^W \sigma_x(0,y)\,dy = P$. Photoelastic studies indicate that $\sigma_x(0,W) \approx 0.7\,\frac{P}{W-R}$ and $\sigma_y(0,W) \approx 0.9\,\frac{P}{W-R}$. Calculation of the stress concentration factor may be made using these requirements instead of the equations

$$\int_R^W \sigma_x(0,y)\,dy = P$$

and

$$\tfrac{1}{2}\sigma_y(0,W) + \int_0^h \sigma_y(x,W)\,dx = Q$$

but then the calculation is only a test of the validity of the assumptions of the elastic theory and the approximations of the problem. *

The simplified conditions along the centerline and top edge are therefore

$$\int_R^W \sigma_\theta\left(r,\tfrac{\pi}{2}\right)dr = P$$

and

$$\tfrac{1}{2}W\sigma_y(0,W) + \int_0^h \sigma_y(x,W)\,dx = Q$$

The boundary requirements along the base and the fillet are exact. For the fan blade fillet

$$\sigma_r(R,\theta) = 0$$
$$\tau_{r\theta}(R,\theta) = 0 \qquad 0 \le \theta \le \tfrac{\pi}{2}$$

---

* Subsequent calculations show that use of either set of conditions leads to approximately the same values of K.

$$\sigma_x (h, y) = 0$$

$$\tau_{xy} (h, y) = 0$$

The shoulder on which the reactions were developed is removed and the reaction is applied as a shear stress, $\tau_{r\theta} (r, 0)$. In view of this change, hope for accurate theoretical predictions for $\frac{R}{h} << 1$ and $e = 0$ is diminished although paradoxically the requirement that $\frac{R}{h} << 1$ is very significant to the radial decay of the perturbation stresses, σ_r' , σ_θ' , $\tau_{r\theta}'$. Comparison of theoretical calculations with experimental evidence corroborated this contention.

The reaction **P** is distributed as a shear along the edge y = 0, $R \leq x \leq h$ such that

$$\int_R^h \tau_{r\theta} (r, 0)\, dr = P$$

Control over the exact distribution of the horizontal pressures is sacrificed.

$$\int_R^h \sigma_\theta (r, 0)\, dr = Q$$

Together with these integral interpretations, two other conditions are added to clarify the picture.

$$\int_R^h r\, \sigma_\theta (r, 0)\, dr = - Pl + QR_o$$

with the assumption that the load center is at ℓ from the fillet tangency point. R_o is the distance from the center of the fillet to the resultant of the side stress integral.

The second condition is, for the case of the distributed load,

$$\sigma_\theta(R, \theta_o) = -\frac{P}{e}\sin^2\theta_o + \sigma_Q \cos^2\theta_o, \quad \theta_o = \tan^{-1}\frac{e}{R}$$

This is an approximation to the condition $\sigma_y(R, -e) = \sigma_Q$. If θ_o is small, then $\sigma_\theta(R, \theta_o) \simeq \sigma_y(R, -e)$; but since it has a component in the direction of the distributed load, by Mohr's circle $\sigma_\theta(R, \theta_o) = -\frac{P}{e}\sin^2\theta_o$, $\sigma_Q = 0$, θ_o very small. σ_θ is approximately zero.*

The point load condition is represented in a similar manner. In order to apply such a loading physically some small shoulder e is required outboard of the fillet tangency point. The stress $\sigma_\theta(R, \theta_o) = 0$ where $\theta_o = \tan^{-1}\frac{e}{R}$ corresponds to the condition $\sigma_y(R, -e) = 0$. It is possible that the choice of e or θ_o will affect K and this must be investigated.

A summary of the simplified boundary requirements is presented here.

$$\sigma_r(R, \theta) = 0$$

$$\tau_{r\theta}(R, \theta) = 0, \qquad 0 \le \theta \le \frac{\pi}{2}$$

---

* Calculations show that $\sigma_\theta(R, \theta_o) = 0$ yield higher values for K than $\sigma_\theta(R, \theta_o) = -\frac{P}{e}\sin^2\theta_o$ for $w = h$, and $0.1 \le \frac{R}{h} \le 0.35$. These values differ by five percent at most.

$$\sigma_x(h, y) = 0$$

$$\tau_{xy}(h, y) = 0, \qquad 0 \le y \le w$$

$$\tau_{xy}(x, w) = 0 \qquad -w \le x \le h$$

$$\frac{1}{2} w \sigma_y(0, w) + \int_0^h \sigma_y(x, w)\, dx = Q$$

$$\int_R^w \sigma_\theta\left(r, \frac{\pi}{2}\right) dr = P$$

$$\int_R^h \sigma_\theta(r, 0)\, dr = Q$$

$$\int_R^h r\, \sigma_\theta(r, 0)\, dr = -Pl + QR_0$$

$$\sigma_\theta(R, \theta_0) = -\frac{P}{e} \sin^2\theta_0 + \sigma_Q \cos^2\theta_0$$

for distributed load

$$= \sigma_Q \cos^2\theta_0$$

for point load

$$\theta_0 = \tan^{-1}\frac{e}{R}$$

Analysis

In order to satisfy these boundary requirements a stress function in the form of a polynomial of sixth order is chosen. Higher order terms are omitted because their addition increases the algebraic complexity of the problem several fold without a corresponding increase in accuracy. A polynomial in x and y is chosen because it is readily transformed to polar coordinates by the simple relationships $x = r\cos\theta$, $y = r\sin\theta$, and because the stresses, to satisfy the conditions on the straight boundaries, can be derived in terms of symbols which make mathematical representation of the boundaries simple. The polynomial $\varphi(x, y)$ is the sum of five polynomials φ_n, $n = 2, 3, 4, 5, 6$:

$$\varphi(x, y) = \sum_{n=2}^{6} \varphi_n(x, y)$$

where $\varphi_n(x, y)$ satisfies the equation $\nabla^4 \varphi_n = 0$, the compatibility and equilibrium requirements. From each of the polynomials of order greater than two, four arbitrary constants are retained, and from the second order polynomial all three are retained. The polynomial φ (x, y) is

$$\begin{aligned}\varphi(x, y) = {} & a_1 x^2 + a_2 xy + a_3 y^2 \\ & + b_1 x^3 + b_2 x^2 y + b_3 x y^2 + b_4 \\ & + c_1 x^4 + c_2 x^3 y - 3(c_1 + c_4) x^2 y^2 + c_3 x y^3 + c_4 y^4 \\ & + d_1 x^5 + d_2 x^4 y + d_3 x^3 y^2 - (5d_4 + d_2) x^2 y^3\end{aligned}$$

$$-(5d_1 + d_3)\, xy^4 + d_4 y^5$$

$$+ f_1 x^6 + f_2 x^5 y + 5(f_4 - 2f_1) x^4 y^2 - \frac{5}{3}(f_2 + f_3) x^3 y^3$$

$$+ 5(f_1 - 2f_4) x^2 y^4 + f_3 x y^5 + f_4 y^6$$

The stresses may be derived from this stress function

$$\sigma_x = \frac{\partial^2 \varphi}{\partial y^2} = 2a_3 + 2b_3 x + 6b_4 y - 6(c_1 + c_4) x^2 + 6c_3 xy + 12c_4 y^2$$
$$+ 2d_3 x^3 - 6(5d_4 + d_2) x^2 y - 12(5d_1 + d_3) x y^2 + 20 d_4 y^3$$
$$+ 10(f_4 - 2f_1) x^4 - 10(f_2 + f_3) x^3 y + 60(f_1 - 2f_4) x^2 y^2$$
$$+ 20 f_3 x y^3 + 30 f_4 y^4$$

$$\sigma_y = \frac{\partial^2 \varphi}{\partial x^2} = 2a_1 + 6b_1 x + 2b_2 y + 12c_1 x^2 + 6c_2 xy - 6(c_1 + c_4) y^2$$
$$+ 20 d_1 x^3 + 12 d_2 x^2 y + 6 d_3 x y^2 - 2(5d_4 + d_2) y^3$$
$$+ 30 f_1 x^4 - 120 f_1 x^2 y^2 + 10 f_1 y^4 + 20 f_2 x^3 y + 60 f_4 x^2 y^2$$
$$- 10 f_2 x y^3 - 10 f_3 x y^3 - 20 f_4 y^4$$

$$-\tau_{xy} = \frac{\partial^2 \varphi}{\partial x \partial y} = a_2 + 2b_2 x + 2b_3 y + 3c_2 x^2 - 12(c_1 + c_4) xy + 3c_3 y^2$$
$$+ 4 d_2 x^3 + 6 d_3 x^2 y - 6(5d_4 + d_2) x y^2 - 4(5d_1 + d_3) y^3$$
$$+ 5 f_2 x^4 + 40(f_4 - 2f_1) x^3 y - 15(f_2 + f_3) x^2 y^2$$
$$+ 40(f_1 - 2f_4) x y^3 + 5 f_3 y^4$$

The boundary condition implying symmetry may then be applied: $-\tau_{xy}(x, w) = 0, \quad -w \le x \le h$ This gives rise

to the following set of equations:

$$a_2 + 2b_2 h + 3c_2 h^2 + 4d_2 h^3 + 5 f_2 h^4 = 0$$

$$2b_3 - 12(c_1 + c_4)h + 6d_3 h^2 + 40(f_4 - 2f_1)h^3 = 0$$

$$3c_3 - 6(5d_4 + d_2)h - 15(f_2 + f_3)h^2 = 0$$

$$-4(5d_1 + d_3) + 40(f_1 - 2f_4)h = 0$$

$$5 f_3 = 0$$

The shear on the bottom must vanish:- $\tau_{xy}(h, y) = 0, \quad 0 \le y \le w.$

$$a_2 + 2b_3 w + 3c_3 w^2 - 4(5d_1 + d_3)w^3 + 5 f_3 w^4 = 0$$

$$2b_2 - 12(c_1 + c_4)w - 6(5d_4 + d_2)w^2 + 10(f_1 - 2f_4)w^3 = 0$$

$$3c_2 + 6d_3 w - 15(f_2 + f_3)w^2 = 0$$

$$4d_2 + 40(f_4 - 2f_1)w = 0$$

$$5 f_2 w = 0$$

and the normal stress on the bottom must vanish; $\sigma_x(h, y) = 0, \quad 0 \le y \le w.$

$$2a_3 + 2b_3 h - 6(c_1 + c_4)h^2 + 2d_3 h^3 + 10(f_4 - 2f_1)h^4 = 0$$

$$6b_4 + 6c_3 h - 6(5d_4 + d_2)h^2 - 10(f_2 + f_3)h^3 = 0$$

$$12c_4 - 12(5d_1 + d_3)h + 60(f_1 - 2f_4)h^2 = 0$$

$$20 d_4 + 20 f_3 h = 0$$

$$30 f_4 = 0$$

From these simultaneous equations, all of the arbitrary constants can be expressed in terms of five remaining constants, a_1, b_1, c_1, d_3, and f_1 as follows:

$$a_1 = a_1$$

$$a_2 = -12c_1hw - 80w^3hf_1 - 140wh^3f_1 + 6wh^2d_3$$

$$a_3 = -3c_1h^2 - 45h^4f_1 + 2h^3d_3$$

$$b_1 = b_1$$

$$b_2 = 6c_1w + 30f_1wh^2 + 40f_1w^3$$

$$b_3 = 6c_1h + 70f_1h^3 - 3h^2d_3$$

$$b_4 = -20wh^2f_1$$

$$c_1 = c_1$$

$$c_2 = -2d_3w$$

$$c_3 = 40f_1wh$$

$$c_4 = 5f_1h^2$$

$$d_1 = 2f_1h - \frac{d_3}{5}$$

$$d_2 = 20f_1w$$

$$d_3 = d_3$$

$$d_4 = 0$$

$$f_1 = f_1$$

$$f_2 = 0$$

$$f_3 = 0$$

$$f_4 = 0$$

$\varphi(x, y)$ now retains five arbitrary constants and is given by the following expression:

$$\begin{aligned}\varphi(x,y) = {} & a_1 x^2 + a_2 xy + a_3 y^2 \\ & + b_1 x^3 + b_2 x^2 y + b_3 x y^2 + b_4 y^3 \\ & + c_1 (x^4 - 3x^2y^2) + c_2 x^3 y + c_3 x y^3 \\ & + c_4 (y^4 - 3x^2y^2) + d_1 (x^5 - 5x y^4) \\ & + d_2 (x^4 y - x^2 y^3) + d_3 (x^3 y^2 - x y^4) \\ & + f_1 (x^6 - 10 x^4 y^2 + 5 x^2 y^4)\end{aligned}$$

$\varphi(x,y)$ may be transformed to $\varphi(r, \theta)$ by the relations, $x = r \cos\theta$, $y = r \sin\theta$ yielding

$$\begin{aligned}\varphi(r,\theta) = {} & a_1 r^2 \cos^2\theta + a_2 r^2 \cos\theta \sin\theta + a_3 r^2 \sin^2\theta \\ & + b_1 r^3 \cos^3\theta + b_2 r^3 \cos^2\theta \sin\theta + b_3 r^3 \cos\theta \sin\theta \\ & + b_4 r^3 \sin^3\theta + c_1 r^4 (\cos^4\theta - 3\cos^2\theta \sin^2\theta) \\ & + c_2 r^4 \cos^3\theta \sin\theta + c_3 \cos\theta \sin^3\theta \\ & + c_4 r^4 (\sin^4\theta - 3\cos^2\theta \sin^2\theta) \\ & + d_1 r^5 (\cos^5\theta - 5\cos\theta \sin^4\theta) + d_2 r^5 \cos^4\theta \sin\theta \\ & - d_2 r^5 (\cos^2\theta \sin^3\theta) + d_3 r^5 (\cos^3\theta \sin^2\theta - \sin^4\theta \cos\theta) \\ & + f_1 r^6 (\cos^6\theta - 10\cos^4\theta \sin^2\theta + 5\cos^2\theta \sin^4\theta) .\end{aligned}$$

By use of trigonometric relationships, $\varphi(r,\theta)$ may be arranged in the following way:

$$\varphi(r,\theta) = \left(\frac{a_1 r^2}{2} + \frac{a_3 r^2}{2}\right) + \left(\frac{b_2 r^3}{4} + \frac{3b_4 r^3}{4}\right)\sin\theta$$

$$+ \left(\frac{3}{4}b_1 r^3 + \frac{1}{4}b_3 r^3\right)\cos\theta + \left(\frac{a_2 r^2}{2} + \frac{c_2 r^4}{4} + \frac{c_3 r^4}{4}\right)\sin 2\theta$$

$$+ \left(\frac{a_1 r^2}{2} - \frac{a_3 r^2}{2} + \frac{c_1 r^4}{2} - \frac{c_4 r^4}{2}\right)\cos 2\theta$$

$$+ \left(\frac{b_2 r^3}{4} - \frac{b_4 r^3}{4} + \frac{d_2 r^5}{8}\right)\sin 3\theta$$

$$+ \left(\frac{b_1 r^3}{4} - \frac{b_3 r^3}{4} + \frac{5 r^5 d_1}{4} + \frac{d_3 r^5}{8}\right)\cos 3\theta$$

$$+ \left(\frac{c_2 r^4}{8} - \frac{c_3 r^4}{8}\right)\sin 4\theta + \left(\frac{c_1 r^4}{2} + \frac{c_4 r^4}{2} + \frac{f_1 r^6}{2}\right)\cos 4\theta$$

$$+ \frac{1}{8} d_2 r^5 \sin 5\theta - \left(\frac{r^5 d}{4} + \frac{r^5 d_3}{8}\right)\cos 5\theta$$

$$+ \frac{f_1 r^6}{2}\cos 6\theta$$

or $\varphi(r,\theta) = A_1 r^2 + B_1 r^3 \cos\theta + C_1 r^3 \sin\theta$

$$+ (D_1 r^2 + D_2 r^4)\cos 2\theta + (E_1 r^2 + E_2 r^4)\sin 2\theta$$

$$+ (F_1 r^3 + F_2 r^5)\cos 3\theta + (G_1 r^3 + G_2 r^5)\sin 3\theta$$

$$+ (H_1 r^4 + H_2 r^6)\cos 4\theta + J_1 r^4 \sin 4\theta$$

$$+ K_1 r^5 \cos 5\theta + M_1 r^5 \sin 5\theta + N_1 r^6 \cos 6\theta$$

where

$$A_1 = \frac{1}{2}(a_1 + a_3)$$

$$B_1 = \frac{3}{4} b_1 + \frac{1}{4} b_3$$

$$C_1 = \frac{1}{4} b_2 + \frac{3}{4} b_3$$

$$D_1 = \frac{1}{2}(a_1 - a_2)$$

$$D_2 = \frac{1}{2}(c_1 - c_4)$$

$$E_1 = \frac{1}{2} a_2$$

$$E_2 = \frac{1}{4}(c_2 + c_3)$$

$$F_1 = \frac{1}{4}(b_1 - b_3)$$

$$F_2 = \frac{5}{4} d_1 + \frac{1}{8} d_3$$

$$G_1 = \frac{1}{4}(b_2 - b_4)$$

$$G_2 = \frac{1}{8} d_2$$

$$H_1 = \frac{1}{2}(c_1 + c_4)$$

$$H_2 = \frac{1}{2} f_1$$

$$J_1 = \frac{1}{8}(c_2 - c_3)$$

$$K_1 = -\frac{1}{4} d_1 - \frac{1}{8} d_3$$

$$M_1 = \frac{1}{8} d_2$$

$$N_1 = \frac{1}{2} f_1$$

To this stress function a perturbation function $\varphi'(r,\theta)$ may be added. $\varphi'(r,\theta)$ is chosen from the general solution in polar coordinates (page 114, Reference 11).

$$\varphi'(r,\theta) = A_0 \ln r + \frac{B_2}{r}\cos\theta + \frac{C_2}{r}\sin\theta$$
$$+\left(\frac{D_3}{r^2} + D_4\right)\cos 2\theta + \left(\frac{E_3}{r^2} + E_4\right)\sin 2\theta$$
$$+\left(\frac{F_3}{r^3} + \frac{F_4}{r}\right)\cos 3\theta + \left(\frac{G_3}{r^3} + \frac{G_4}{r}\right)\sin 3\theta$$
$$+\left(\frac{H_3}{r^4} + \frac{H_4}{r^2}\right)\cos 4\theta + \left(\frac{J_3}{r^4} + \frac{J_4}{r^2}\right)\sin 4\theta$$
$$+\left(\frac{K_3}{r^5} + \frac{K_4}{r^3}\right)\cos 5\theta + \left(\frac{M_3}{r^5} + \frac{M_4}{r^3}\right)\sin 5\theta$$
$$+\left(\frac{N_3}{r^6} + \frac{N_4}{r^4}\right)\cos 6\theta$$

The total stress function $\varphi(r,\theta) + \varphi'(r,\theta)$, hereinafter called $\varphi_T(r,\theta)$ is

$$\varphi_T(r,\theta) = A_0 \ln r + A_1 r^2 + \left(B_1 r^3 + \frac{B_2}{r}\right)\cos\theta + \left(C_1 r^3 + \frac{C_2}{r}\right)\sin\theta$$
$$+\left(D_1 r^2 + D_2 r^4 + \frac{D_3}{r^2} + D_4\right)\cos 2\theta + \left(E_1 r^2 + E_2 r^4 + \frac{E_3}{r^2} + E_4\right)\sin 2\theta$$
$$+\left(F_1 r^3 + F_2 r^5 + \frac{F_3}{r^3} + \frac{F_4}{r}\right)\cos 3\theta + \left(G_1 r^3 + G_2 r^5 + \frac{G_3}{r^3} + \frac{G_4}{r}\right)\sin 3\theta$$
$$+\left(H_1 r^4 + H_2 r^6 + \frac{H_3}{r^4} + \frac{H_4}{r^2}\right)\cos 4\theta + \left(J_1 r^4 + \frac{J_3}{r^4} + \frac{J_4}{r^2}\right)\sin 4\theta$$
$$+\left(K_1 r^5 + \frac{K_3}{r^5} + \frac{K_4}{r^3}\right)\cos 5\theta + \left(M_1 r^5 + \frac{M_3}{r^5} + \frac{M_4}{r^3}\right)\sin 5\theta$$
$$+\left(N_1 r^6 + \frac{N_3}{r^6} + \frac{N_4}{r^4}\right)\cos 6\theta$$

Addition of these perturbation terms destroys exact satisfaction of the boundary conditions along the straight edges, but if these perturbation stresses decay with r their magnitude along the straight boundaries is small.

The functions $\varphi_n(r, \theta)$ are of the general form

$$\varphi_n = \left(P_{n1} r^n + P_{n2} r^{n+2} + P_{n3} r^{-n} + P_{n4} r^{2-n}\right) \begin{matrix}\sin \\ \cos\end{matrix} n\theta.$$

In polar coordinates, $\tau_{r\theta} = -\frac{\partial}{\partial r}\left(\frac{1}{r}\frac{\partial \varphi}{\partial \theta}\right)$.

$$-\frac{\partial}{\partial r}\left(\frac{1}{r}\frac{\partial \varphi}{\partial \theta}\right) = \pm n\left[(n-1)P_{n1} r^{n-2} + (n+1)P_{n2} r^n - (n+1)P_{n3} r^{-n-2} + (1-n)P_{n4} r^{-n}\right] \begin{pmatrix}\sin \\ \cos\end{pmatrix} n\theta$$

The requirement that $\tau_{r\theta}(R, \theta) = 0, 0 \le \theta \le \frac{\pi}{2}$, requires for both the sine and cosine functions that

$$(n-1)P_{n1} R^{n-2} + (n+1)P_{n2} R^n - (n+1)P_{n3} R^{-n-2} + (1-n)P_{n4} R^{-n} = 0.$$

Furthermore $\sigma_r = \frac{1}{r}\frac{\partial \varphi}{\partial r} + \frac{1}{r^2}\frac{\partial^2 \varphi}{\partial \theta^2}$. For the sine functions and the cosine functions,

$$\sigma_{rn} = \left[n(1-n)P_{n1} r^{n-2} + (n+2-n^2)P_{n2} r^n - n(n+1)P_{n3} r^{-n-2} + (2-n-n^2)P_{n4} r^{-n}\right] \begin{matrix}\sin \\ \cos\end{matrix} n\theta.$$

To satisfy the condition that $\sigma_r(R, \theta) = 0$, $0 \le \theta \le \frac{\pi}{2}$,

$$n(1-n)P_{n1} R^{n-2} + (n+2-n^2)P_{n2} R^n - n(n+1)P_{n3} R^{-n-2} + (2-n-n^2)P_{n4} R^{-n} = 0$$

From the preceding equations, P_{n3} and P_{n4} can be determined in terms of P_{n1} and P_{n2}. Multiplying the first by and subtracting from the second, we obtain

$$P_{n4} = -n P_1 R^{2n-2} - (1-n) P_2 R^{2n}$$

Substituting this value into the first equation we have

$$P_{n3} = (n-1) P_1 R^{2n} + n P_2 R^{2n+2}$$

and therefore φ_n, $n \geq 2$, can be determined to satisfy the fillet boundary conditions:

$$\varphi_n(r,\theta) = P_{n1}\left[r^n + (n-1)\frac{R^{2n}}{r^n} - n\frac{R^{2n-2}}{r^{n-2}} \right] \begin{matrix} \sin \\ \cos \end{matrix} n\theta$$

$$+ P_{n2}\left[r^{n+2} + n\frac{R^{n+2}}{r^n} - (1-n)\frac{R^{2n}}{r^{n-2}} \right] \begin{matrix} \sin \\ \cos \end{matrix} n\theta$$

For $n = 0, 1$

$$\varphi_0(r,\theta) = P_{01}(r^2 - 2R^2 \ln r)$$

$$\varphi_1(r,\theta) = P_{11}\left(r^3 + \frac{R^4}{r}\right) \begin{matrix} \sin \\ \cos \end{matrix} \theta$$

The total stress function is, therefore:

$$\varphi_T(r,\theta) = A_1(r^2 - 2R^2 \ln r) + B_1\left(r^3 + \frac{R^4}{r}\right)\cos\theta + C_1\left(r^3 + \frac{R^4}{r}\right)\sin\theta$$

$$+ D_1\left(r^2 + \frac{R^4}{r^2} - 2R^2\right)\cos 2\theta + D_2\left(r^4 + 2\frac{R^6}{r^2} - 3R^4\right)\cos 2\theta$$

$$+ E_1\left(r^2 + \frac{R^4}{r^2} - 2R^2\right)\sin 2\theta + E_2\left(r^4 + 2\frac{R^6}{r^2} - 3R^4\right)\sin 2\theta$$

$$+ F_1\left(r^3 + 2\frac{R^6}{r^3} - 3\frac{R^4}{r}\right)\cos 3\theta + F_2\left(r^5 + 3\frac{R^8}{r^3} - 4\frac{R^6}{r}\right)\cos 3\theta$$

$$+ G_1\left(r^3 + 2\frac{R^6}{r^3} - 3\frac{R^4}{r}\right)\sin 3\theta + G_2\left(r^5 + 3\frac{R^8}{r^3} - 4\frac{R^6}{r}\right)\sin 3\theta$$

$$+ H_1\left(r^4 + 3\frac{R^8}{r^4} - 4\frac{R^6}{r^2}\right)\cos 4\theta + H_2\left(r^6 + 4\frac{R^{10}}{r^4} - 5\frac{R^8}{r^2}\right)\cos 4\theta$$

$$+ J_1\left(r^4 + 3\frac{R^8}{r^4} - 4\frac{R^6}{r^2}\right)\sin 4\theta + K_1\left(r^5 + 4\frac{R^{10}}{r^5} - 5\frac{R^8}{r^3}\right)\cos 5\theta$$

$$+ M_1\left(r^5 + 4\frac{R^{10}}{r^5} - 5\frac{R^8}{r^3}\right)\sin 5\theta + N_1\left(r^6 + 5\frac{R^{12}}{r^6} - 6\frac{R^{10}}{r^4}\right)\cos 6\theta$$

The constants A_1, B_1, ..., in terms of the constants a_1, b_1, c_1, ... become

$$A_1 = 0.5a_1 - 1.5c_1h^2 - 22.5f_1h^4 + 1.0d_3h^3$$

$$B_1 = 0.75b_1 + 1.5c_1h + 17.5f_1h^3 - 0.75d_3h^2$$

$$C_1 = 1.5c_1w + 7.5f_1h^2w + 10f_1w^3 - 15f_1wh^2$$

$$D_1 = 0.5a_1 + 1.5c_1h^2 + 22.5f_1h^4 - d_3h^3$$

$$D_2 = 0.5c_1 - 2.5f_1h^2$$

$$E_1 = -6c_1wh - 40f_1w^3h - 70f_1wh^3 + 3d_3wh^2$$

$$E_2 = -0.5d_3w + 10f_1wh$$

$$F_1 = 0.25b_1 - 1.5c_1h - 17.5f_1h^3 + 0.75d_3h^2$$

$$F_2 = 2.5f_1h - 0.125d_3$$

$$G_1 = 1.5c_1w + 12.5f_1wh^2 + 10f_1w^3$$

$$G_2 = 2.5f_1w$$

$$H_1 = 0.5c_1 + 2.5f_1h^2$$

$$H_2 = 0.5f_1$$

$$J_1 = -5.0f_1wh - 0.25d_3w$$

$$K_1 = -0.125f_1h - 0.120d_3$$

$$M_1 = 2.5f_1w$$

$$N_1 = 0.5f_1$$

From the stress function $\varphi_T(r,\theta)$, $\sigma_\theta = \frac{\partial^2 \varphi}{\partial r^2}$ may be derived.

$$\sigma_\theta(r,\theta) = 2A_1\left(1+\frac{R^2}{r^2}\right) + B_1\left(6r+2\frac{R^4}{r^3}\right)\cos\theta + C_1\left(6r+2\frac{R^4}{r^3}\right)\sin\theta$$

$$+ D_1\left(2+6\frac{R^4}{r^4}\right)\cos 2\theta + D_2\left(12r^2+12\frac{R^6}{r^4}\right)\cos 2\theta$$

$$+ E_1\left(2+6\frac{R^4}{r^4}\right)\sin 2\theta + E_2\left(12r^2+12\frac{R^6}{r^4}\right)\sin 2\theta$$

$$+ F_1\left(6r+24\frac{R^6}{r^5}-6\frac{R^4}{r^3}\right)\cos 3\theta + F_2\left(20r^3+36\frac{R^8}{r^5}-8\frac{R^6}{r^3}\right)\cos 3\theta$$

$$+ G_1\left(6r+24\frac{R^6}{r^5}-6\frac{R^4}{r^3}\right)\sin 3\theta + G_2\left(20r^3+36\frac{R^8}{r^5}-8\frac{R^6}{r^3}\right)\sin 3\theta$$

$$+ H_1\left(12r^2+60\frac{R^8}{r^6}-24\frac{R^6}{r^4}\right)\cos 4\theta + H_2\left(30r^4+80\frac{R^{10}}{r^6}-30\frac{R^8}{r^4}\right)\cos 4\theta$$

$$+ J_1\left(12r^2+60\frac{R^8}{r^6}-24\frac{R^6}{r^4}\right)\sin 4\theta + K_1\left(20r^3+120\frac{R^{10}}{r^7}-60\frac{R^8}{r^5}\right)\cos 5\theta$$

$$+ M_1\left(20r^3+120\frac{R^{10}}{r^7}-60\frac{R^8}{r^4}\right)\sin 5\theta + N_1\left(30r^4+210\frac{R^{12}}{r^8}-120\frac{R^{10}}{r^6}\right)\cos 6\theta$$

The first boundary condition, the integral over the top surface may then be applied.

$$\int_R^w \sigma_\theta\left(r,\frac{\pi}{2}\right) dr = P$$

If terms of the order R^3/h^3 and R^4/h^4 are neglected because $R/h < 1$, $R^2/h^2 << 1$, then,

$$P = 2A_1 w\left(1-\frac{R^2}{w^2}\right) + C_1 w^2\left(3-\frac{R^2}{w^2}\right) - 2D_1 w - 4D_2 w^3$$

$$- 3G_1 w^2 - 5G_2 w^4 + 4H_1 w^3 + 6H_2 w^5 + 5M_1 w^4 - 6N_1 w^5$$

In terms of a_1, b_1, c_1, ...,

$$P = -a_1 W\left(\frac{R^2}{W^2}\right) - c_1 h^2 W\left(6 + 3\frac{R}{W} + 1.5\frac{R^2}{h^2}\right) - f_1 W h^4\left(90 + 45\frac{R^2}{W^2}\right)$$

$$- f_1 W^3 h^2\left(40 + 7.5\frac{R^2}{W^2}\right) + 10 f_1 W^5 \frac{R^2}{W^2} + d_3 W h^3\left(4 + 2\frac{R^2}{W^2}\right)$$

The moment equation is applied next.

$$QR_o - Pl = \int_R^h r\,\sigma_\theta(r, o)\,dr$$

$$QR_o - Pl = A_1 h^2\left[1 + \frac{R^2}{h^2}\left(2 \ln \frac{h}{R} - 1\right)\right] + 2B_1 h^3 + D_1 h^2\left(1 + 2\frac{R^2}{h^2}\right) + 3D_2 h^4$$

$$+ 2F_1 h^3 + 4F_2 h^5 + 3H_1 h^4 + 5H_2 h^6 + 4K_1 h^5 + 5N_1 h^6$$

and in terms of a_1, b_1, ...,

$$QR_o - Pl = a_1 h^2\left(1 + 2\frac{R^2}{h^2} \ln \frac{h}{R}\right) + c_1 h^4\left(3 - 3\frac{R^2}{h^2} \ln \frac{h}{R} + 4.5\frac{R^2}{h^2}\right)$$

$$f_1 h^6\left(14.5 - 45\frac{R^2}{h^2} \ln \frac{h}{R} + 67.5\frac{R^2}{h^2}\right) + d_3 h^5\left(-0.980 + 4\frac{R^2}{h^2} \ln \frac{h}{R} - 4\frac{R^2}{h^2}\right)$$

The integral of the forces normal to the sides of the base is Q.

$$Q = 2A_1 h\left(1 - R^2/h^2\right) + 3B_1 h^2 + 2D_1 h + 4D_2 h^3 + 3F_1 h^2 + 5F_2 h^4$$

$$+ 4H_1 h^3 + 6H_2 h^5 + 5K_1 h^4 + 6N_1 h^5$$

and in terms of a_1, ...,

$$Q = 2a_1 h\left(1 - \frac{R^2}{h^2}\right) + 3b_1 h^2 + c_1 h^3\left(4 - 3\frac{R^2}{h^2}\right) + f_1 h^5\left(17.875 - 45\frac{R^2}{h^2}\right)$$

$$+ d_3 h^4\left(-1.225 + 2\frac{R^2}{h^2}\right)$$

The boundary condition along the centerline

$$Q = \int_0^h \sigma_y (x, w)\, dx + \frac{1}{2} w\, \sigma_y (0, w)$$

may then be applied.

$$\int_0^h \sigma_y (x, w)\, dx = 2 a_1 h + 3 b_1 h^2 + c_1 h^3 \left(6 \frac{w^2}{h^2} + 4\right) + f_1 h^5 \left(16 + 70 \frac{w^2}{h^2} + 50 \frac{w^4}{h^4}\right) - d_3 h^4 \left(1 + 3 \frac{w^2}{h^2}\right)$$

$$\sigma_y (0, w) = 2 a_1 + 6 c_1 w^2 + 30 f_1 w^2 h^2 + 50 f_1 w^4$$

$$\frac{1}{2} w\, \sigma_y (0, w) = a_1 w + 3 c_1 w^3 + 15 f_1 w^3 h^2 + 25 f_1 w^5$$

$$\therefore \quad Q = a_1 h \left(2 + \frac{w}{h}\right) + 3 b_1 h^2 + c_1 h^3 \left(4 + 6 \frac{w^2}{h^2} + 3 \frac{w^3}{h^3}\right) + f_1 h^5 \left(16 + 70 \frac{w^2}{h^2} + 15 \frac{w^3}{h^3} + 50 \frac{w^4}{h^4} + 25 \frac{w^5}{h^5}\right) + d_3 h^4 \left(-1 - 3 \frac{w^2}{h^2}\right)$$

The final condition concerning the fillet stress is manifest in several forms.

$$\sigma_\theta (R, 0) = 4 A_1 + 8 B_1 R + 8 D_1 + 24 D_2 R^2 + 24 F_1 R + 48 F_2 R^3 + 48 H_1 R^2 + 80 H_2 R^4 + 80 K_1 R^3 + 120 N_1 R^4$$

In terms of a_1, b_1, ...,

$$\sigma_\theta(R,\theta) = 6a_1 + 12b_1R + c_1h^2\left(6 - 24\frac{R}{h} + 36\frac{R^2}{h^2}\right)$$

$$+ f_1h^4\left(90 - 280\frac{R}{h} + 60\frac{R^2}{h^2} + 110\frac{R^3}{h^3} + 100\frac{R^4}{h^4}\right)$$

$$+ d_3h^3\left(-4 + 12\frac{R}{h} - 15.6\frac{R^3}{h^3}\right)$$

When the loading shoulder is small, then $\sigma_\theta(R,\theta_o) \approx \sigma_Y(R,-e) - \sigma_Q$ where $\theta_o = \tan^{-1}\frac{e}{R}$ for the case of the point load but in the case of the distributed load it is assumed that $\sigma_\theta(R,\theta_o) = -\frac{p}{e}\sin^2\theta_o + \sigma_Q\cos^2\theta_o$.

$$\sigma_\theta(R,\theta_o) = \sigma_\theta(R, h, w, a_1, b_1, c_1, f_1, d_3, \theta_o)$$

and for each specific case must be calculated from the equation on page 47.

In summary, the equations governing the fillet stress are

$$\sigma_\theta(R,\theta_o) = \sigma_Q\cos^2\theta_o - \frac{p}{e}\sin^2\theta_o, \qquad \ell/h \ll 1$$

$$\frac{p}{w} = -a_1\left(\frac{R^2}{h^2}\right) - c_1h^2\left(6 + 3\frac{R^2}{w^2} + 1.5\frac{R^2}{h^2}\right) - f_1h^4\left(90 + 45\frac{R^2}{w^2}\right)$$

$$- f_1w^2h^2\left(40 + 7.5\frac{R^2}{w^2}\right) + 10f_1w^4\frac{R^2}{w^2} + d_3h^3\left(4 + 2\frac{R^2}{w^2}\right)$$

$$\frac{Q}{h} = 2a_1\left(1 - \frac{R^2}{h^2}\right) + 3b_1h + c_1h^2\left(4 - 3\frac{R^2}{h^2}\right) + f_1h^4\left(17.875 - 45\frac{R^2}{h^2}\right)$$

$$+ d_3h^3\left(-1.225 + 2\frac{R^2}{h^2}\right)$$

$$\frac{QR_o}{h^2} - \frac{Pl}{h^2} = a_1\left(1 + 2\frac{R^2}{h^2}\ln\frac{h}{R}\right) + c_1 h^2\left(3 - 3\frac{R^2}{h^2}\ln\frac{h}{R} + 4.5\frac{R^2}{W^2}\right)$$

$$+ f_1 h^4\left(14.5 - 45\frac{R^2}{h^2}\ln\frac{h}{R} + 67.5\frac{R^2}{h^2}\right)$$

$$+ d_3 h^3\left(-0.980 + 4\frac{R^2}{h^2}\ln\frac{h}{R} - 4\frac{R^2}{h^2}\right)$$

$$\frac{Q}{h} = a_1\left(2 + \frac{W}{h}\right) + 3b_1 h + c_1 h^2\left(4 + 6\frac{W^2}{h^2} + 3\frac{W^3}{h^3}\right)$$

$$+ f_1 h^4\left(16 + 70\frac{W^2}{h^2} + 15\frac{W^3}{h^3} + 50\frac{W^4}{h^4} + 25\frac{W^5}{h^5}\right)$$

$$+ d_3 h^3\left(-1 - 3\frac{W^2}{h^2}\right)$$

These equations constitute an array of simultaneous linear algebraic equations which may be represented in matrix form:

$$\left[\ C_{ij}\ \right]\left[\ x_i\ \right] = \left[\ P_j\ \right]$$

The solution is

$$\left[\ x_i\ \right] = \left[\ C_{ij}^{-1}\ \right]\left[\ P_j\ \right]$$

The maximum fillet stress may then be determined and the stress concentration factor determined.

$$K = \frac{\sigma_{\text{fillet max.}}}{\dfrac{P}{W-R}}$$

IV. COMPARISON BETWEEN THEORY AND EXPERIMENT

In order to compare these theoretical calculations with experiment, a sample case is chosen. It is assumed that $w = h$. In order to simplify the algebra, the following substitutions are made: $u = b_1 h$ $x = c_1 h^2$, $y = f_1 h^4$ and $z = d_3 h^3$. Under these circumstances, and for $Q = 0$ the equations reduce to:

$$-a_1 \frac{R^2}{h^2} - x\left(6 + 4.5\frac{R^2}{h^2}\right) - y\left(130 + 42.5\frac{R^2}{h^2}\right) + z\left(4 + 2\frac{R^2}{h^2}\right) = \frac{P}{h}$$

$$3a_1 + 3u + 13x + 176y - 4z = 0$$

$$2\left(1 - \frac{R^2}{h^2}\right)a_1 + 3u + \left(4 - 3\frac{R^2}{h^2}\right)x + y\left(17.875 - 45\frac{R^2}{h^2}\right) + z\left(-1.225 + 2\frac{R^2}{h^2}\right) = 0$$

$$\left(1 + 2\frac{R^2}{h^2}\ln\frac{h}{R}\right)a_1 + 2u + x\left(3 - 3\frac{R^2}{h^2}\ln\frac{h}{R} + 4.5\frac{R^2}{h^2}\right)$$

$$+ \left(14.5 - 45\frac{R^2}{h^2}\ln\frac{h}{R} + 67.5\frac{R^2}{h^2}\right)y + z\left(-0.98 + 4\frac{R^2}{h^2}\ln\frac{h}{R} - 4\frac{R^2}{h^2}\right) = -\frac{P\ell}{h^2}$$

$\sigma_\theta(R, \theta_0) = -\frac{P}{e}\sin^2\theta$, for distributed load

$= 0$, for point load

Calculations were made at various R/h values for both distributed and point loads. The distributed conditions were that $\ell = e/2$ and $\sigma_\theta(R, \theta_0) = 0$, $\theta_0 = \tan^{-1}\frac{e}{R}$. The point loads were characterized by the condition $\sigma_\theta(R, \theta_0) = 0$. The distributed load calculations are shown in Figure 28.

Another computation for R/h = 0.33 corresponding to R/b = 0.25 and c/b = 0.5 was made for varying ℓ/h ratios with point load reactions. The results are shown in Figure 29.

One recessed fillet problem was also calculated. Using the boundary condition $\sigma_\theta\left(R, -\frac{\pi}{2}\right) = 0$ for a point load on the center of the shoulder and for R/b = 0.25, c/b = 0.5, f/b = 0.75, e/h = 0.09, ℓ/b = 0.29 a stress concentration factor of 10.3 was calculated. Experiments indicated a factor of 8. Agreement of this sort is remarkable considering that no attempt has been made to satisfy boundary conditions on the outboard side of the loading shoulder.

V. CRITIQUE

For small values of R/b, the theory and experiment differ by substantial amounts. Examination of the simplified theory shows its main weaknesses: namely the non-satisfaction of boundary conditions along the straight edges if the perturbation stresses do not die rapidly with r, the assumptions regarding x_o to approximate the integral of the normal forces along the centerline, the choice of $\sigma_\theta(R,\theta_o) \approx \sigma_y(R,-e)$ and the lack of higher order terms.

Lack of higher order terms reduces the number of conditions which may be imposed on the face, y = 0, and limits the shear gradient $\frac{\partial \tau_{r\theta}}{\partial r}\Big|_{\substack{r=R \\ \theta=0}}$ at the fillet tangency point. Were one higher order term added no additional conditions could be imposed on the problem, but if two higher order terms were added, then the condition $\sigma_y(h,-e) = 0$ could be added together with an integral condition on one of the straight boundaries to minimize any non-satisfaction of boundary conditions due to the perturbation stresses. This condition with the summation $\int_R^h \sigma_\theta(r,0)\,dr = Q$ and moment summation $\int_R^h r\,\sigma_\theta(r,0)\,dr = -Pl + QR_o$ would restrict the distribution along the face y = 0 to a much greater extent than it is now restricted. A better approximation to the shear gradient at the fillet tangency would also result. Unfortunately much additional algebra would also result because at least two higher order terms would have to be added to permit introduction of the condition $\sigma_y(h,-e) = 0$

The integration along the centerline is only an approximation. For small R/b calculations show $\sigma_x(0,w) > 0.7\,\frac{P}{w-R}$ the approximate experimentally observed value and therefore the stress

$\sigma_\theta\left(R, \frac{\pi}{2}\right)$ is less than it should be since $\int_R^w \sigma_\theta\left(r, \frac{\pi}{2}\right) dr = P$.

An alternative formulation of this requirement has been suggested. Instead of an integral of the normal forces over the centerline, the deflection in the y direction, $v(x, w) = 0$. This condition can not be applied because with stresses having terms up to and including the fourth order, the deflection would have terms up and including the fifth order. Were this condition applied six constants including the constant from integration of the strain field would be required. No other conditions could then be imposed on the problem.

From each polynomial which satisfies $\nabla^4 \varphi = 0$, a maximum of four arbitrary constants is supplied. If the final polynomial chosen is of order N, where $N \geq 2$, the number of arbitrary constants supplied is 4N-5. For each application of a straight edge stress boundary condition, N-1 conditions are imposed and for a straight edge displacement boundary condition N requirements are imposed. Whenever N is even, however, one condition for the centerline shear to vanish is the same as one condition for the base shear to vanish. If three straight edges are subjected to "exact" boundary conditions then for N even 3(N-1) -1 constants are required or for N odd 3 (N-1) constants are required. In the case N = 6, 19 arbitrary constants are supplied but application of three exact boundary conditions uses 14 of these leaving five for approximate conditions.

Were a displacement condition required along the centerline, then a total of 4(N-1) + 5 = 4N + 1 constants would be required if N is even and 4N constants if N is odd. Since the total constants supplied

by a function whose highest order is N is 4N-5, it is impossible for the supply, 4N-5, to equal the demand 4N + 1 if N is even (or 4N if N is odd) because there is no real integer value for N which satisfies the requirement 4N + 1 = 4N - 5 (or 4N = 4N - 5). It is therefore seen that it is impossible to apply an exact displacement condition on the centerline unless one of the other exact conditions is omitted. Relaxing one of the exact conditions along the base to apply the displacement boundary condition shows no promise for increasing the accuracy for K.

If only one additional condition over the present analysis is required then 3(N - 1) - 1 + 6 = 4N - 5 for N even or 3(N - 1) + 6 = 4N - 5 for N odd, so N must equal at least 8.

Another reason for disagreement between theory and experiment is now satisfaction of equilibrium since the boundary conditions on the straight edges were applied before the perturbation stresses were added to the solution. The perturbation stresses do not completely vanish on the straight boundaries. This discrepancy is greatest for large R/b or R/h.

$\int_R^h \sigma_\theta \left(r, \frac{\pi}{2}\right) dr = P$ for $w = h$ yielded the equation

$$\frac{P}{h} = -a_1 \frac{R^2}{h^2} - x\left(6 + 4.5\frac{R^2}{h^2}\right) - y\left(130 + 42.5\frac{R^2}{h^2}\right) + z\left(4 + 2\frac{R^2}{h^2}\right)$$

By equilibrium considerations

$$\int_R^h \tau_{r\theta}(r, 0)\, dr = P$$

This equation yields the result

$$\frac{P}{h} = x\left(-6 + 21\frac{R^2}{h^2}\right) + y\left(-130 + 435\frac{R^2}{h^2}\right) + z\left(4 - 12\frac{R^2}{h^2}\right)$$

These equations are identical only in the first order $\left(\frac{R^2}{h^2} \approx 0\right)$, but large R/h terms yield values for P/h which differ by as much as ten percent. For this reason, experimental and theoretical agreement is not expected for large R/h.

An investigation of the point load condition shows that when ℓ/h = 0 (P applied at the fillet tangency point) the choice of θ_0 makes a significant effect on K (about 15 percent). (Figure 29.) When $\ell/h > 0.03$ however and $e > \ell$ of course, the effect on K of a change in e is small. The calculations for point loads are therefore uncertain by about this amount.

If the theory sheds any light on the experiments, the experimental values must be high for small R/b. One systematic error which has not been removed from the experimental results is the error due to creep which at c/b = 0.5 should not exceed 5 percent. In the region where R/b is small the finite width of the edge may have introduced a systematic or personal calibration error but certainly of no large percentage. Errors of this sort would make the theory and experiment more reconcilable.

VI. FURTHER APPLICATIONS

Thermal Stresses

If the member is in a temperature field, additional body force terms may be added to the present solution and the stress function modified accordingly. If the temperature gradients and boundary temperature are known, the effect of these gradients on the stresses in the fillet may be studied.

Three Dimensional Axially Symmetric Application

Results of this two dimensional analysis indicate that, if an eighth order polynomial is chosen, the axially symmetric distribution solution may be obtained in an analogous fashion complicated only by the additional hoop stresses. These stresses arise due to the radial displacements and therefore a crude estimation of them should be possible. If the hoop stresses can be estimated, then they can be treated as body forces and the axially symmetric solution obtained.

REFERENCES

1. F. T. Morrison and R. G. Sturm, "The World's Largest Forming Press", Mechanical Engineering, March 1953, p. 191.

2. H. D. McGinness, "Static Tests of Curtiss-Wright Fan Blade in Retention Assembly", C.W.T. Report K-76, September 1, 1950.

3. H. D. McGinness, "An Experimental Study of the Stress Distribution in Two Dimensional Fan Blade Specimens Under Static Load", C.W.T. Report K-81, December 14, 1949.

4. H. D. McGinness, "An Experimental Study of the Stress Distribution in Three Dimensional Fan Blade Specimens Under Static Load", C.W.T. Report K-82, December 14, 1949.

5. H. D. McGinness, "An Experimental Study of the Stress Distribution in C.W.T. Fan Blade No. 2 Test Specimen Under Static Load", C.W.T. Report K-88, November 24, 1950.

6. H. D. McGinness, "An Experimental Study of the Stress Distribution in Curtiss-Wright Fan Blades Under Operating Conditions", C.W.T. Report T-38, October 1950.

7. Unofficial Summary of Two and Three Dimensional Propeller Hub Tests. N.A.C.A., Moffett Field, June 1949.

8. "New Fan for Farnborough", Flight, April 20, 1950, p. 485.

9. M. M. Frocht, "Photoelasticity", Vol. I, John Wiley & Sons, Inc., New York, 1941.

10. GALCIT, "Report on a Photoelastic Conference at the California Institute of Technology", February 17, 1953.

11. S. Timoshenko, "Theory of Elasticity", McGraw-Hill Book Company, Inc., New York, 1934.

12. R. E. Matzdorff, GALCIT Thesis "Castable Plastics in Photoelastic Stress Analysis", June 1949.

13. Eastman Kodak Company, Industrial Photographic Division, Rochester 4, New York, "Sensitized Materials for the Scientific and Industrial Laboratory", Bulletin F1-39, July 1951.

14. Rohm & Haas Co., Resinous Products Division, Washington Square, Philadelphia, Pa., "The Paraplex 'P' Series Resins", Bulletin M-7-50.

15. Cast Optics Corporation, Riverside, Conn., "Optically Clear Rigid Plastic Sheets", Brochure.

16. Cast Optics Corporation, Riverside, Conn., "CR-39 Transparent Plastic Sheet", Brochure.

17. H. Neuber, "Kerbspannungslehre", Julius Springer, Berlin, 1937, p. 160

18. Raymond J. Roark, "Formulas for Stress and Strain", McGraw-Hill Book Company, Inc., New York, 1943, p. 334.

19. H. Kober, "Conformal Representations", Dover Publications, Inc., 1952.

APPENDIX I.

The materials from which the models were made are thermo-setting resins. CR-39 can be purchased in plates of thicknesses less than one inch, but P-43 must be cast in the laboratory. Neither of these materials is entirely new; they have been used commercially for several years, but their application to photoelasticity is relatively unexploited. Since their photoelastic properties are very good compared to conventional materials and since they can be cast or purchased having surfaces comparable to polished plate glass, their use greatly reduces model preparation time, one of the deterrents to frequent use of photoelastic investigations.

These materials machine readily but develop thermal stresses along the machined edges unless care is taken to prevent chatter or vibration between the tool and edge. There is, as for the conventional materials, a preferred direction of cut called the "inward" cut. The tool rotary speed must be either very high or low to minimize these edge stresses, but the finish cuts may be as deep as 0.020 inches compared to a finish cut of 0.005 inches for Bakelite (page 351, Reference 9). Models which are as satisfactory as those made from the conventional materials can therefore be prepared in a matter of hours. Compare this procedure with that needed for Bakelite models! (Section 10.16, page 349, and Section 10.21, page 360, Reference 9).

These materials are less susceptible to time-edge-stresses than

are Bakelite and Catalin. CR-39 may be annealed from time to time to remove these and other residual stress effects; annealing, however, has little effect on Bakelite and P-43 stresses.

The main disadvantages of the thermosetting plastics are, in general, their low fringe values and poor creep characteristics. The fringe value for the 5460A radiation was measured by a simple tension test. (Figure 30.) Various tensile specimens were placed in universal joints and subjected to a pure tensile load through these joints. Load was applied until a given fringe order appeared; then small load increments were added or substracted until maximum darkness or brightness occurred. The load was measured and plotted against the fringe number; the specimen was then loaded to the next fringe order and the process repeated. The fringe value in psi shear* per fringe per unit thickness was obtained from the slope of this curve:

$$f = \frac{2}{b} \frac{\Delta W}{\Delta n}$$

Several tests were conducted with P-43 and CR-39 and the initial fringe values were plotted against room temperature. (Figure 31.) In the case of P-43, there was a slight downward trend of the fringe value with temperature, but for CR-39 the data was not spread over a large enough temperature range to determine a trend. The fringe

---

* The stress optic law is $\frac{p-q}{2} = \frac{nf}{t}$. f is here defined in <u>psi shear</u> because $\frac{p-q}{2} = \tau$ max. f is differentiated from f_1 in <u>psi</u> which is defined by the equation $p - q = \frac{nf_1}{t}$. $f_1 = 2f$.

value for P-43 at room temperature is 82.0 psi shear per inch thickness per fringe for = 5460A; for CR-39 the fringe value is 44.5. The maximum error is about 1 per cent for CR-39, less than 2 per cent for P-43. The larger error in fringe value for P-43 is due to the fact that specimens were cut from different castings which in turn had been annealed in slightly different ways. The fringe value for Bakelite 61-893 is 43.0 (page 348, Reference 9).

The creep characteristics are worse for these materials than for Bakelite. Several experiments were conducted to verify this fact and the results are shown in Figures 32, 33, 34 and 35.

In the first experiment, each of several tensile specimens was loaded until four fringes appeared. The load was left on but adjusted every half hour to bring the fringe order back to four. This approach was used because the laboratory was not in possession of a compensator which would have permitted accurate determination of fractional fringe orders. It was assumed that reduction of load to maintain a given fringe order was comparable to measurements of a fractional fringe order arising under a constant load. The loads were plotted against time as percentages of the initial fourth fringe load (Figure 32). The required loads decreased with time.

The results of this experiment pointed out two different concepts of fringe value: the first was the concept used to determine the material fringe value - that $f = \frac{2}{b} \frac{\Delta W}{\Delta n}$; the second, that $f' = \frac{2}{b} \frac{W_{final}}{n_{final}}$. Within the accuracy of the load measurements in the initial fringe value

number. The percent change in f' at 8 or 9 fringe orders should therefore be somewhat less than the change in f' at 3 or 4 fringe orders where the creep tests were conducted. Further evidence to support this contention is the fact that the change in the load to produce the first fringe was near 50 per cent in two hours but due to the fact that these loads were small and could not be measured to less than $\pm$ 5 per cent, that evidence is judiciously omitted here.

The creep phenomenon was significant to the model studies because tests were conducted consecutively on the same basic model. The initial load application lasted only ten minutes but results of the creep tests nevertheless indicated that the fringe orders at the fillets would change by small amounts even in this short time. After a photograph of a loaded model had been taken, the model base height, C , was cut down. This operation took about three-quarters of an hour. The model was then reloaded and photographed for the fringe order corresponding to the new configuration. About five configurations were cut from each basic model. In view of the short loaded time and the relatively long unloaded time it was assumed that the residual stresses from loading would have ample time to disappear and that the fringe value would not vary from test to test. If the total loaded time was the important factor then this assumption was incorrect and creep played an important role.

To decide which, if either, of these contentions was correct another experiment was designed and conducted. The fringe values,

of several tensile models were measured but the fourth fringe load was left on for about one-half hour. The load was then removed and the fringe value determined as previously; this procedure was repeated four times. With regard to the ratio of loaded time to unloaded time this test was much more severe than an actual model loading cycle.

The results showed that the final fringe value f' decreased with time (Figure 33) but also that the fringe values f, excluding the zero point, increased slightly with time (Figure 35). This corroborated the findings of the uninterrupted creep studies and in view of the fact that the unloaded time was small compared to the loaded time this should have been anticipated.

To further clarify the situation, another experiment was conducted which closely simulated actual test conditions. A model of average R/b and c/b ratios was loaded for ten minutes, photographed and then unloaded for about 50 minutes. This cycle was repeated four times and the fringe orders in the fillets compared.

The results (Figure 34) indicated that the fringe order near seven fringes increased about two per cent in four tests. The resultant final fringe value, f', near seven fringes may therefore be interpreted as decreasing about two per cent. In the same loaded time at the four fringe level, the decrease in f' was about eight per cent (Figure 33). It appears therefore that total loaded time is not a significant parameter in the model studies but that relaxation time and the effects of

stress and fringe order on the percentage decay of fringe value are important. More tests with more precise load and fringe measuring equipment would have to be made to ascertain the roles that each of these effects plays in the creep picture; further research in this direction is recommended.

In another test, tensile models of CR-39 from which fringe value had been determined were heat treated after testing and allowed to cool for a day. It was seen that after the second annealing the fringe value decreased substantially but that if the specimen was permitted to "rest" for about two weeks, the original fringe value was recovered.

Both P-43 and CR-39 are brittle fracture materials and are very notch sensitive.

Many other casting and high temperature tests were conducted with P-43 to determine its suitability to the frozen stress techniques of three dimensional photoelasticity but these tests will not be reported here since they have little bearing on the two dimensional study.

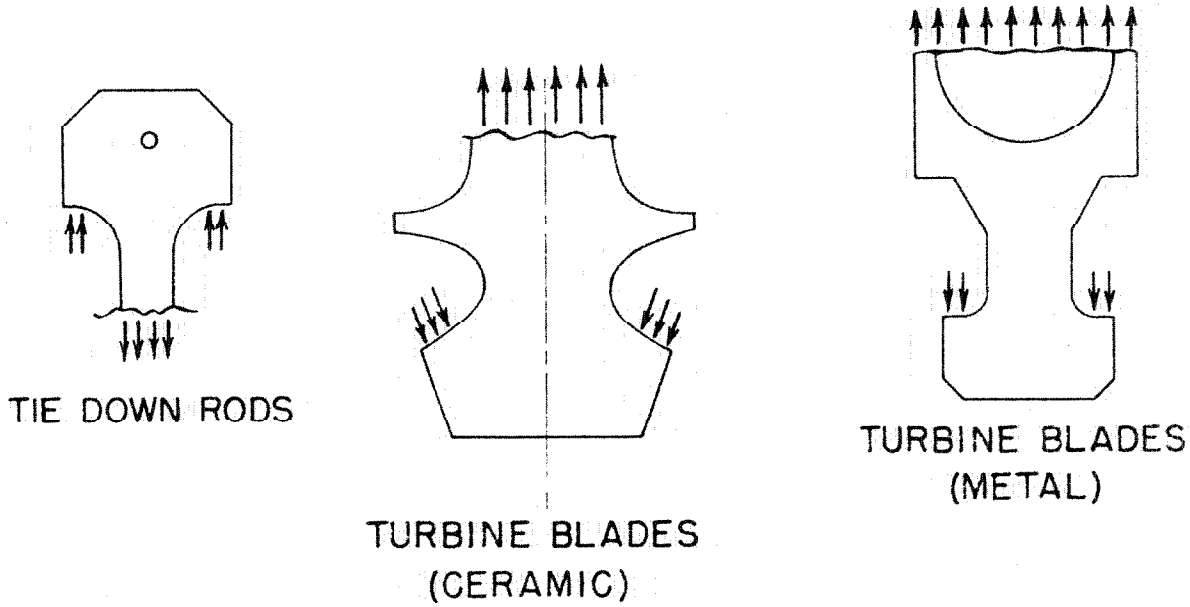

TWO DIMENSIONAL APPLICATIONS

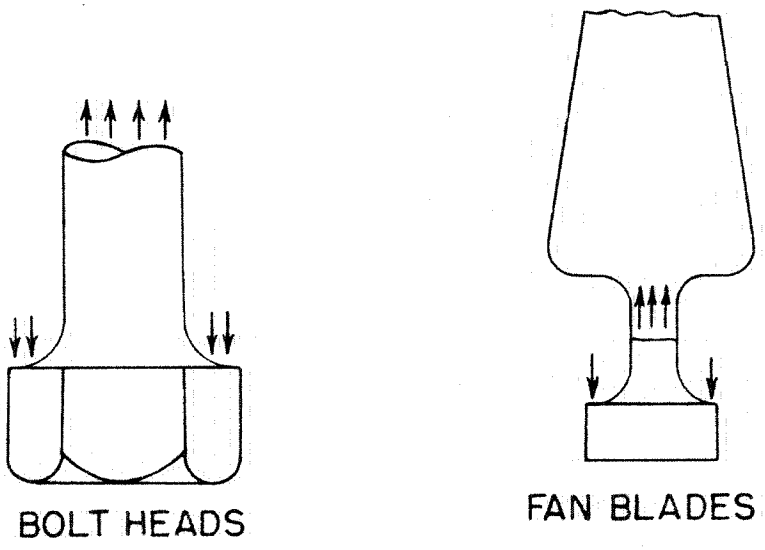

THREE DIMENSIONAL APPLICATIONS

FIGURE 1

FILLET STRESS CONCENTRATIONS
FROM STATIC OR CENTRIFUGAL LOADING

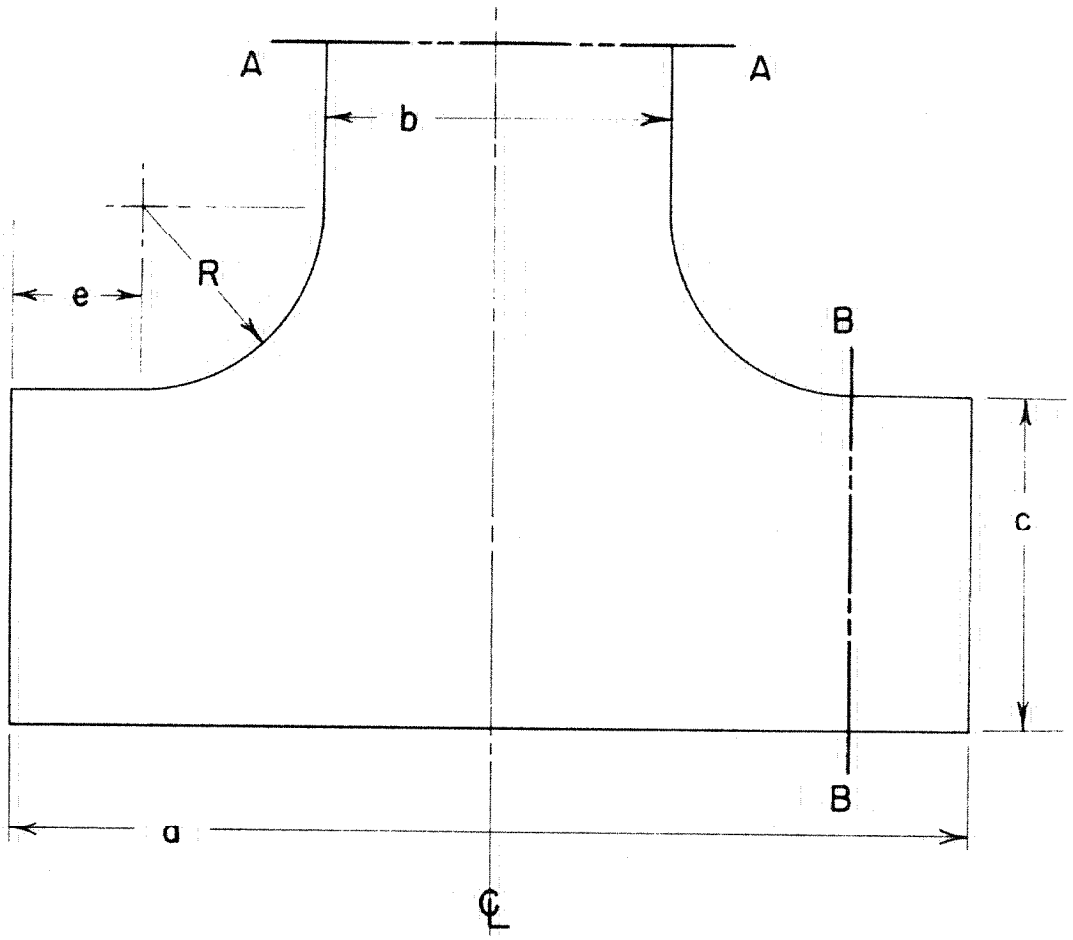

FIGURE 2

BASIC CONTOUR AND NOMENCLATURE

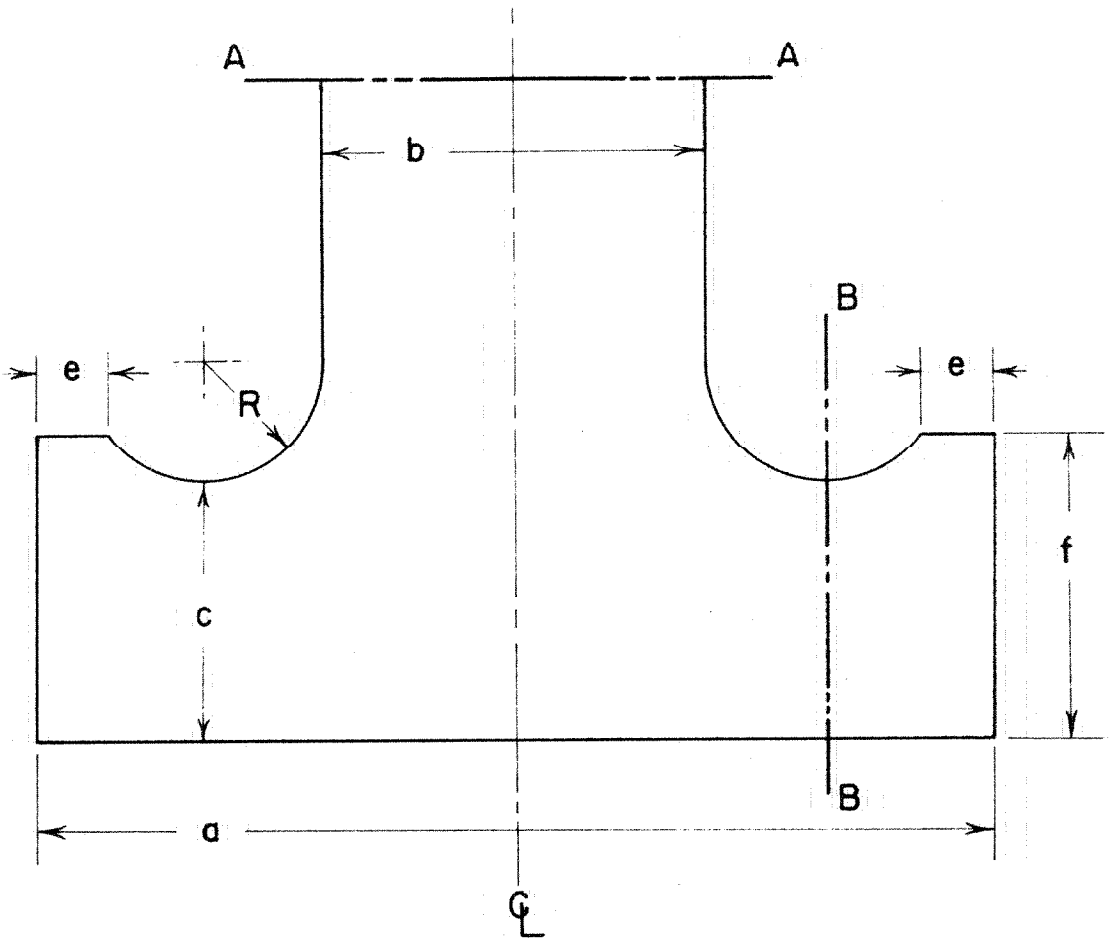

FIGURE 3

CONTOUR WITH RECESSED FILLETS

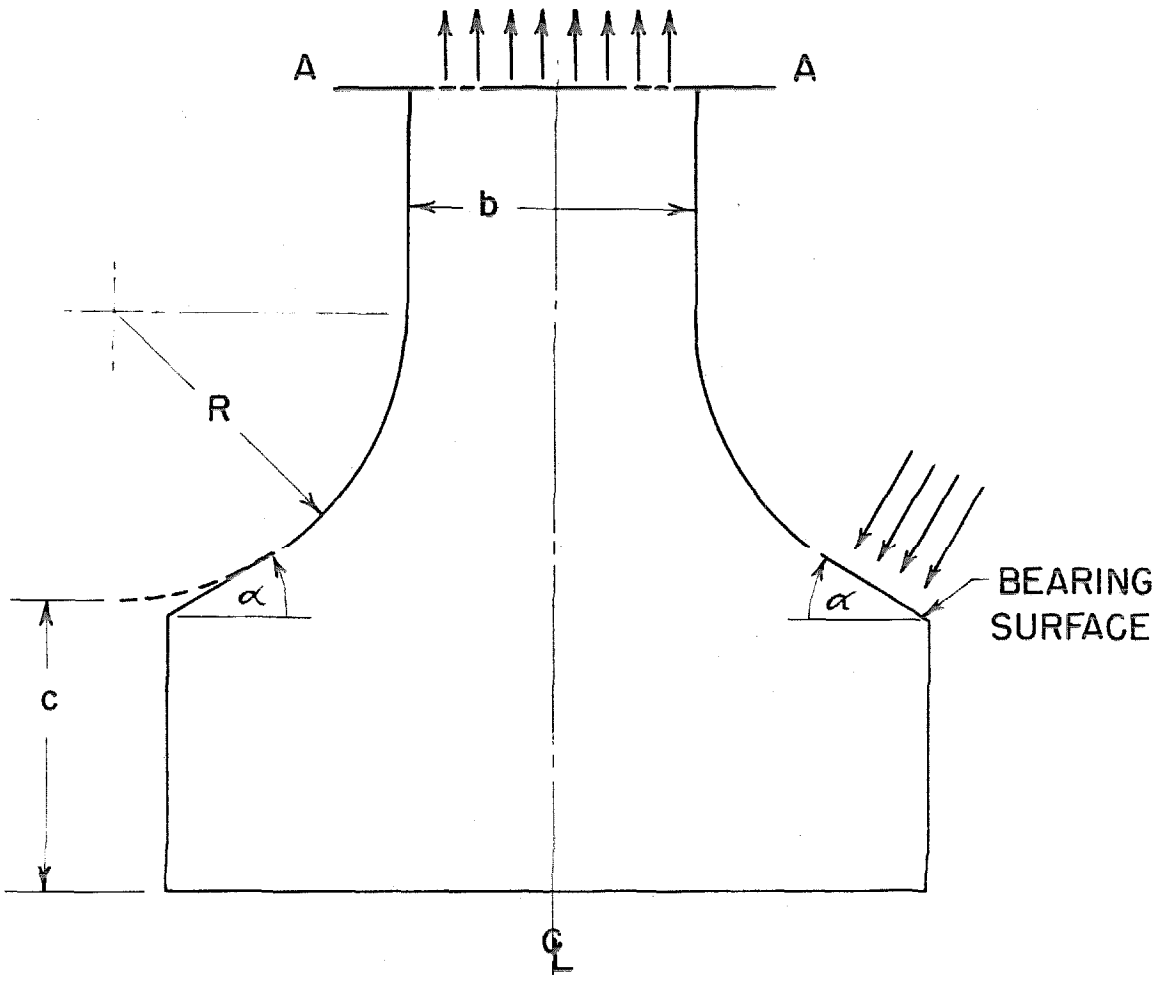

FIGURE 4

CONTOUR WITH INCLINED BEARING SURFACES

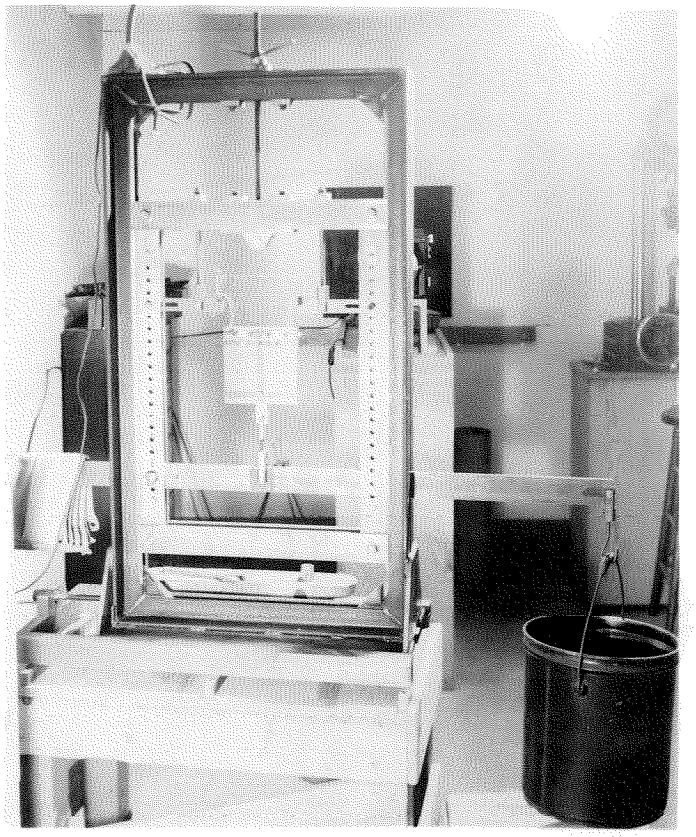

FIGURE 5

LOADING FRAME WITH TYPICAL TWO DIMENSIONAL PROPELLER-BUTT MODEL

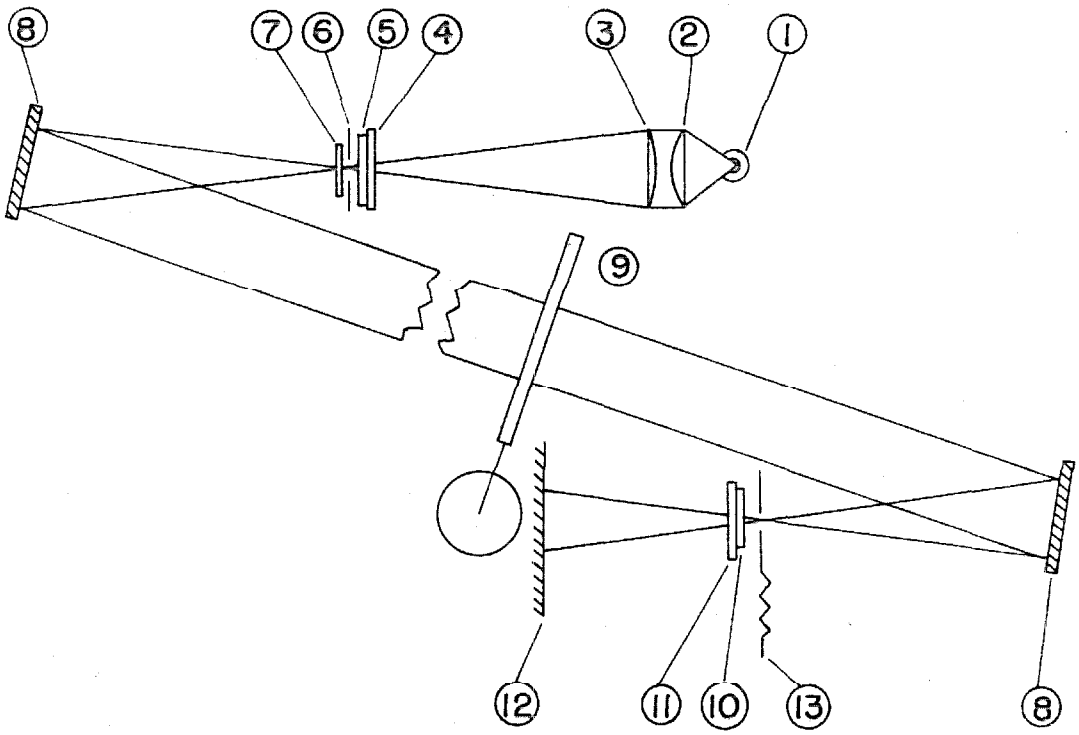

FIGURE 6

SCHEMATIC OF PHOTOELASTICITY LABORATORY

1	Mercury Vapor Lamp, G.E. AH-4, 100 watts		
2	Plano-convex Condensing Lens, 4.5" dia., f/1		
3	Plano-convex Condensing Lens, 4.5" dia., f/4.5		
4	Polarizer	5	Quarter Wave Plate
6	Stop, 3/16" dia.; at focal point of mirror		
7	Wratten 77A Filter		
8	Spherical Mirrors, 8" dia., f/4.9		
9	Loading Frame		
10	Quarter Wave Plate	11	Analyzer
12	Viewing Screen & Film Holder	13	Focal Plane Shutter

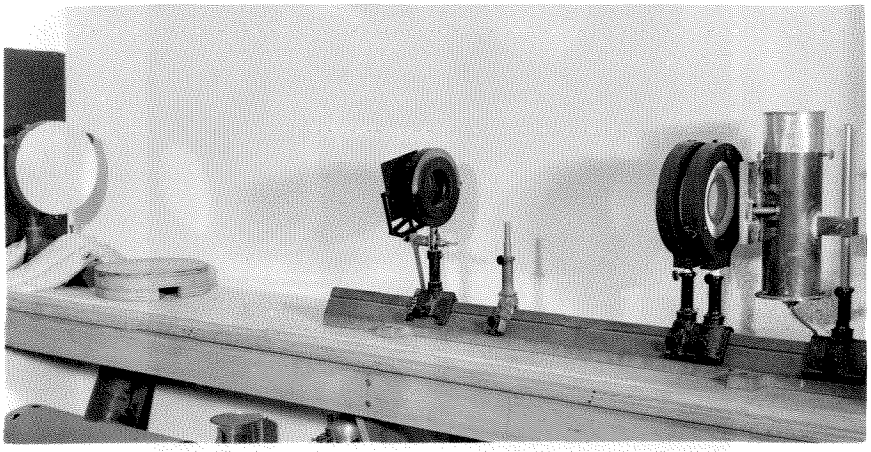

FIGURE 7

POLARISCOPE SHOWING LIGHT SOURCE, CONDENSING LENSES, POLARIZER, QUARTER WAVE PLATE, STOP TO WHICH FILTER IS ATTACHED, AND FIELD MIRROR

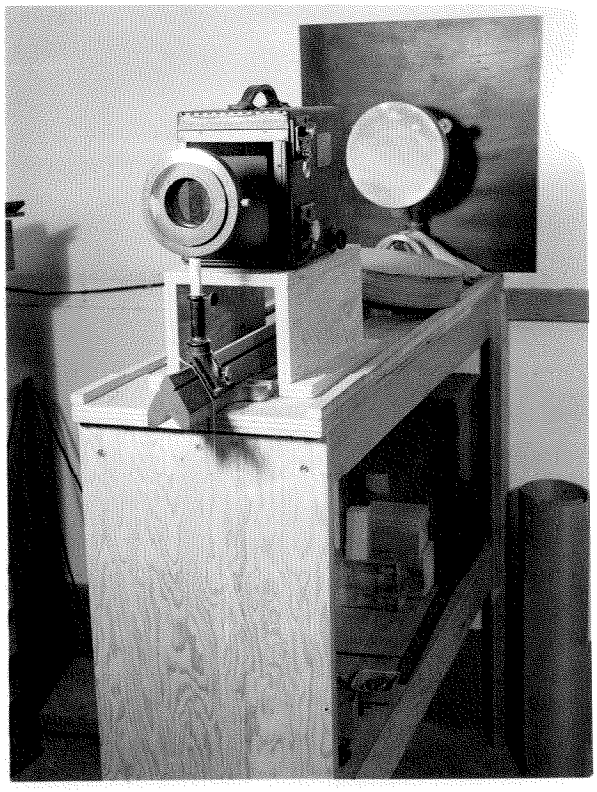

FIGURE 8

POLARISCOPE SHOWING MIRROR, FOCAL PLANE SHUTTER, QUARTER-WAVE PLATE, AND ANALYZER

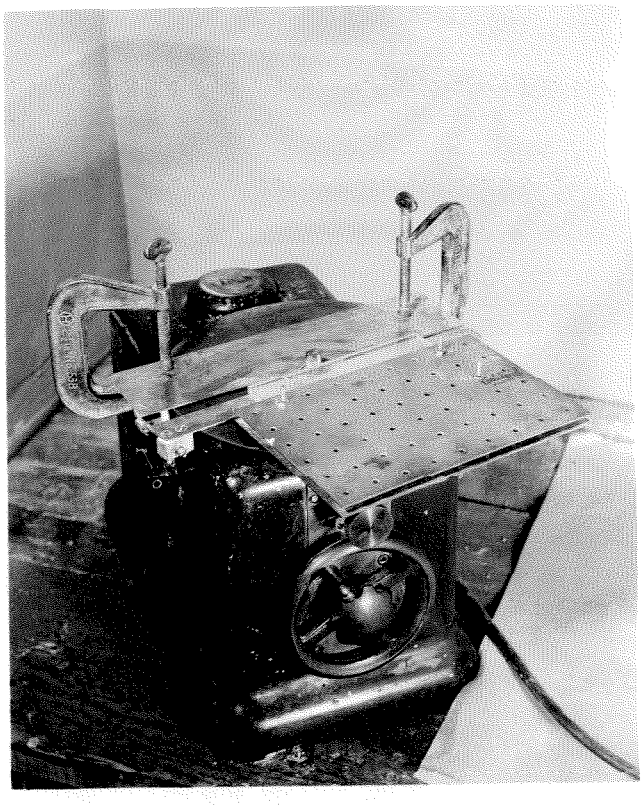

FIGURE 9

HAND ROUTER WITH JIG AND GUIDE

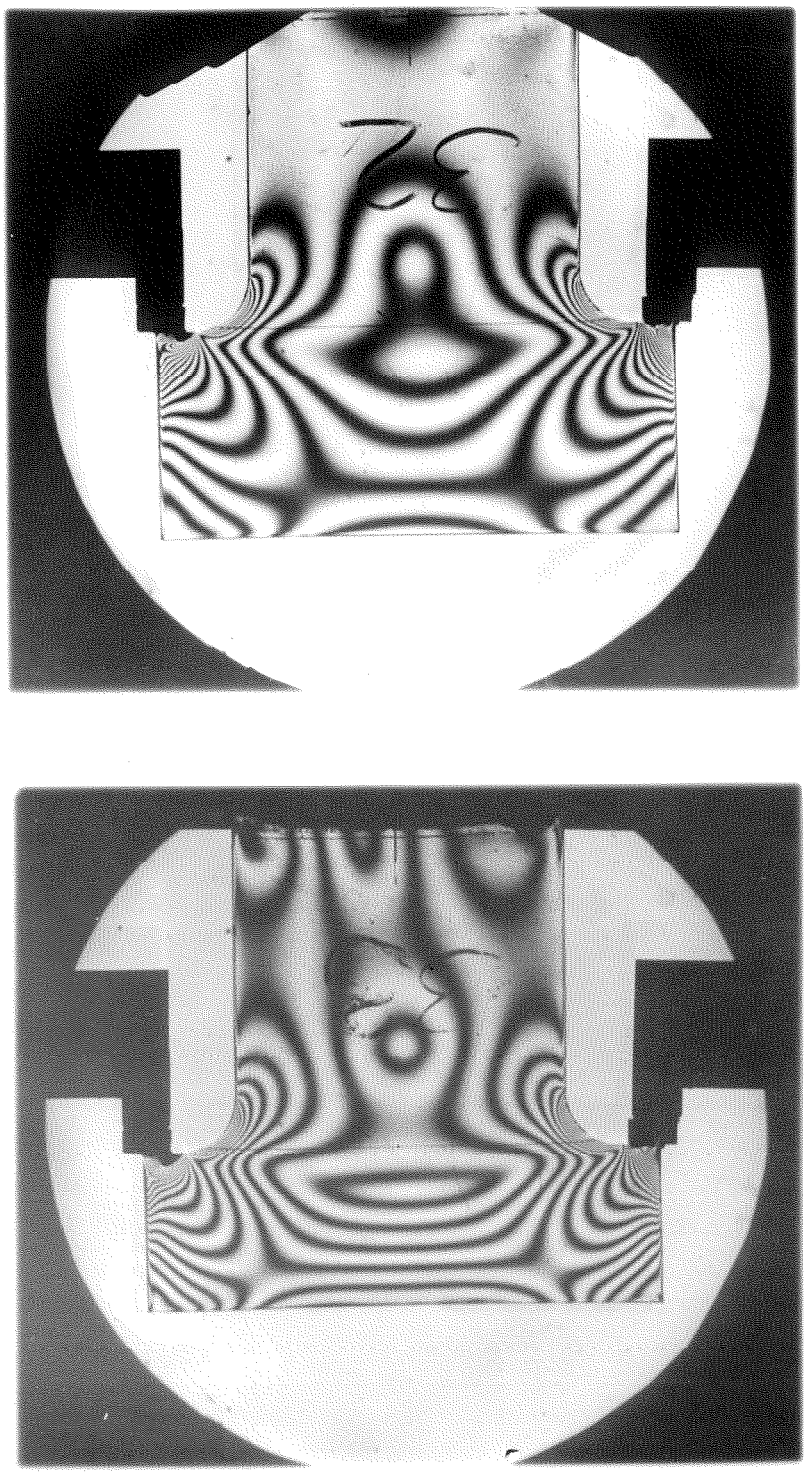

FIGURE 10

DISTRIBUTED LOAD TEST SHOWING EFFECT OF BASE HEIGHT ON STRESS CONCENTRATION. $R/b = .16$, ABOVE: $c/b = .63$, BELOW: $c/b = .48$

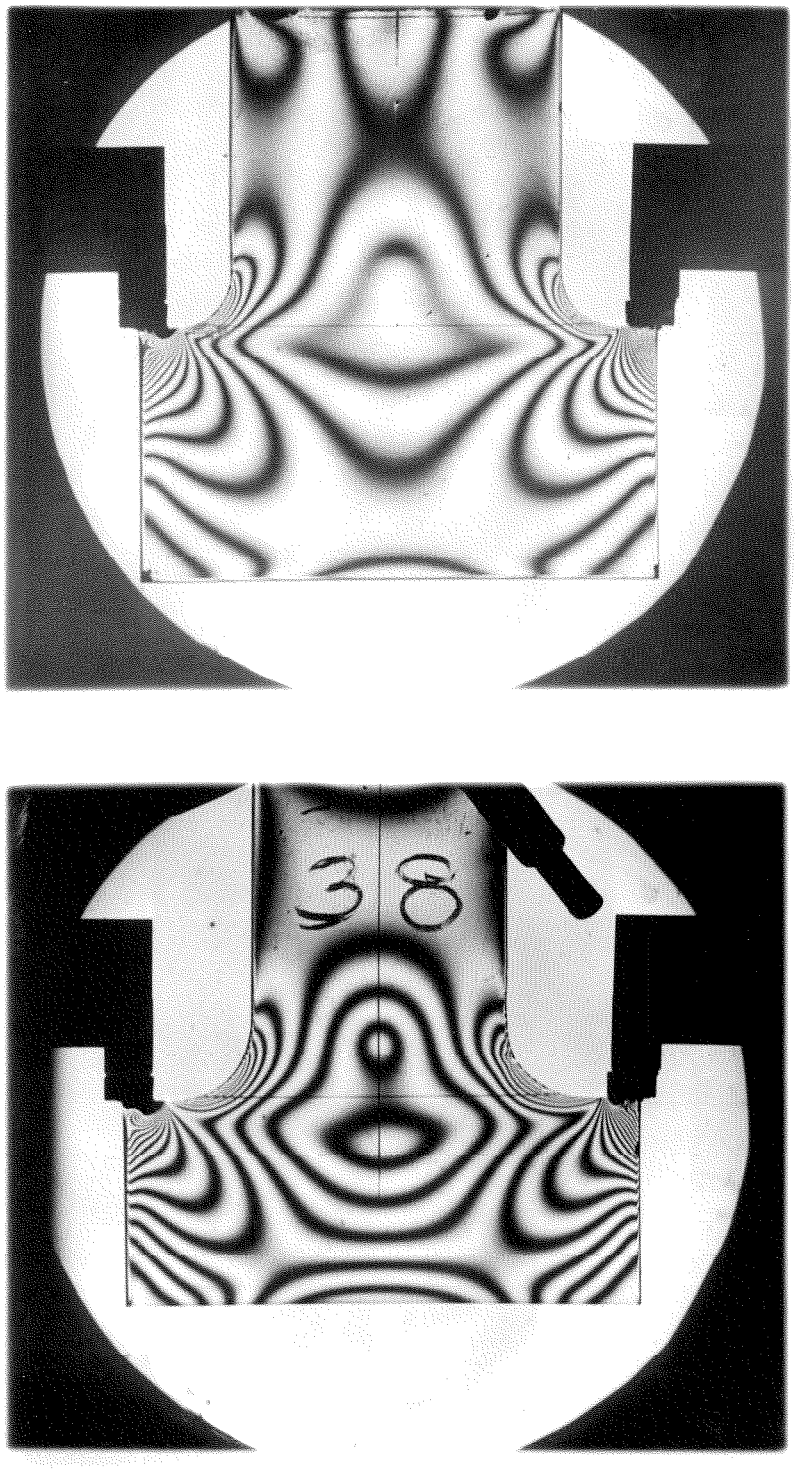

FIGURE 11

DISTRIBUTED LOAD TEST SHOWING EFFECT OF RADIUS ON STRESS CONCENTRATION. ABOVE: $R/b = .16$, $c/b = .76$ BELOW: $R/b = .30$, $c/b = .81$

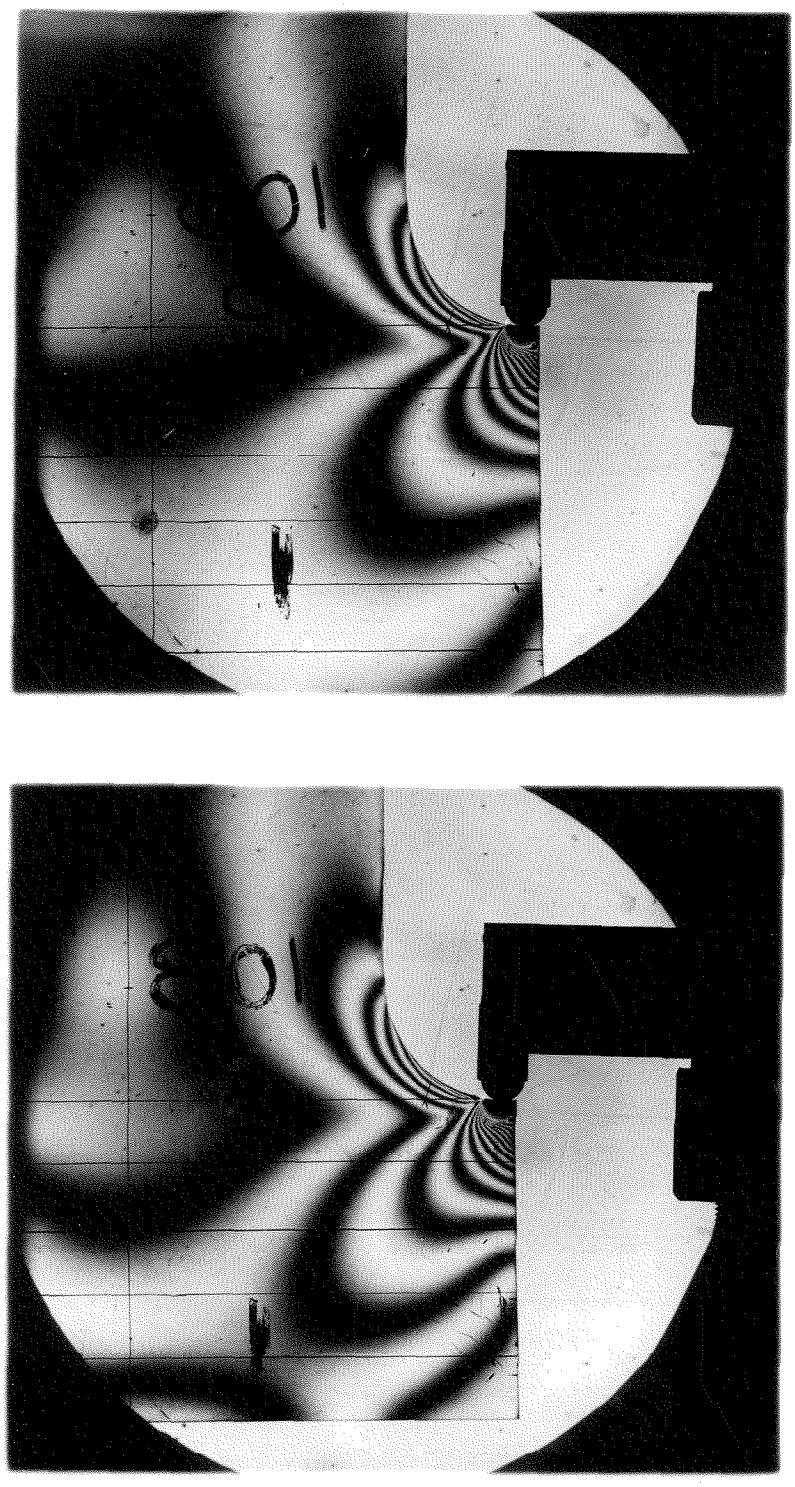

FIGURE 12

POINT LOAD TEST SHOWING EFFECT OF BASE HEIGHT ON STRESS CONCENTRATION. ABOVE: $R/b = .23$, $c/b = .6$ BELOW: $R/b = .23$, $c/b = .4$

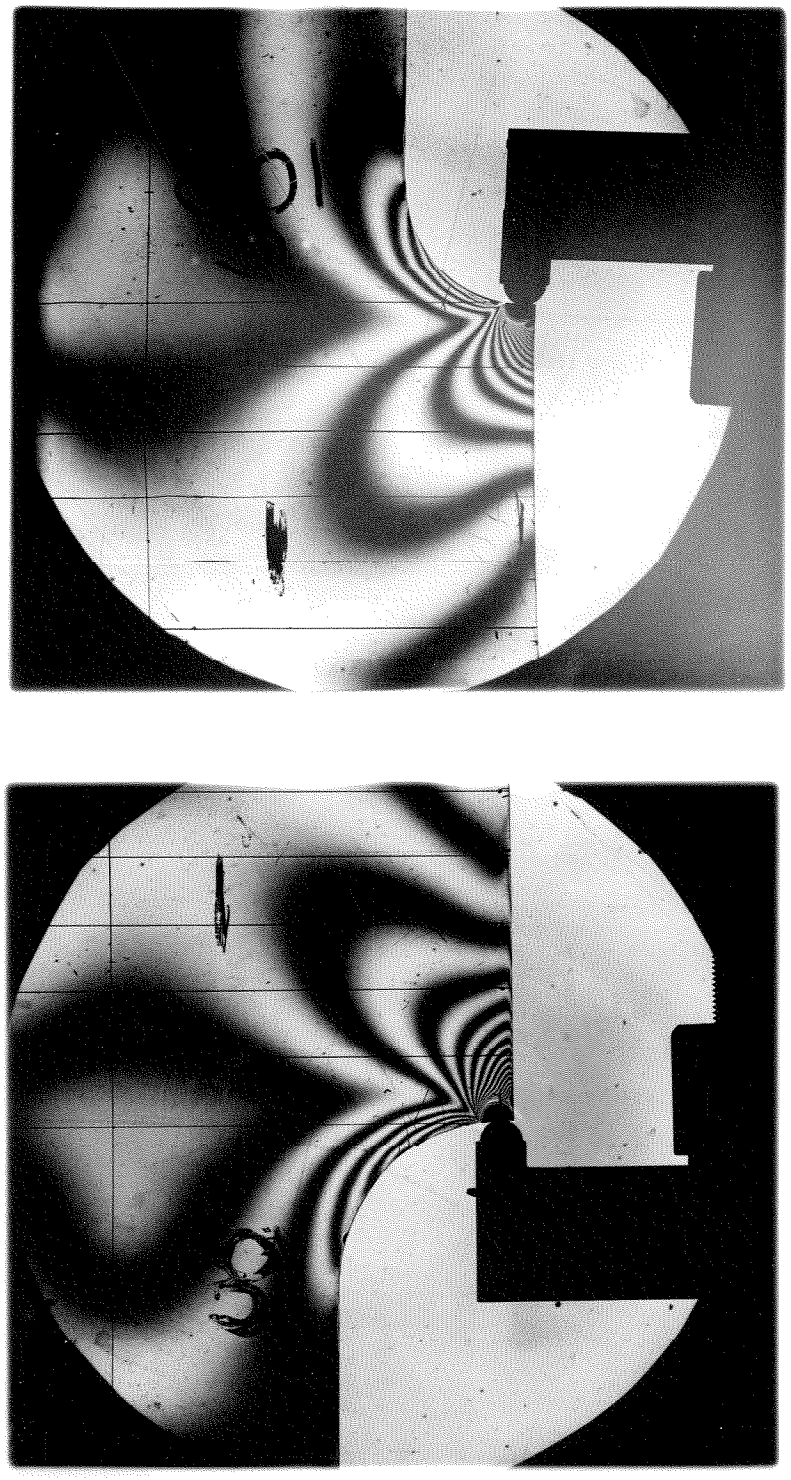

FIGURE 13

POINT LOAD TEST SHOWING EFFECT OF RADIUS ON STRESS CONCENTRATION. ABOVE: $R/b = .23$, $c/b = .5$ BELOW: $R/b = .35$, $c/b = .5$

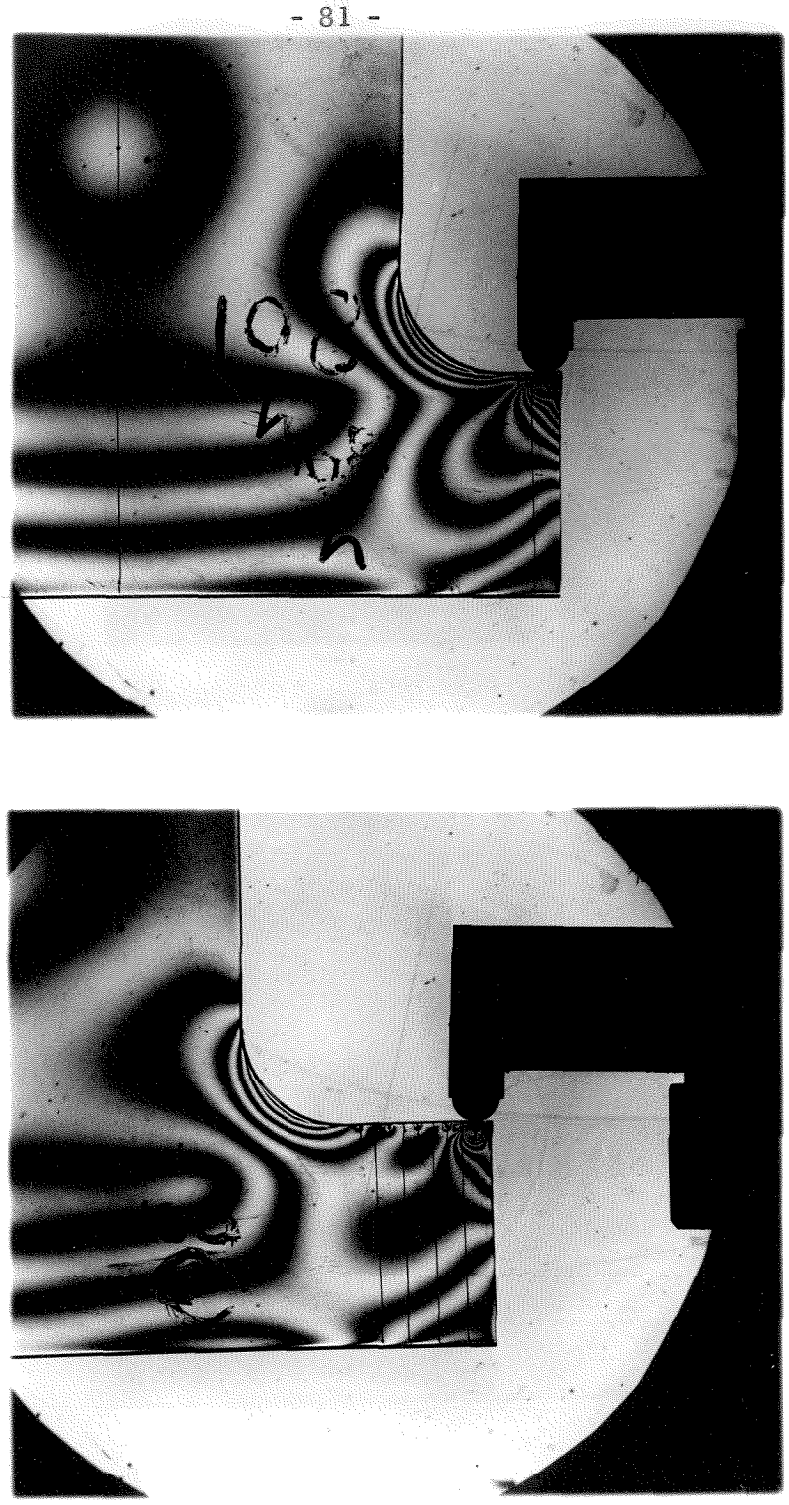

FIGURE 14

POINT LOAD TEST SHOWING EFFECT OF LOAD DISTANCE ON STRESS CONCENTRATION. $R/b = .18$, $c/b = .4$ ABOVE: $e/b = .05$ LOAD = 70 # BELOW: $e/b = .20$ LOAD = 70 #

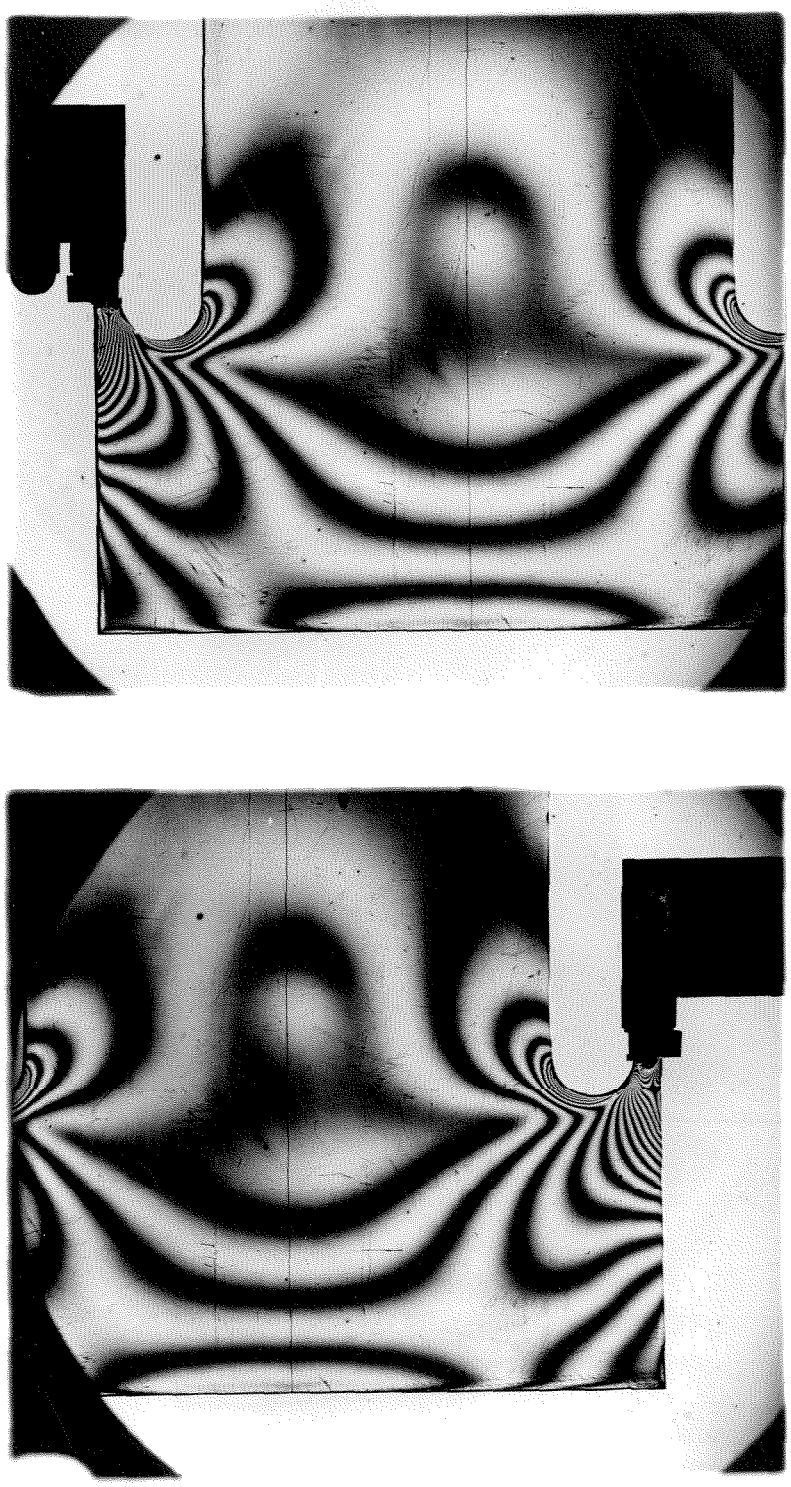

FIGURE 15

RECESSED FILLET TEST; $R/b = .075$, $c/b = .55$, $\ell/b = .175$, $K \approx 8$

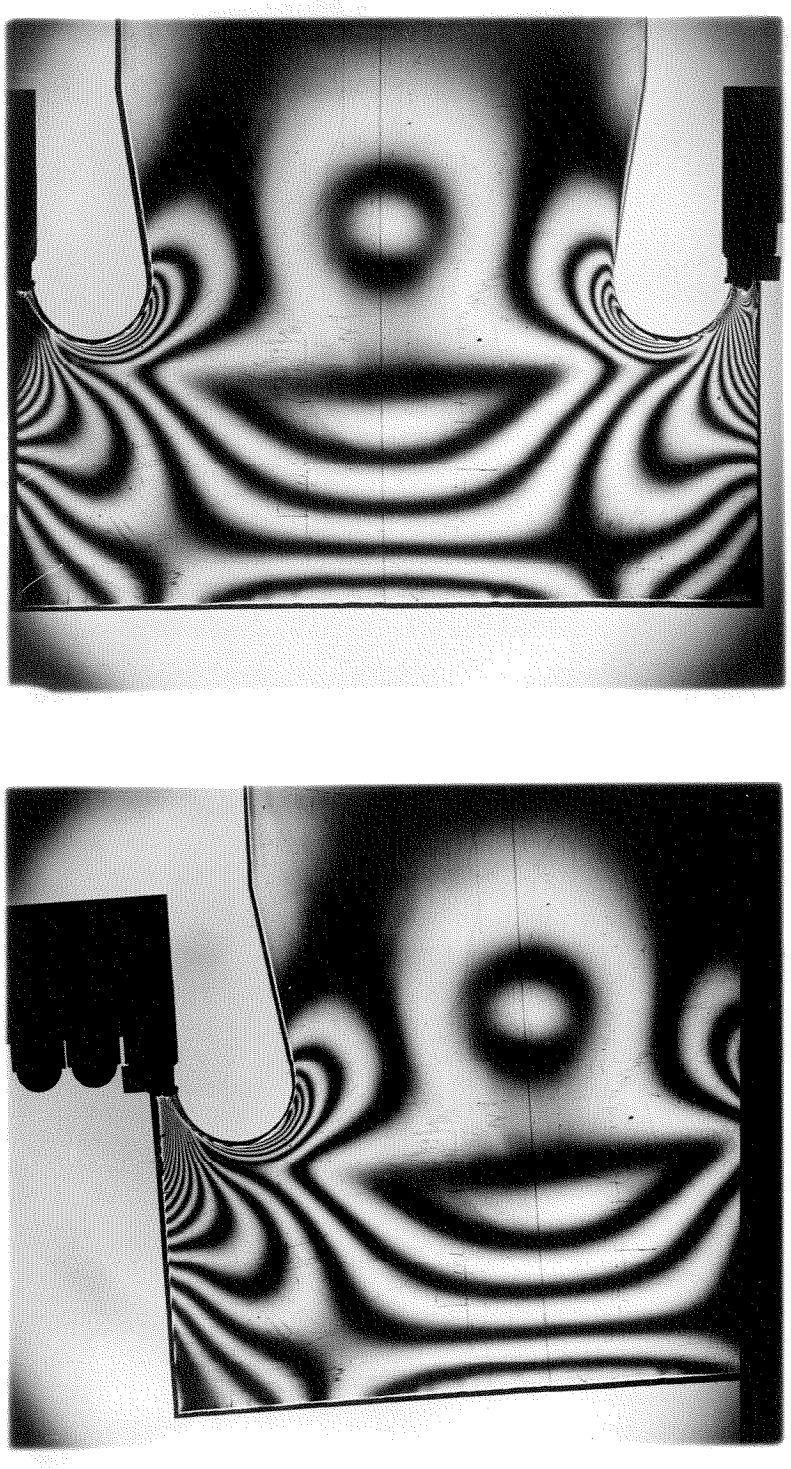

FIGURE 16

RECESSED FILLET TEST; $R/b = .13$, $c/b = .58$, $\ell/b = .29$, $K \approx 6.6$

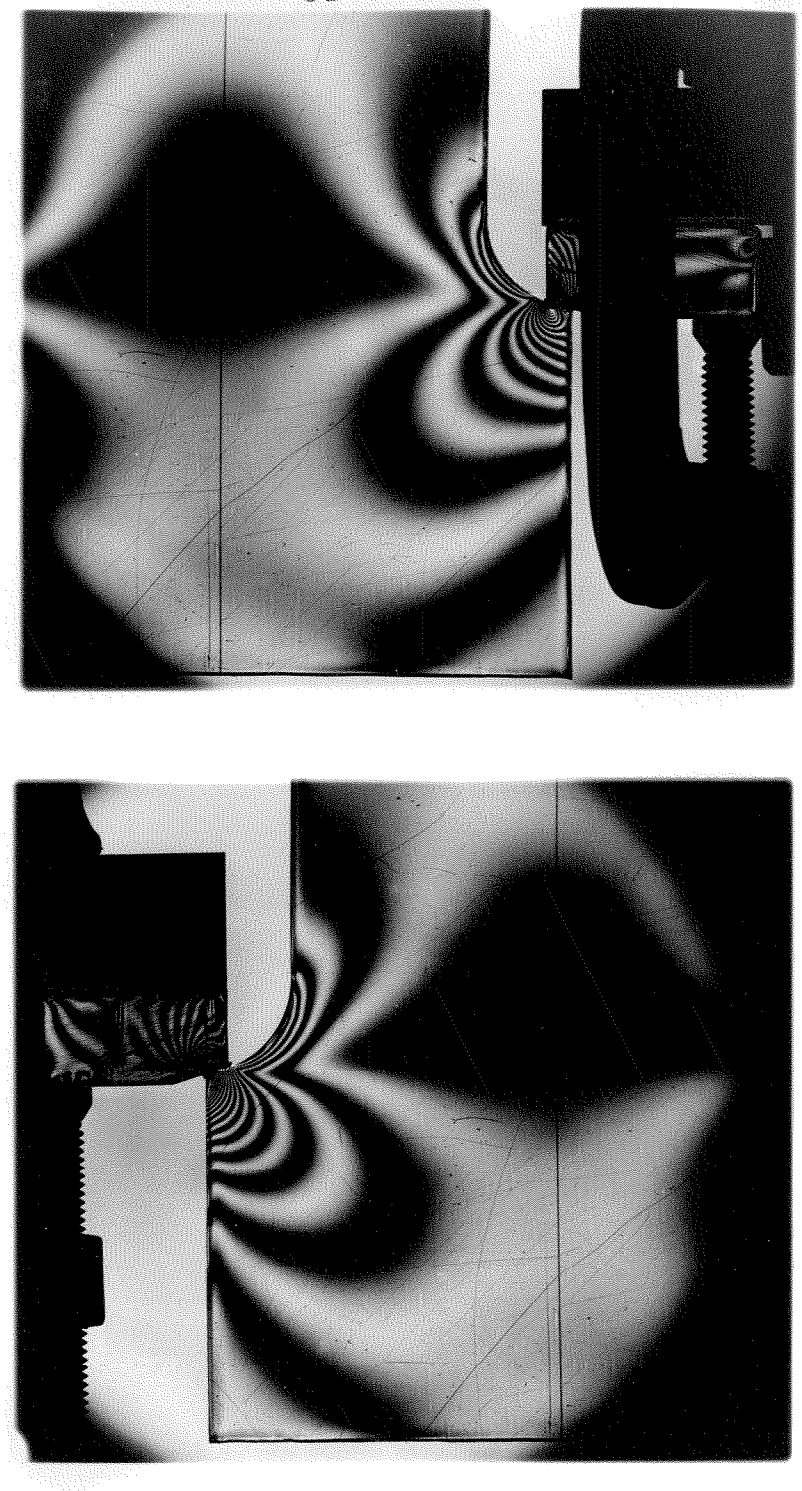

FIGURE 17

INCLINED FILLET; $R/b = .21$, $c/b = .71$, $\alpha = 18.5°$

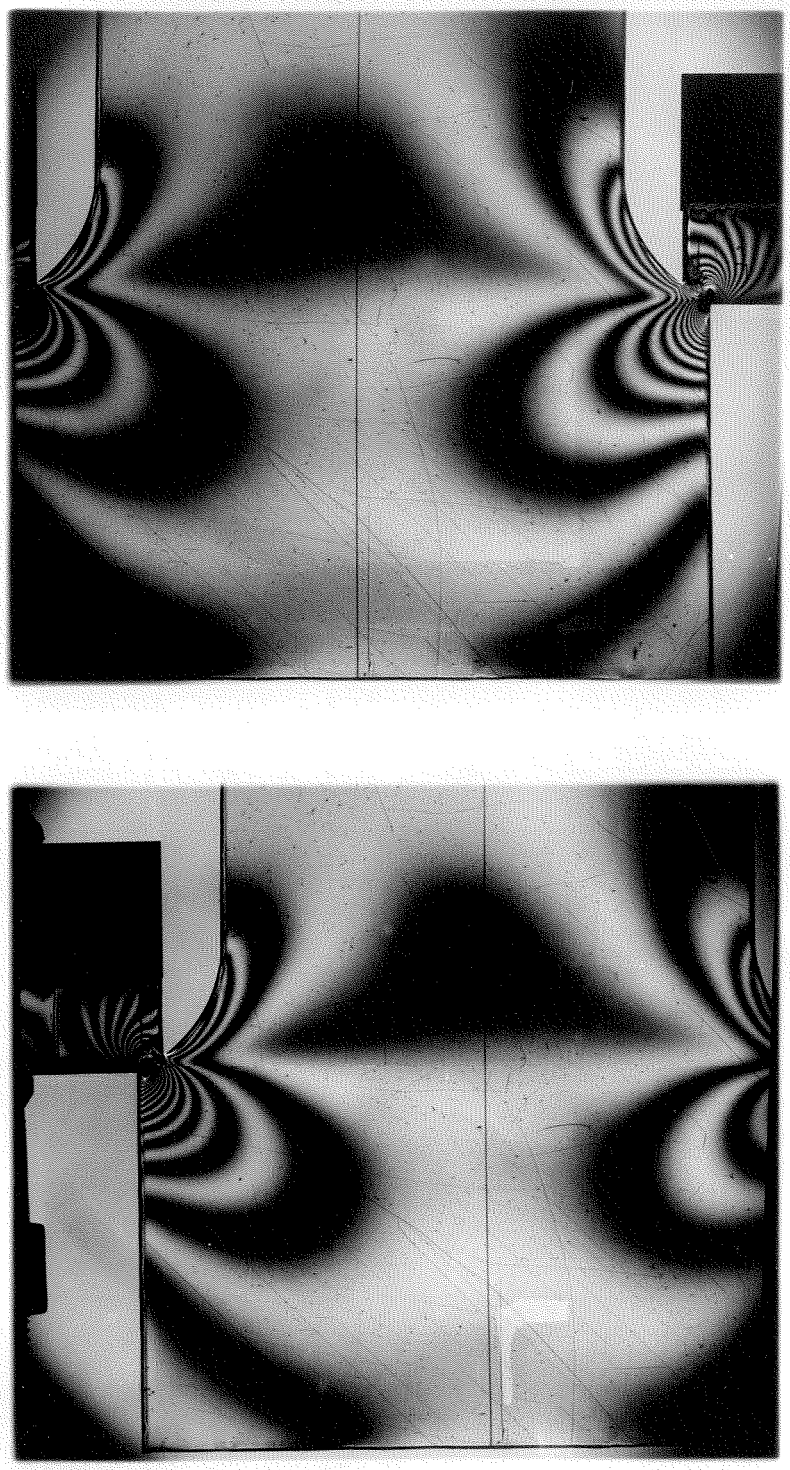

FIGURE 18

INCLINED FILLET; $R/b = .333$, $c/b = .66$, $\alpha = 38°$, $K = 4$

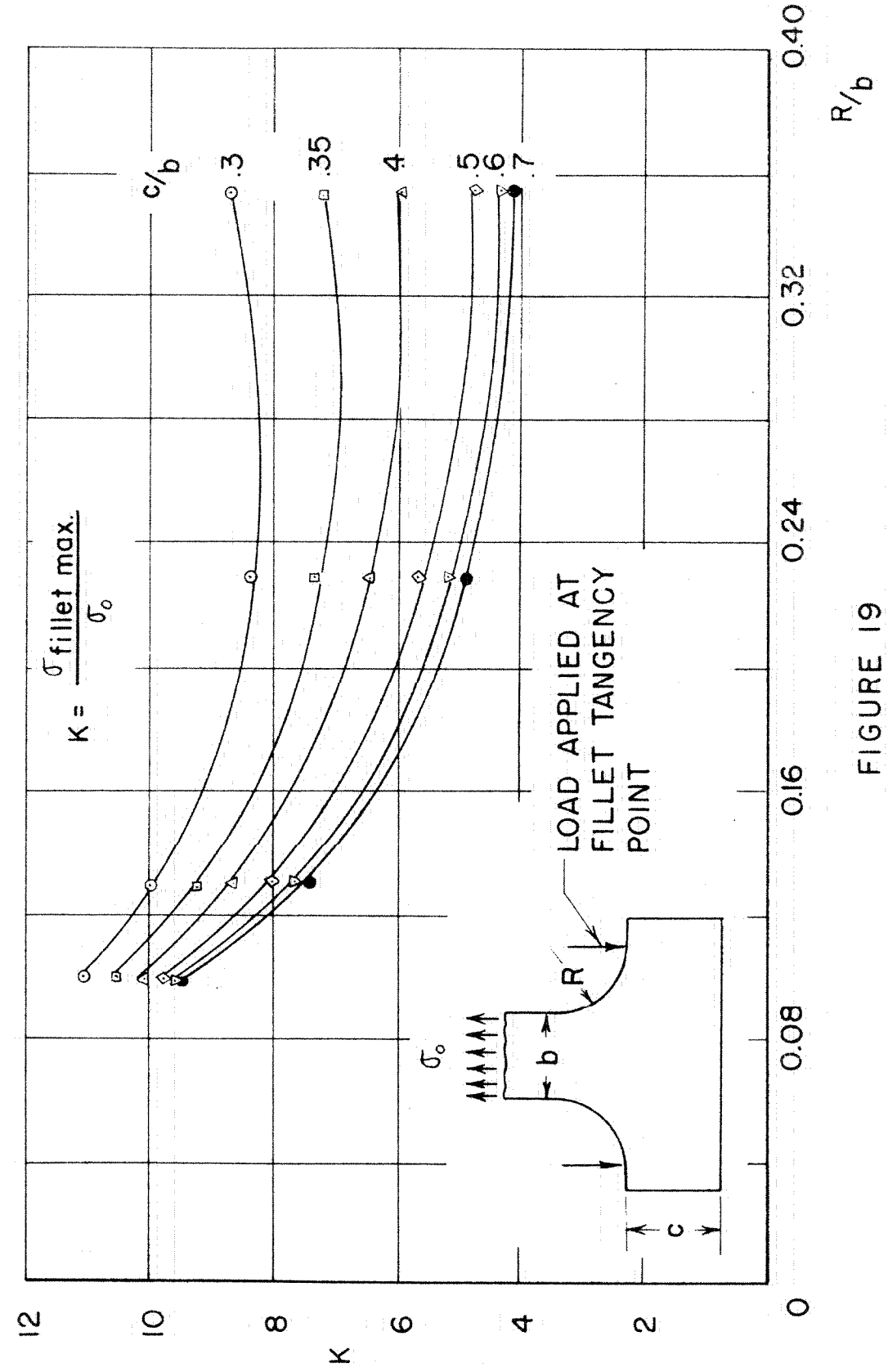

FIGURE 19

POINT LOAD EXPERIMENTAL RESULTS

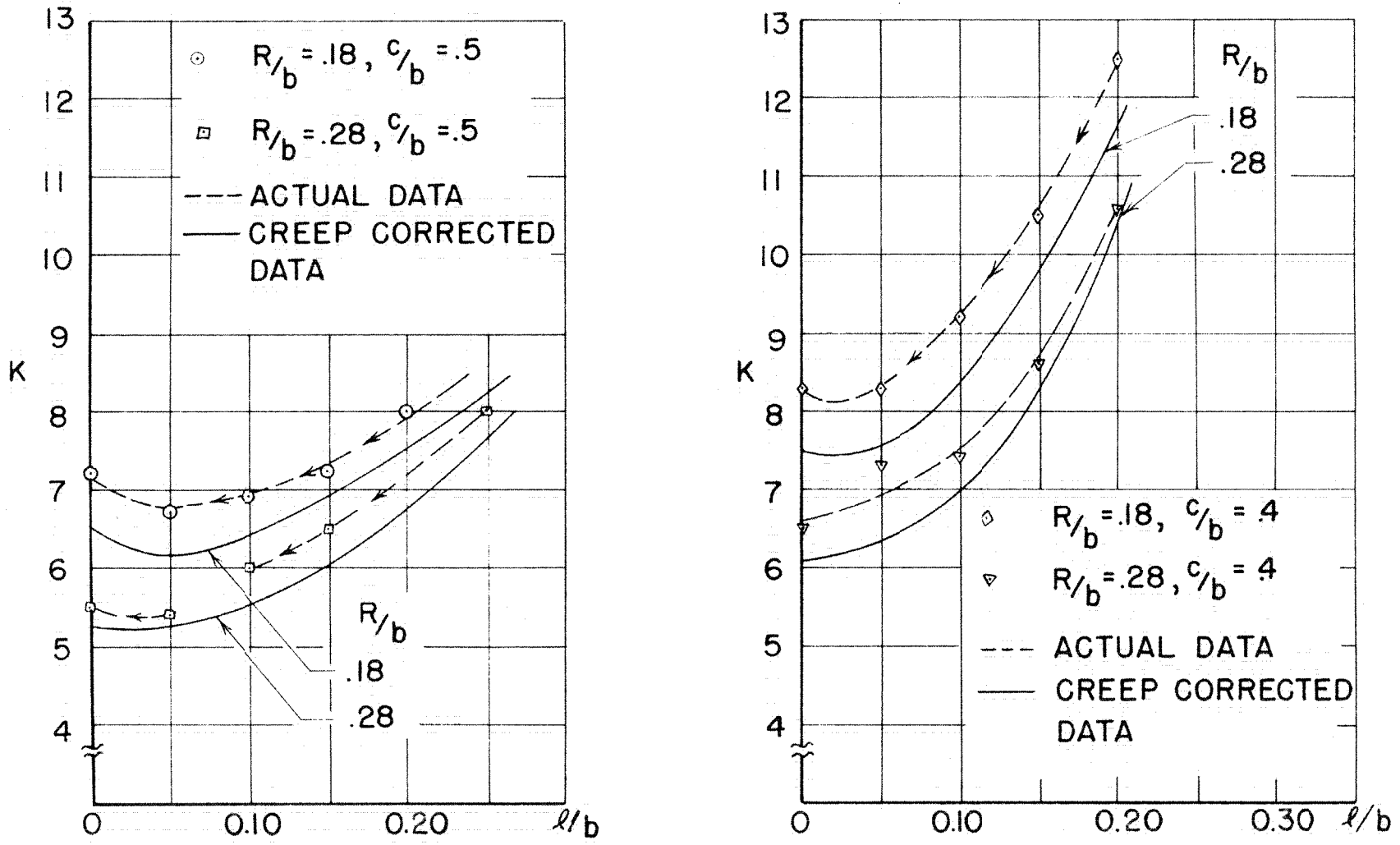

FIGURE 20
EFFECT OF DISTANCE BETWEEN POINT REACTIONS AND FILLET TANGENCIES

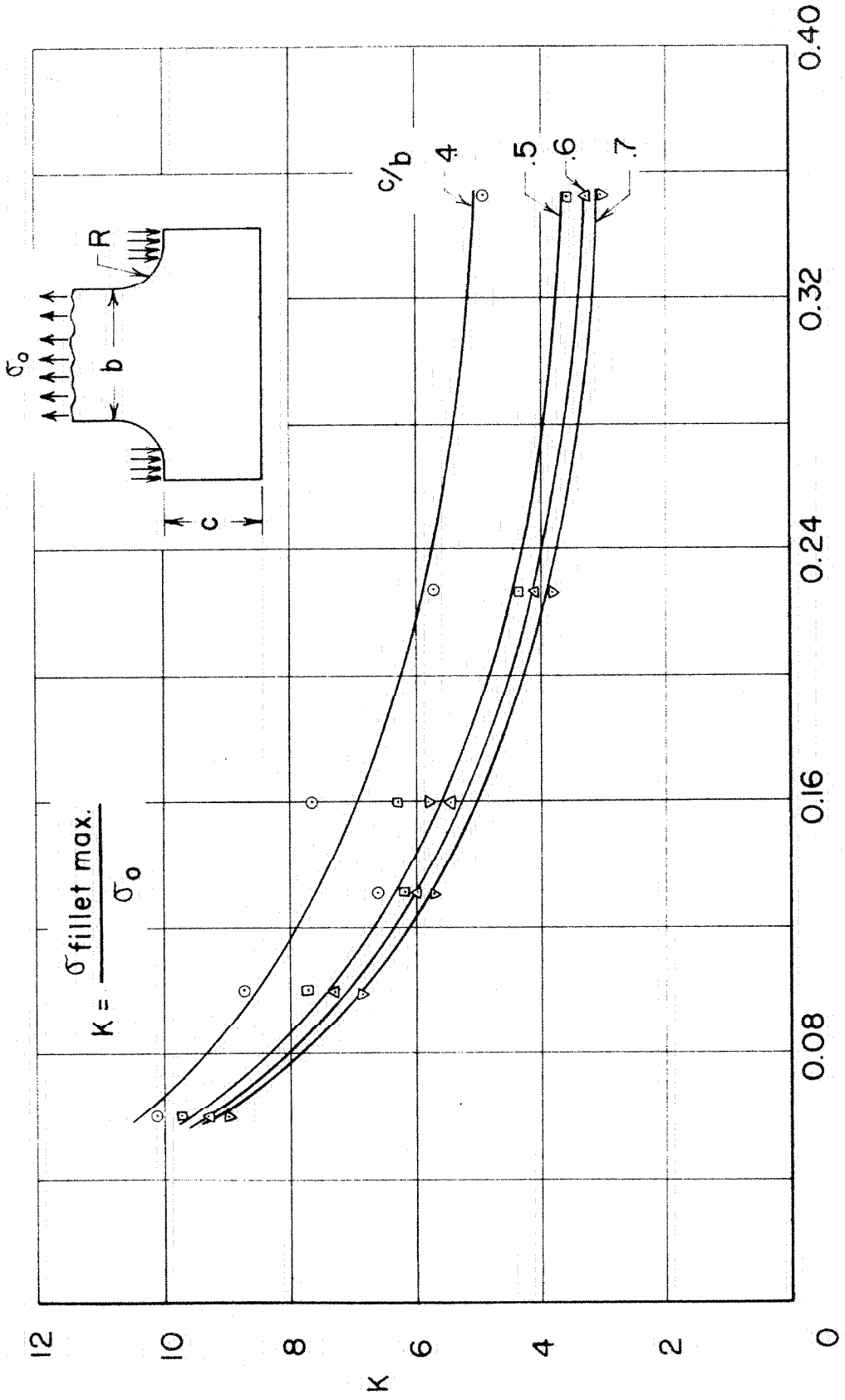

FIGURE 21

DISTRIBUTED LOAD EXPERIMENTAL RESULTS

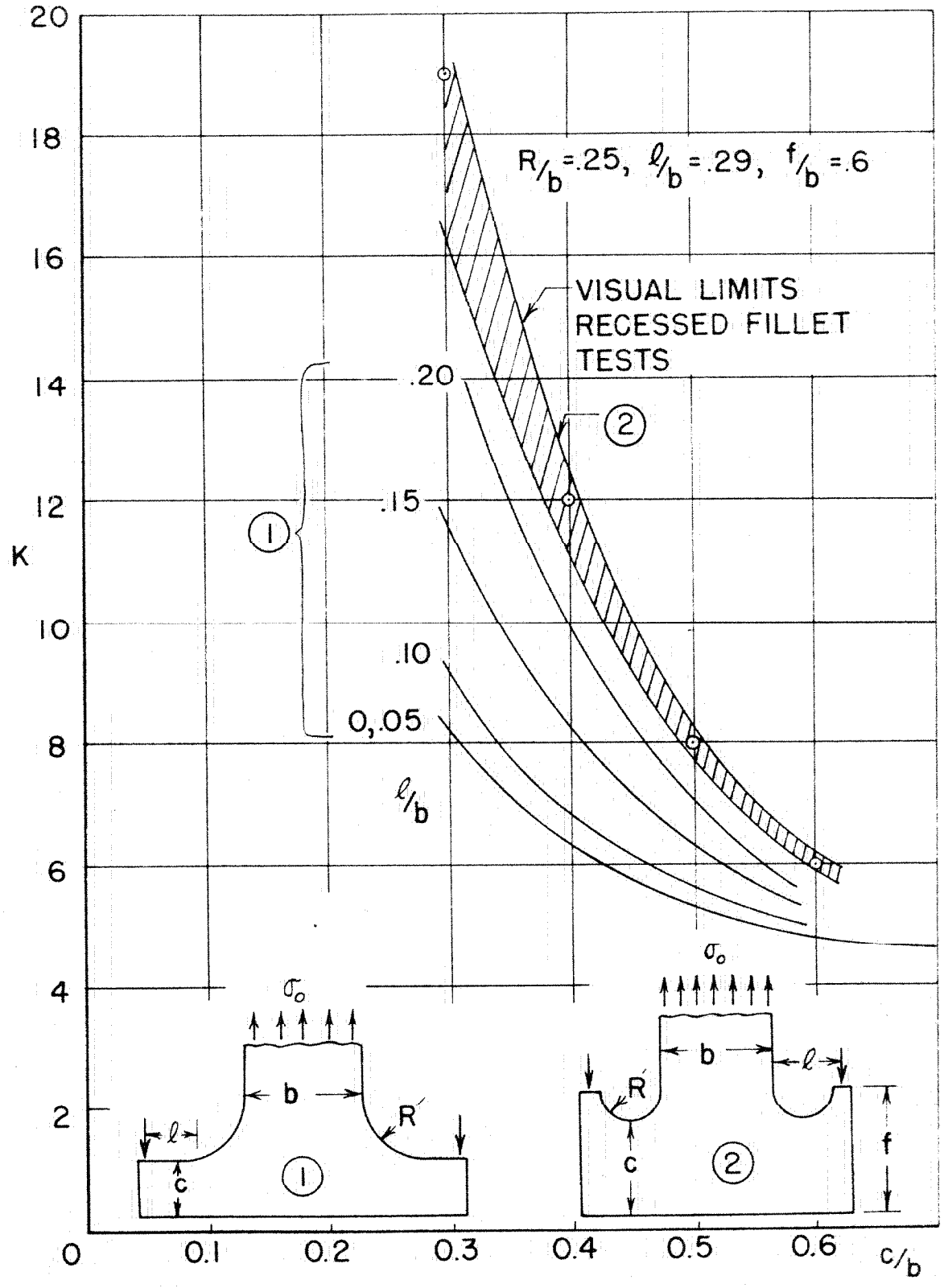

FIGURE 22

EFFECTS OF RECESSED FILLET WITH POINT LOADS

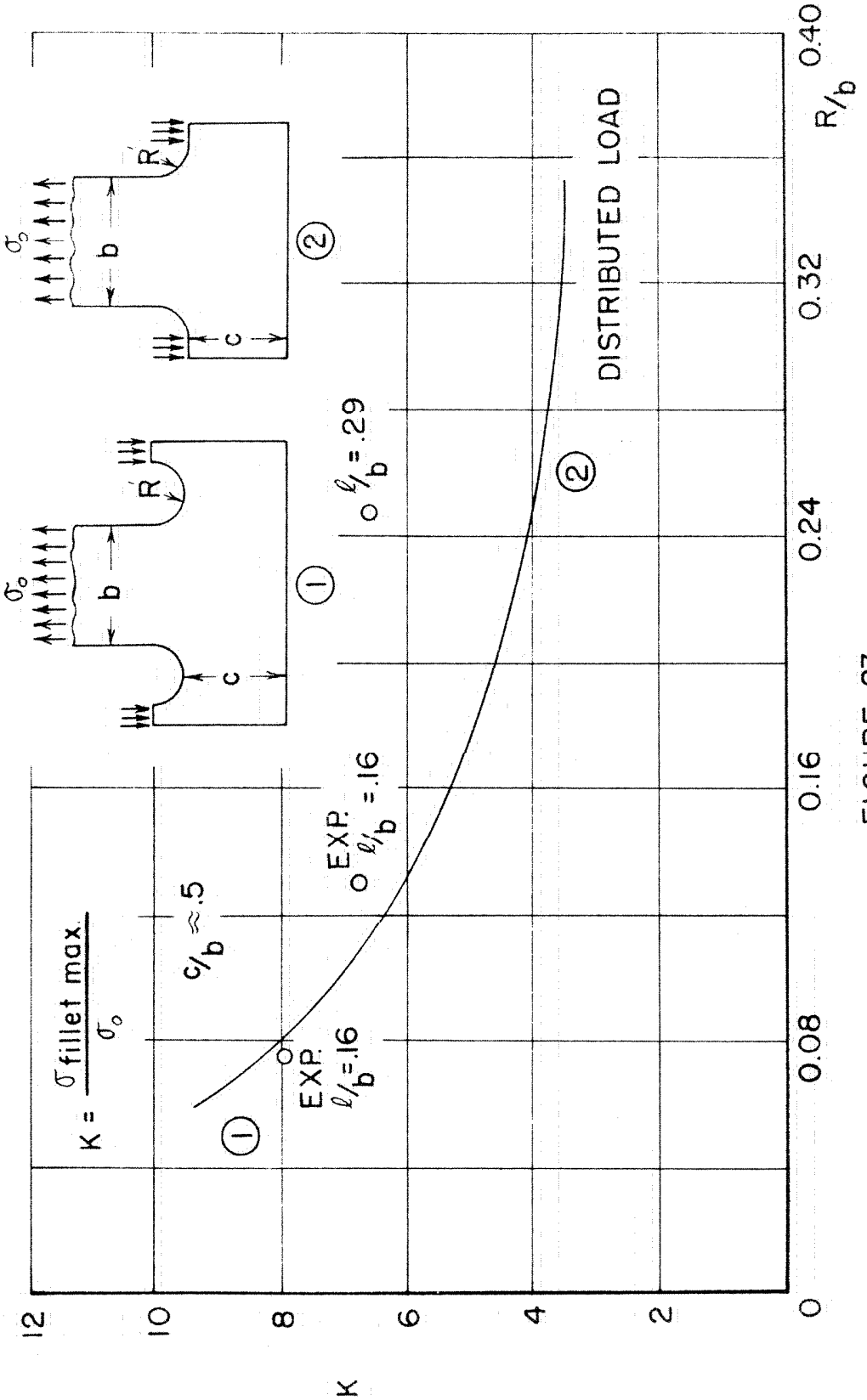

FIGURE 23

EFFECTS OF RECESSED FILLETS WITH DISTRIBUTED LOAD

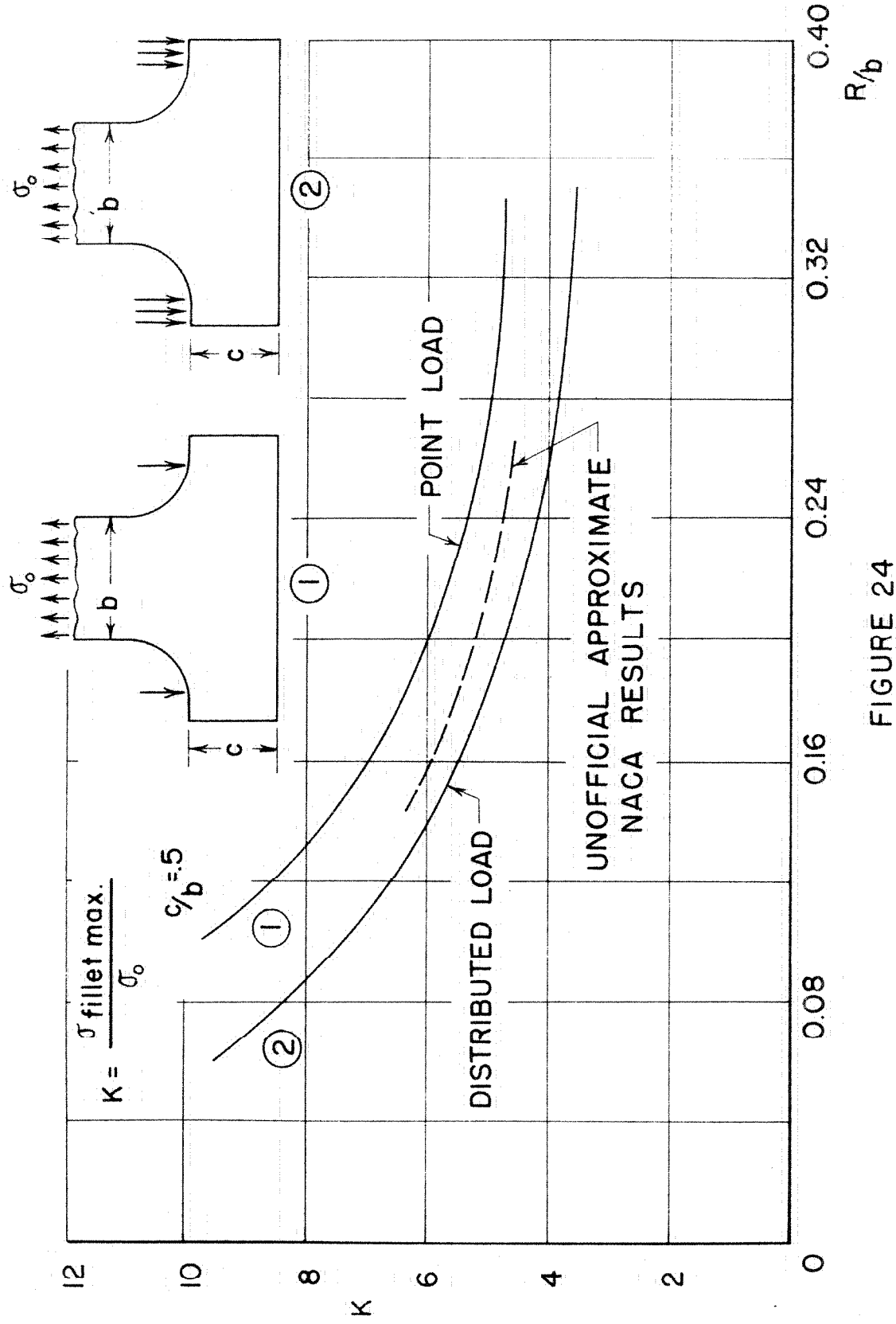

FIGURE 24

COMPARISON OF EXPERIMENTAL RESULTS

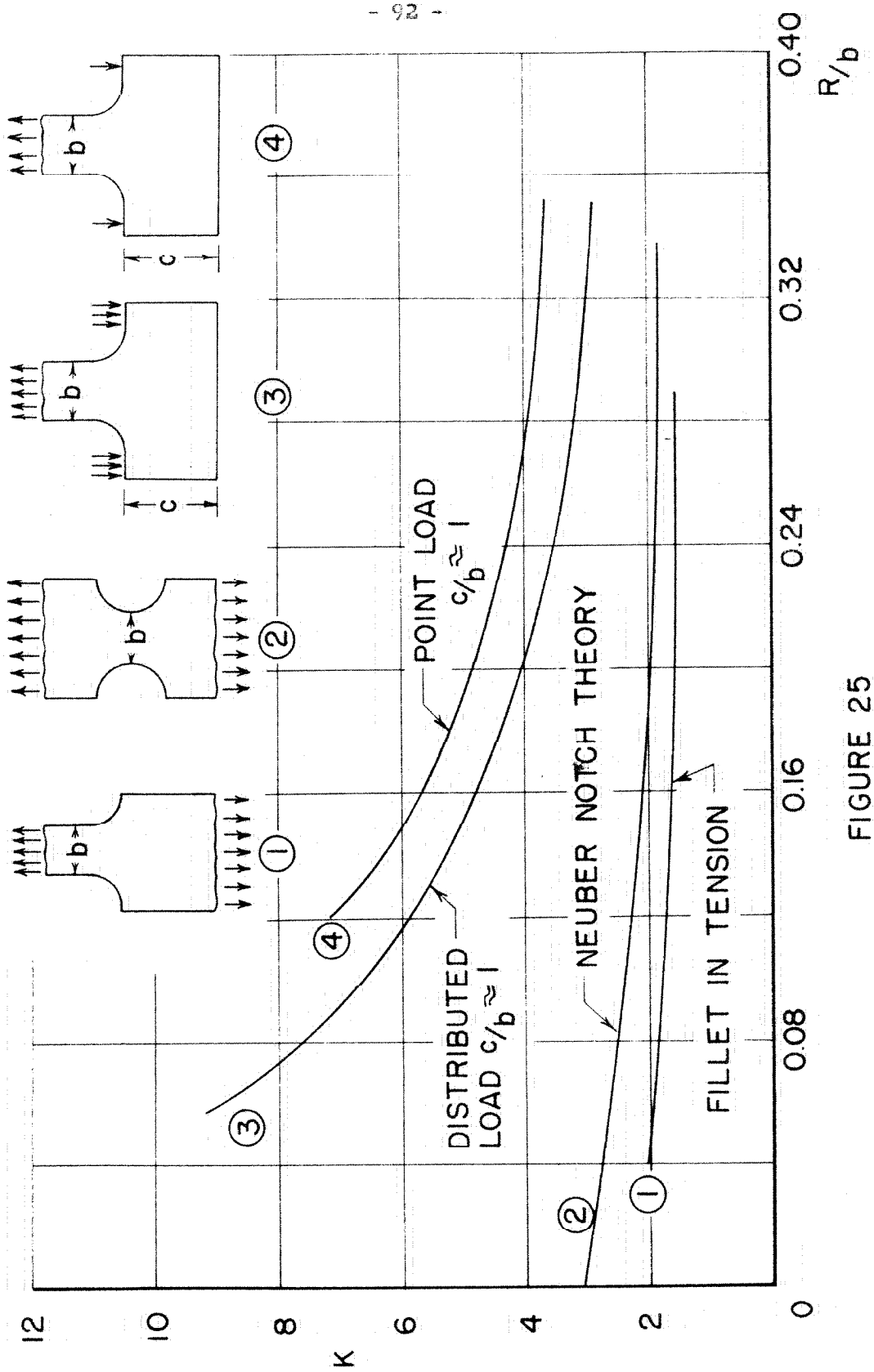

FIGURE 25

COMPARISON OF STRESS CONCENTRATION FACTORS

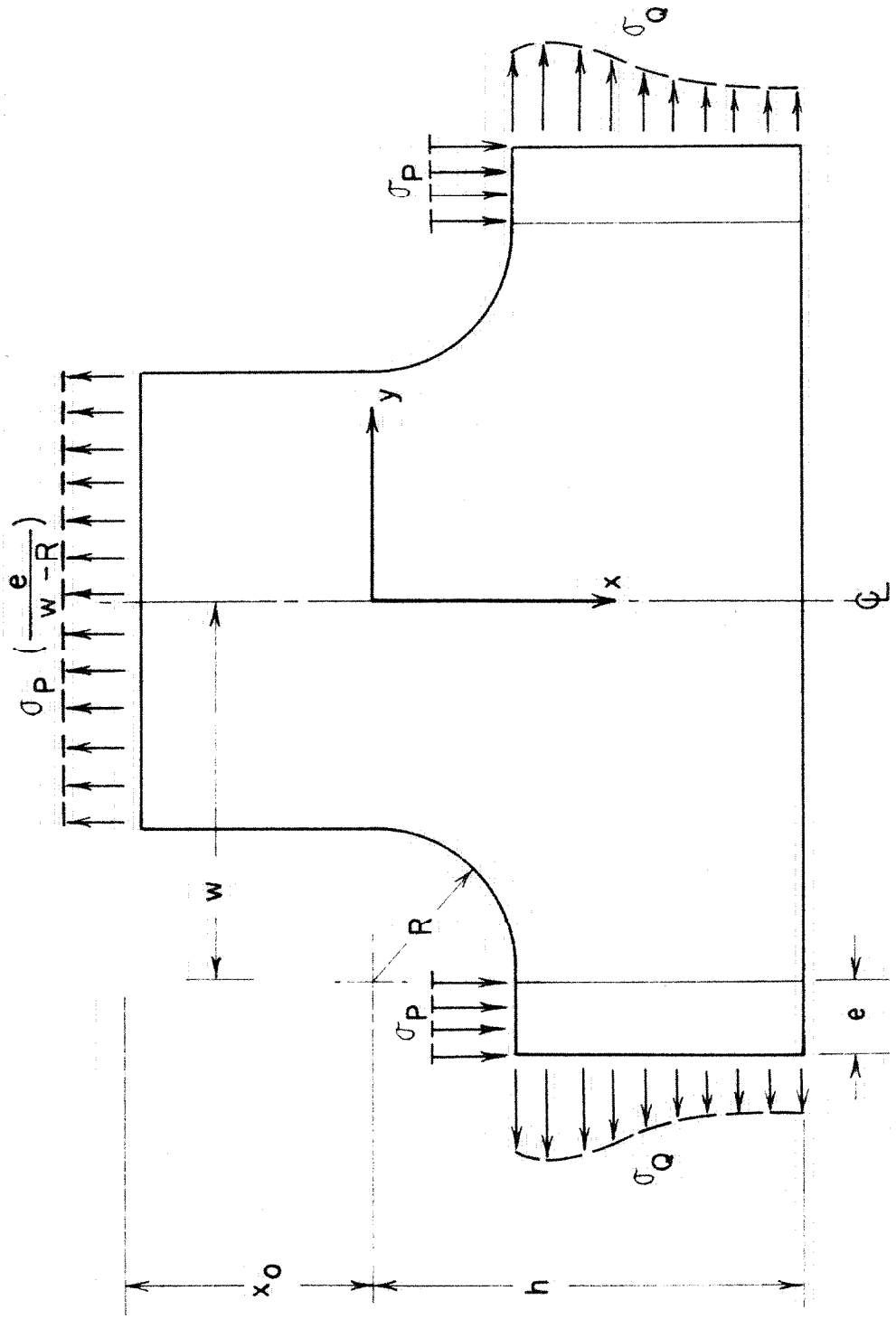

FIGURE 26

STATICALLY EQUIVALENT, AXIALLY SYMMETRIC PROBLEM

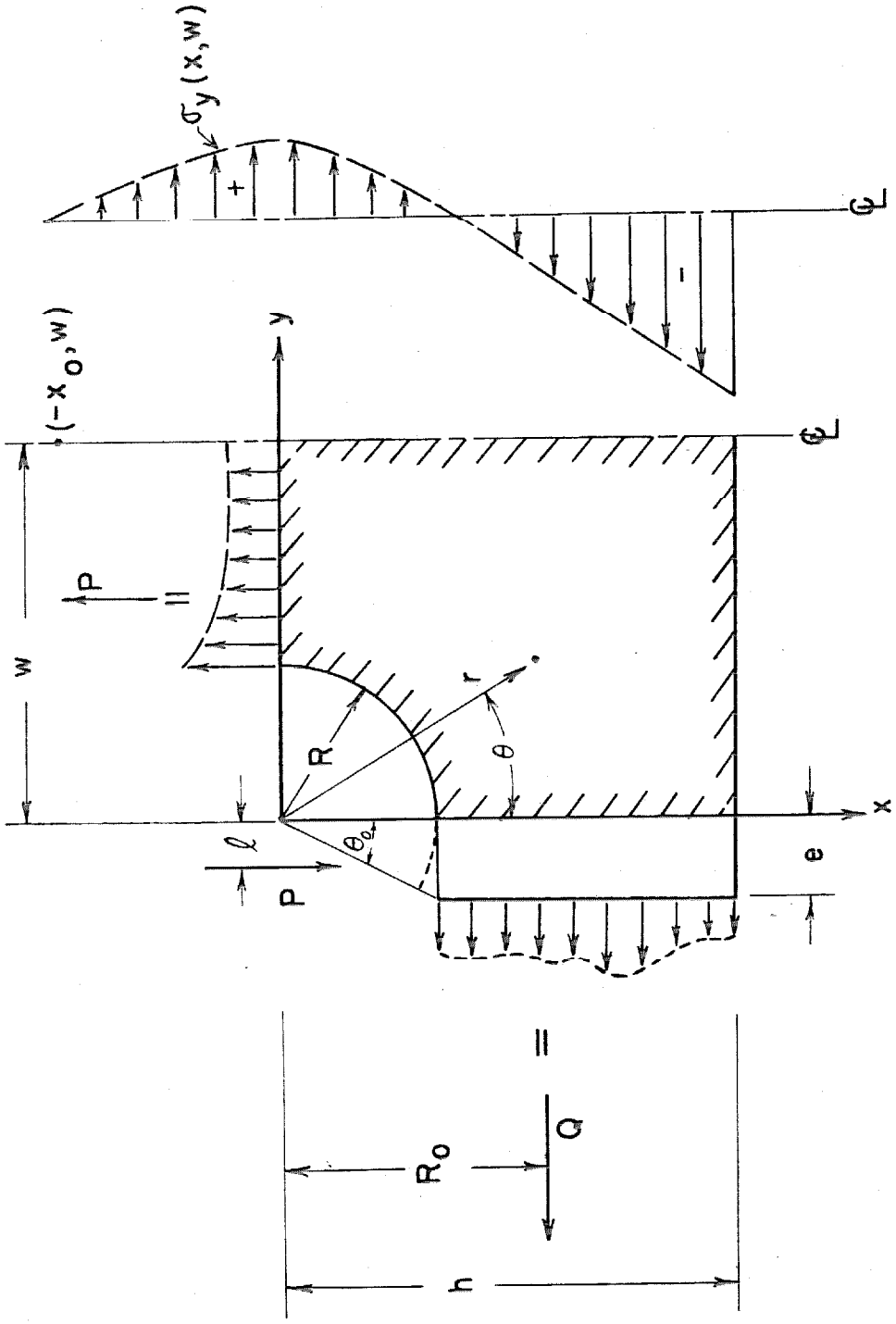

FIGURE 27
SIMPLIFIED PROBLEM FOR THEORETICAL STUDY

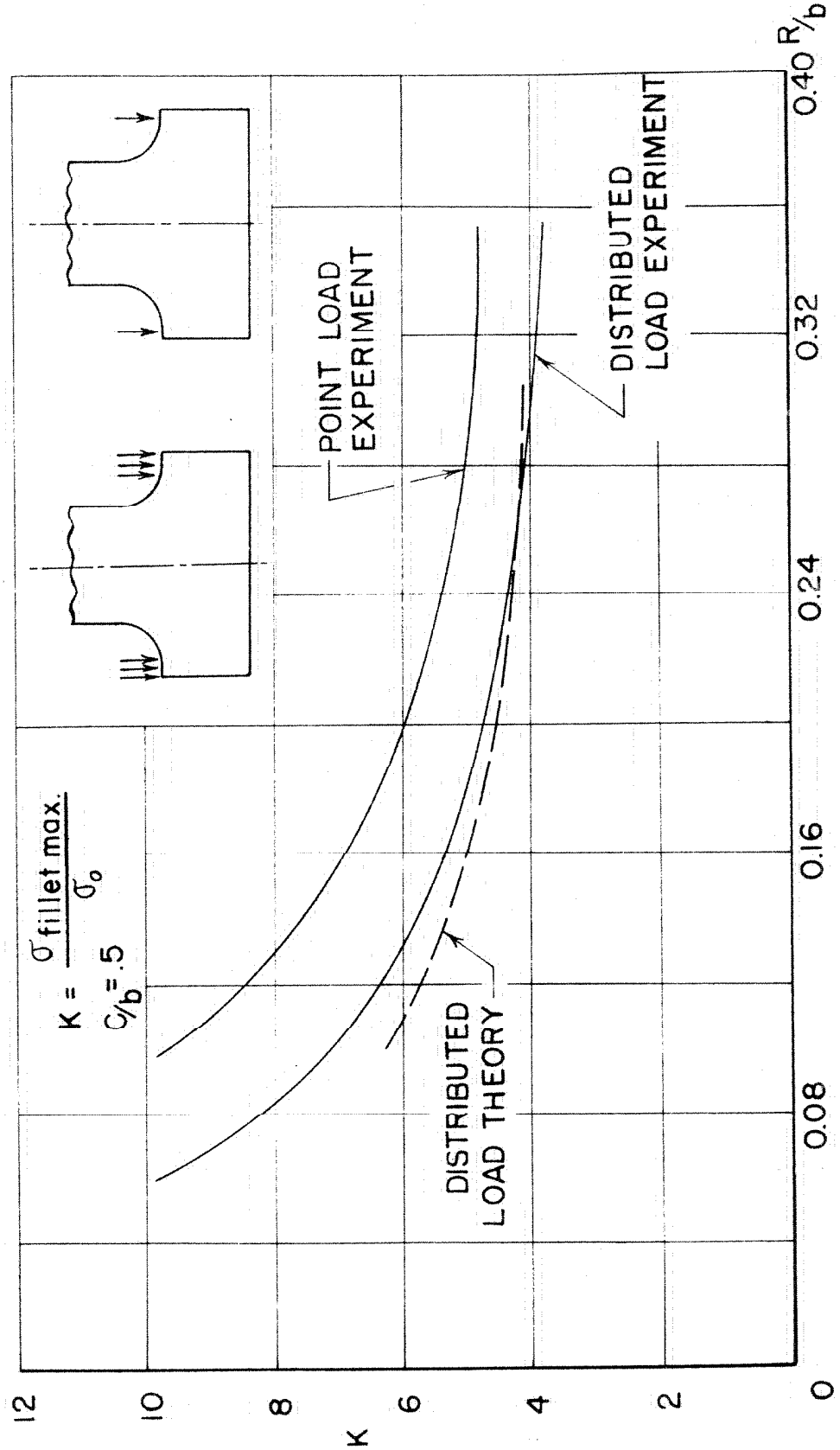

FIGURE 28

COMPARISON BETWEEN THEORY AND EXPERIMENT

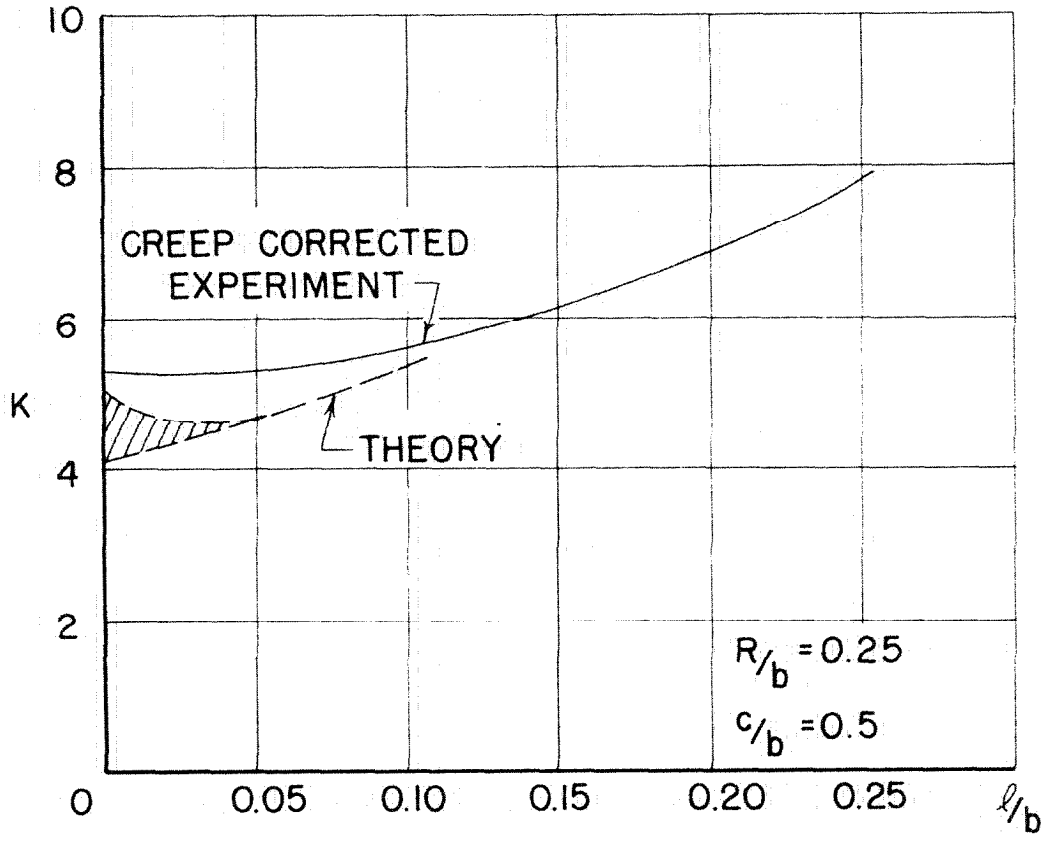

FIGURE 29

COMPARISON BETWEEN THEORY AND EXPERIMENT

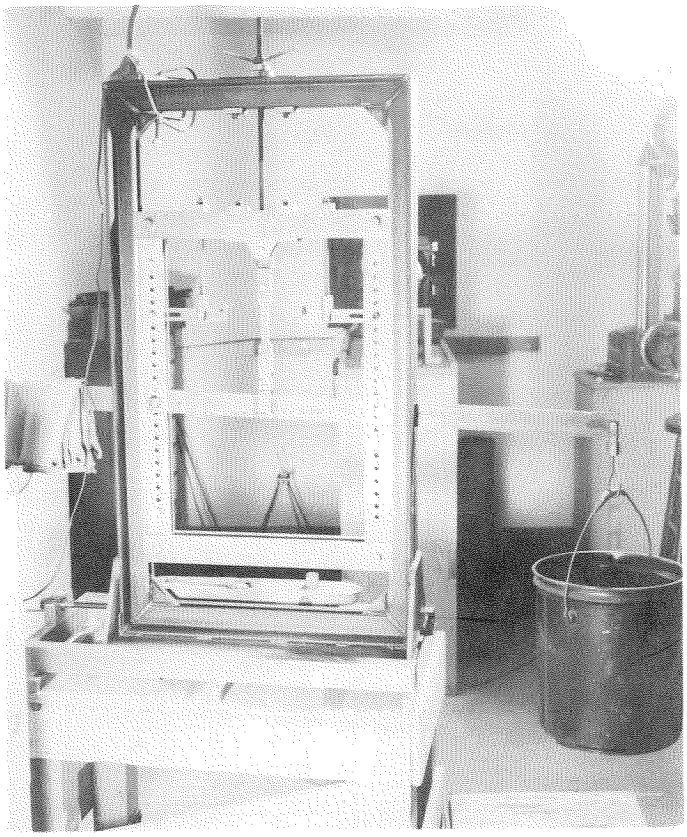

FIGURE 30

LOADING FRAME WITH TENSILE SPECIMEN;
TYPICAL FRINGE VALUE TEST

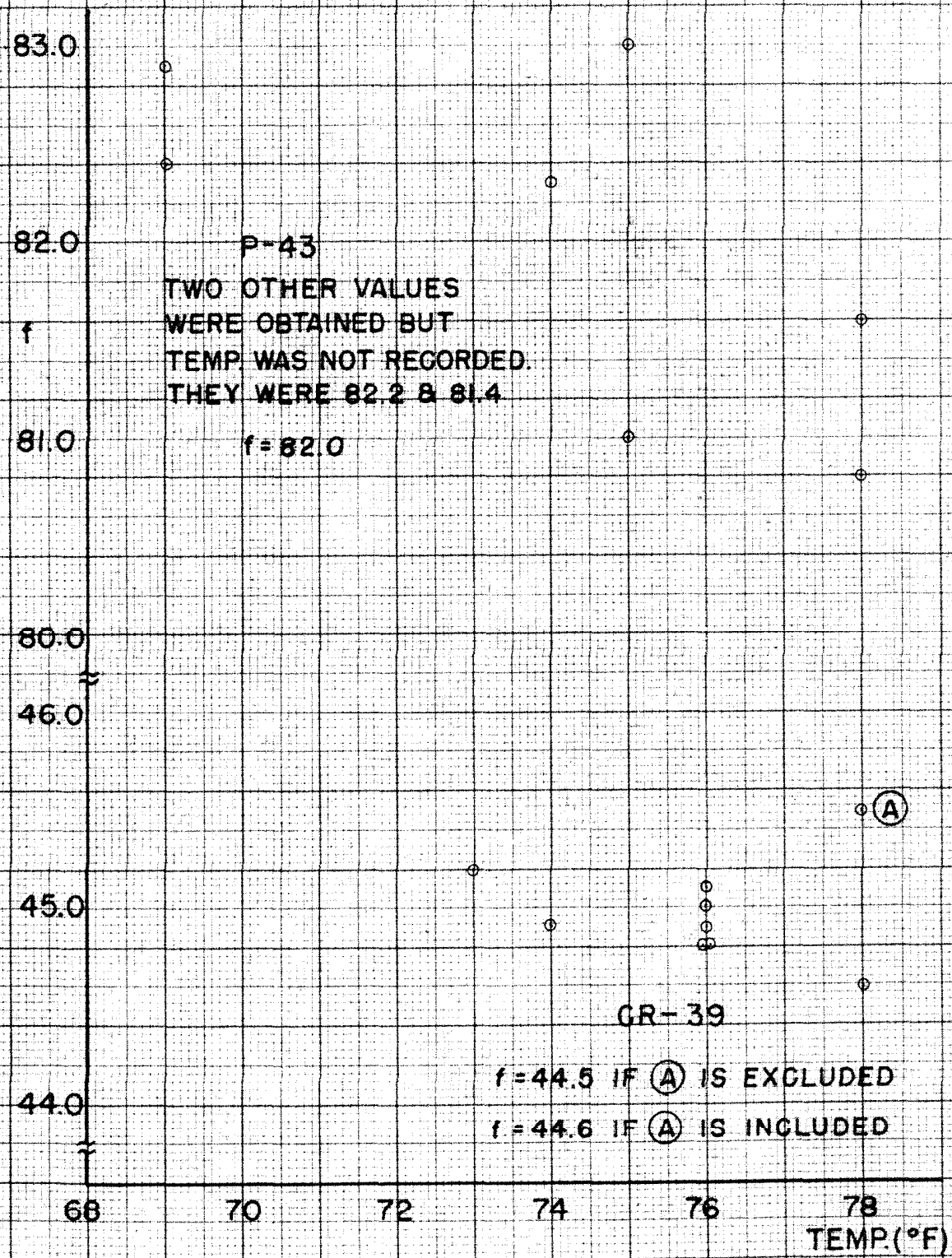

FIGURE 31

INITIAL FRINGE VALUES FOR P-43 AND CR-39

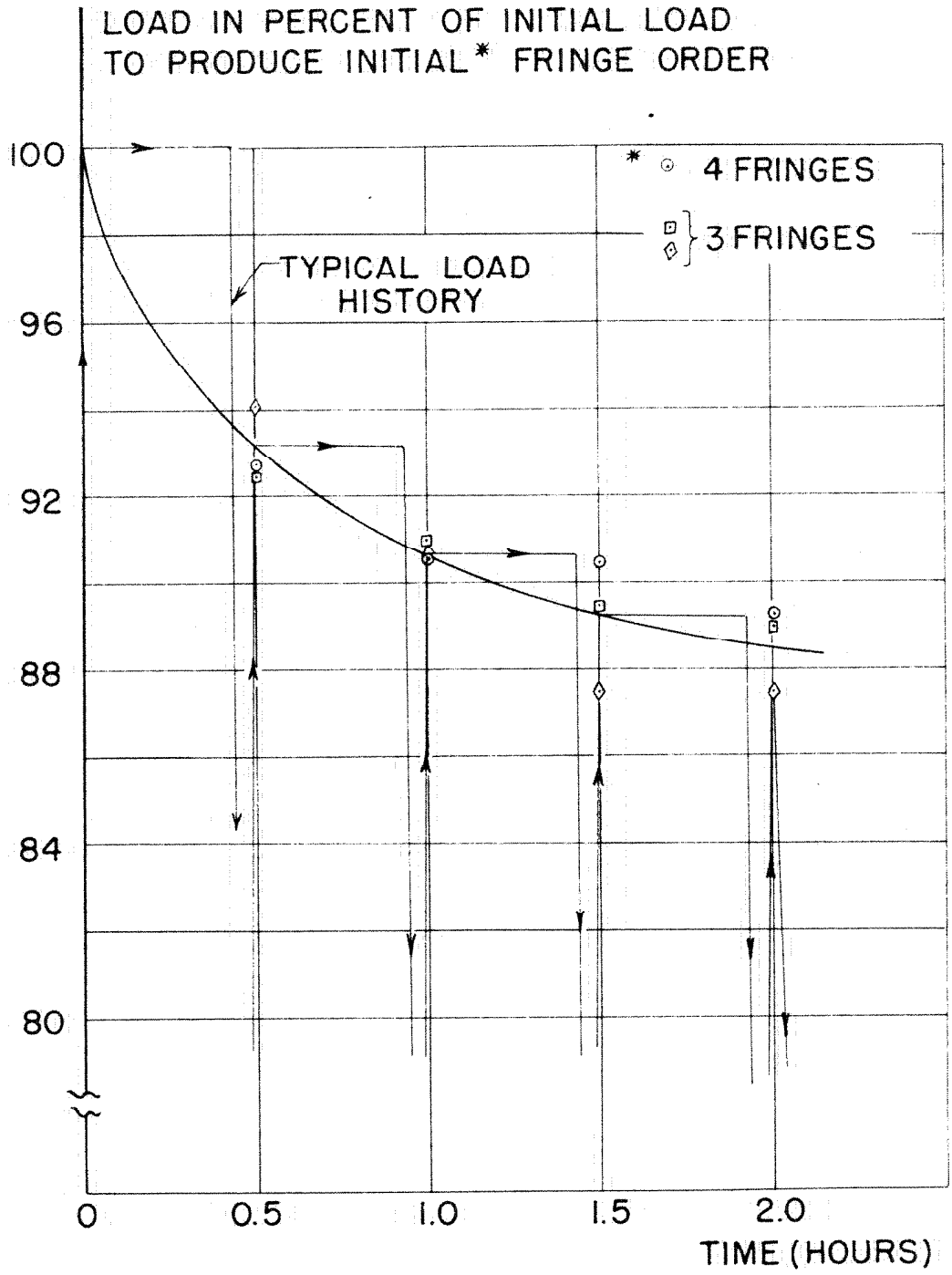

FIGURE 33

CREEP CHARACTERISTICS OF CR-39
WITH LOAD INTERRUPTION (STRESS NEAR 1500 PSI)

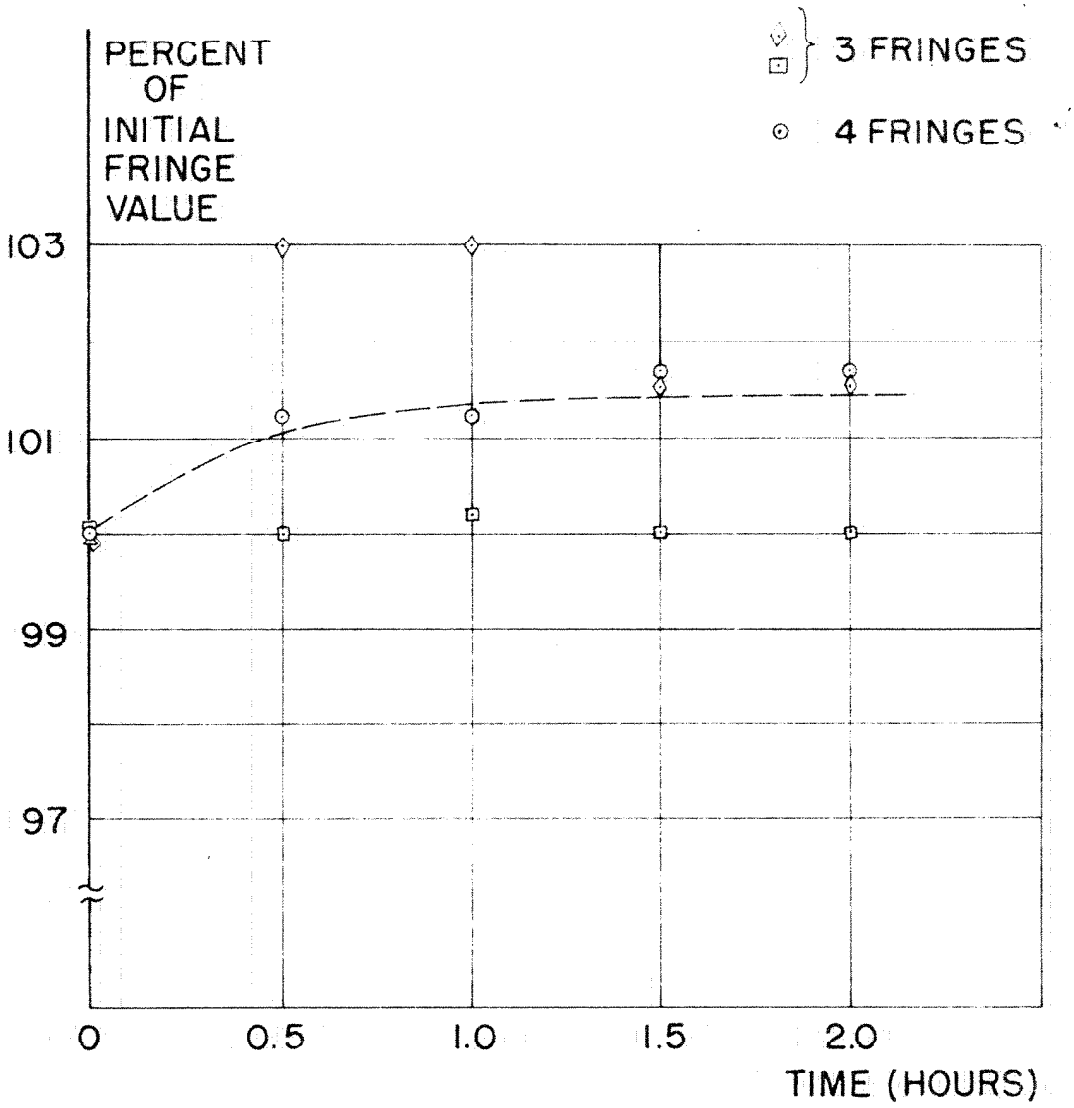

FIGURE 34

VARIATION OF FRINGE VALUE WITH TIME

WHERE $f = \frac{2}{\omega} \frac{\Delta W}{\Delta n}$

LOAD CYCLE IS SHOWN IN FIGURE 33

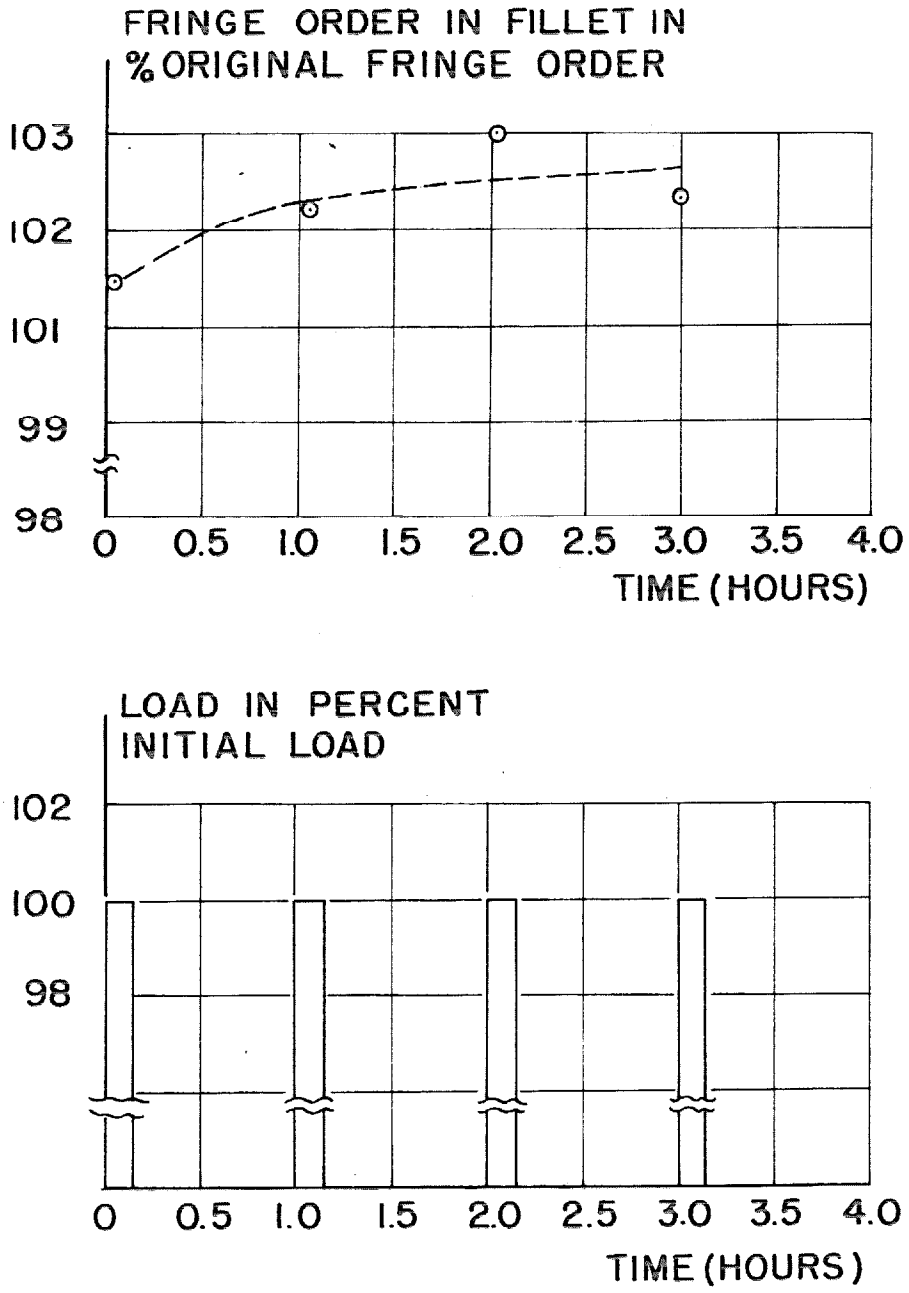

FIGURE 35

VARIATION OF FRINGE ORDER WITH REPEATED TESTS